National Library
of Canada

Acquisitions and
Bibliographic Services Branch

395 Wellington Street
Ottawa, Ontario
K1A 0N4

Bibliothèque nationale
du Canada

Direction des acquisitions et
des services bibliographiques

395, rue Wellington
Ottawa (Ontario)
K1A 0N4

Your file Votre référence

Our file Notre référence

NOTICE

The quality of this microform is heavily dependent upon the quality of the original thesis submitted for microfilming. Every effort has been made to ensure the highest quality of reproduction possible.

If pages are missing, contact the university which granted the degree.

Some pages may have indistinct print especially if the original pages were typed with a poor typewriter ribbon or if the university sent us an inferior photocopy.

Reproduction in full or in part of this microform is governed by the Canadian Copyright Act, R.S.C. 1970, c. C-30, and subsequent amendments.

AVIS

La qualité de cette microforme dépend grandement de la qualité de la thèse soumise au microfilmage. Nous avons tout fait pour assurer une qualité supérieure de reproduction.

S'il manque des pages, veuillez communiquer avec l'université qui a conféré le grade.

La qualité d'impression de certaines pages peut laisser à désirer, surtout si les pages originales ont été dactylographiées à l'aide d'un ruban usé ou si l'université nous a fait parvenir une photocopie de qualité inférieure.

La reproduction, même partielle, de cette microforme est soumise à la Loi canadienne sur le droit d'auteur, SRC 1970, c. C-30, et ses amendements subséquents.

Canada

UNIVERSITY OF ALBERTA

SECONDARY STRESSES IN FLEXIBLE COMPOSITE PIPE

by

KEVIN REINHART ©

A thesis submitted to the Faculty of Graduate Studies in partial
fulfilment of the requirements for the degree of Master of Science

Department of

MECHANICAL ENGINEERING

Edmonton, Alberta

Fall, 1995

National Library
of Canada

Acquisitions and
Bibliographic Services Branch

395 Wellington Street
Ottawa, Ontario
K1A 0N4

Bibliothèque nationale
du Canada

Direction des acquisitions et
des services bibliographiques

395, rue Wellington
Ottawa (Ontario)
K1A 0N4

Your file Votre référence

Our file Notre référence

THE AUTHOR HAS GRANTED AN IRREVOCABLE NON-EXCLUSIVE LICENCE ALLOWING THE NATIONAL LIBRARY OF CANADA TO REPRODUCE, LOAN, DISTRIBUTE OR SELL COPIES OF HIS/HER THESIS BY ANY MEANS AND IN ANY FORM OR FORMAT, MAKING THIS THESIS AVAILABLE TO INTERESTED PERSONS.

L'AUTEUR A ACCORDE UNE LICENCE IRREVOCABLE ET NON EXCLUSIVE PERMETTANT A LA BIBLIOTHEQUE NATIONALE DU CANADA DE REPRODUIRE, PRETER, DISTRIBUER OU VENDRE DES COPIES DE SA THESE DE QUELQUE MANIERE ET SOUS QUELQUE FORME QUE CE SOIT POUR METTRE DES EXEMPLAIRES DE CETTE THESE A LA DISPOSITION DES PERSONNE INTERESSEES.

THE AUTHOR RETAINS OWNERSHIP OF THE COPYRIGHT IN HIS/HER THESIS. NEITHER THE THESIS NOR SUBSTANTIAL EXTRACTS FROM IT MAY BE PRINTED OR OTHERWISE REPRODUCED WITHOUT HIS/HER PERMISSION.

L'AUTEUR CONSERVE LA PROPRIETE DU DROIT D'AUTEUR QUI PROTEGE SA THESE. NI LA THESE NI DES EXTRAITS SUBSTANTIELS DE CELLE-CI NE DOIVENT ETRE IMPRIMES OU AUTREMENT REPRODUITS SANS SON AUTORISATION.

ISBN 0-612-06530-8

Canada

University of Alberta

Library Release Form

Name of Author: Kevin Reinhart
Title of Thesis: Secondary Stresses in Flexible Composite Pipe
Degree: Master of Science
Year this Degree Granted: 1995

Permission is hereby granted to the University of Alberta Library to reproduce single copies of this thesis and to lend or sell such copies for private, scholarly, or scientific research purposes only.

The author reserves all other publication and other rights in association with the copyright in the thesis, and except as herinbefore provided, neither the thesis nor any substantial portion thereof may be printed or otherwise reproduced in any material form whatever without the author's prior written permission.

RR#2, Odessa
Ontario
K0H 2H0

Date: JULY 4, 1995

University of Alberta

Faculty of Graduate Studies and Research

The undersigned certify that they have read and recommend to the Faculty of Graduate Studies and Research for acceptance, a thesis entitled **Secondary Stresses in Flexible Composite Pipe** submitted by **Kevin Reinhart** in partial fulfillment of the requirements for the degree of **Master of Science**.

Dr. D.R. Budney (Supervisor)

aw Lipsett

Dr. A.W. Lipsett

Dr. A. Elwi

Date: July 4, 1995

ABSTRACT

The use of flexible composite pipe for the high pressure applications in the oil and gas industry provides the opportunity to overcome many of the problems associated with traditional steel or rigid fibreglass pipelines. The plastic and fibre-reinforced materials employed provide superior chemical resistance to that of steel structures, while and independent, multilayered construction allows structural flexibility. However, design and analysis of such a system is considerably more complex than that of any mono-material construction. Several different models have been developed to deal with the interaction between the individual components.

Global models utilize equations of compatibility, equilibrium and constitutive relations for the composite material to determine growth and rotation (or axial force and torque) developed through internal pressure. A number of simplifying assumptions necessary for these models allow consideration of unidirectional fibre tension only and preclude the modelling of individual components with respect to secondary stresses. These additional stresses are caused by localized bending and have, through experimentation, been shown to cause premature failure of the pipe under internal pressure.

In this thesis, secondary stresses have been studied in detail using finite element analysis. A greater understanding of the factors causing secondary stresses has been achieved and methods of reducing the stress levels have been developed.

ACKNOWLEDGEMENTS

I would like to thank my thesis supervisor, Dr. D.R. Budney, for his continual support and counsel throughout this thesis.

I would also like to thank Mr. Don Wolfe and Composite Technologies Inc. for providing me with the opportunity to work on such an interesting and challenging project, and the support through good times and bad. This project has been supported by Composite Technologies Inc.

Sam Bouey, Roland Freiheit, Kevin Gartner, Jim Lim and Russell Agnew all helped me immeasurably. They gave me endless technical help and personal support, without which I could not have succeeded.

The assistance of Mark Ackerman in keeping the computer system running despite my ability to frequently overload it is very much appreciated.

I would like to acknowledge my parents Bill and Leslie who were always able to reorient me when I wandered.

And to Rob, Matt, Steve, Chris and the rest who regularly ensured that I never suffered from overwork, I owe my sanity.

I would also like to thank Tone, who kept me motivated despite the distance.

TABLE OF CONTENTS

CHAPTER 1
INTRODUCTION 1

CHAPTER 2
PRIMARY LOADING 3

- 2.1 Introduction 3
- 2.2 Pipe Description 3
- 2.3 Loading Conditions 4
- 2.4 Single Radius Model 5
  - 2.4.1 Introduction 5
  - 2.4.2 Strip Stress for the Unrestrained Case 5
  - 2.4.3 Contact Pressure for the Unrestrained Case 6
  - 2.4.4 Contact Pressure for the General Case 7
  - 2.4.5 Contact Pressure for the Fully Restrained Case 10
- 2.5 Multiple Radius Model 10
  - 2.5.1 Introduction 10
  - 2.5.2 Material Properties for the Multiple Radius Model 12
  - 2.5.3 Development of Strip Stress, Torque and Axial Loads 12
  - 2.5.4 Strip Displacements Due to Pipe Deformations 14
  - 2.5.5 System of Equations 19
- 2.6 Inherent Limitations to the Global Model 21

CHAPTER 3
SECONDARY STRESSES 28

- 3.1 Description of Secondary Stresses 28
  - 3.1.1 Introduction 28
  - 3.1.2 Inner Hoop Layer 28
  - 3.1.3 Observations and Causes of Secondary Stresses 29
  - 3.1.4 Bridge Regions 29

3.2 Critical Stress Regions 30
3.2.1 Introduction 30
3.2.2 Longitudinal Bridge 30
3.2.3 Cross Bridge 31
3.3 Modelling of Critical Stress Regions 31
3.3.1 Introduction 31
3.3.2 Helical Approximation 32
3.3.3 Material Properties 32
3.3.4 Model Geometries 33
3.3.5 Boundary Conditions 34
3.3.5.i *Model L2* 34
3.3.5.ii *Model L1* 36
3.3.6 Failure Criteria 36
3.3.7 Mesh Refinement 37
3.4 Analysis 37

CHAPTER 4
RESULTS 41
4.1 Introduction 41
4.2 Analysis of Reference Model 42
4.2.1 Model L1 42
4.2.2 Model L2 44
4.2.3 Discussion 45
4.3 Cross Bridge Width 47
4.3.1 Model L2 47
4.3.2 Model L1 48
4.3.3 Discussion 48
4.4 Cross Bridge Angle 48
4.4.1 Model L2 48
4.4.2 Model L1 49
4.4.3 Discussion 49

4.5 Percentage of Woven Fabric 49
4.5.1 Model L1 49
4.5.2 Model L2 50
4.5.3 Discussion 50
4.6 Longitudinal Bridge 51
4.6.1 Model L1 51
4.6.2 Discussion 51
4.7 Comparison with 100% Unidirectional Composite 52
4.7.1 Model L1 52
4.7.2 Model L2 53
4.7.3 Discussion 54
4.8 Experimental Results 55

CHAPTER 5
CONCLUSIONS AND RECOMMENDATIONS 90
5.1 Conclusions 90
5.2 Recommendations 92

REFERENCES 93

APPENDIX 1
CYLINDRICAL APPROXIMATION 95

APPENDIX 2
MATERIAL PROPERTIES 98

APPENDIX 3
CONTACT SURFACE PRESSURE GRADIENTS 104

APPENDIX 4
FAILURE CRITERIA 111

APPENDIX 5
MESH REFINEMENT 114

LIST OF FIGURES

Figure 1.1 Schematic of Flexible Composite Pipe 2

Figure 2.1 Radial Equilibrium of Hoop and Helix Structures 22

Figure 2.2 Axial Equilibrium of Hoop and Helix Structures 22

Figure 2.3 One Pitch of Pipe Mapped onto a Plane 23

Figure 2.4 Axial and Radial Deflections 23

Figure 2.5 Circumferential and Radial Deflections 24

Figure 2.6 Schematic of Multiple Radius Model 24

Figure 2.7 Composite Strip Coordinate System 25

Figure 2.8 Schematic of Contact Pressures 25

Figure 2.9 Radial Equilibrium of One Layer 26

Figure 2.10 Axial and Rotational Equilibrium in One Layer 26

Figure 2.11 Axial Growth and Radial Deflection 27

Figure 3.1 Schematic of Inner and Outer Hoop Layers 38

Figure 3.2 Sketch of Model L2, Showing Displacement Constraints 39

Figure 3.3 Sketch of Model L1, Showing Displacement Constraints 40

Figure 4.1 Longitudinal Stress in Unidirectional Composite, Model L1, with Bridges Identified 56

Figure 4.2 Longitudinal Stress in Woven Fabric Composite, Model L1, with Bridges Identified 57

Figure 4.3 Transverse Stress in Unidirectional Composite (psi), Model L1 . . 58

Figure 4.4 Transverse Stress in Woven Fabric Composite (psi), Model L1 . . 58

Figure 4.5 Radial Stress in Unidirectional Composite (psi), Model L1 59

Figure 4.6 Radial Stress in Woven Fabric Composite (psi), Model L1 59

Figure 4.7 Shear Stress S_{TR} in Unidirectional Composite (psi), Model L1 . . . 60

Figure 4.8 Shear Stress S_{TR} in Woven Fabric Composite (psi), Model L1 . . . 60

Figure 4.9 Tsai-Wu Parameters in Unidirectional Composite, Model L1 61

Figure 4.10 Tsai-Wu Parameters in Woven Fabric Composite, Model L1 61

Figure 4.11 Longitudinal Stress in Unidirectional Composite, Model L2, Bridge Regions Identified 62
Figure 4.12 Longitudinal Stress in Unidirectional Composite 'T', Model L2, Bridge Regions Identified 63
Figure 4.13 Longitudinal Stress in Woven Fabric Composite, Model L2, Bridge Regions Identified 64
Figure 4.14 Transverse Stress in Unidirectional Composite (psi), Model L2 . . 65
Figure 4.15 Transverse Stress in Unidirectional Composite (psi), Model L2, 'T' Section 65
Figure 4.16 Transverse Stress in Woven Fabric Composite (psi), Model L2 . . 66
Figure 4.17 Radial Stress in Unidirectional Composite (psi), Model L2 66
Figure 4.18 Radial Stress in Unidirectional Composite (psi), Model L2, 'T' Section 67
Figure 4.19 Radial Stress in Woven Fabric Composite (psi), Model L2 67
Figure 4.20 Shear Stress S_{LR} in Unidirectional Composite (psi), Model L2 . . . 68
Figure 4.21 Shear Stress S_{LR} in Unidirectional Composite, Model L2, 'T' Section 68
Figure 4.22 Shear Stress S_{LR} in Woven Fabric Composite, Model L2 69
Figure 4.23 Shear Stress S_{TR} in Unidirectional Composite (psi), Model L2 . . 69
Figure 4.24 Shear Stress S_{TR} in Unidirectional Composite, Model L2, 'T' Section 70
Figure 4.25 Shear Stress S_{TR} in Woven Fabric Composite (psi), Model L2, View of Top of Bottom Layer of Fabric 70
Figure 4.26 Tsai-Wu Parameters in Unidirectional Composite, Model L2 71
Figure 4.27 Tsai-Wu Parameters in Unidirectional Composite (psi), Model L2, 'T' Section 71
Figure 4.28 Tsai-Wu Parameters in Woven Fabric Composite, Model L2 72
Figure 4.29 Tsai-Wu Parameters in Woven Fabric Composite, Model L2 . . . 72
Figure 4.30 Maximum Shear Stress S_{LR} as a Function of Cross Bridge Width, Model L2 73

Figure 4.31 Maximum Longitudinal Stress as a Function of Cross Bridge Width, Model L2 73

Figure 4.32 Maximum Transverse Stress as a Function of Cross Bridge Width, Model L2 74

Figure 4.33 Maximum Radial Stress as a Function of Cross Bridge Width, Model L2 74

Figure 4.34 Maximum Shear Stress S_{TR} as a Function of Cross Bridge Width, Model L2 75

Figure 4.35 Maximum Tsai-Wu Parameter as a Function of Cross Bridge Width, Model L2 75

Figure 4.36 Maximum Tsai-Wu Parameter as a Function of Cross Bridge Width, Model L1 76

Figure 4.37 Maximum Longitudinal Stress as a Function of Cross Bridge Angle, Model L2 77

Figure 4.38 Maximum Transverse Stress as a Function of Cross Bridge Angle, Model L2 77

Figure 4.39 Maximum Radial Stress as a Function of Cross Bridge Angle, Model L2 78

Figure 4.40 Maximum Shear Stress S_{LR} as a Function of Cross Bridge Angle, Model L2 78

Figure 4.41 Maximum Shear Stress S_{TR} as a Function of Cross Bridge Angle, Model L2 79

Figure 4.42 Maximum Tsai-Wu Parameter as a Function of Cross Bridge Angle, Model L2 79

Figure 4.43 Maximum Tsai-Wu Parameter as a Function of Cross Bridge Angle, Model L1 80

Figure 4.44 Maximum Longitudinal Stress as a Function of Percentage of Woven Fabric, Model L1 81

Figure 4.45 Maximum Transverse Stress as a Function of Percentage of Woven Fabric, Model L1 81

Figure 4.46 Maximum Radial Stress as a Function of Percentage of Woven Fabric, Model L1 82

Figure 4.47 Maximum Shear Stress S_{TR} as a Function of Percentage of Woven Fabric, Model L1 82

Figure 4.48 Maximum Tsai-Wu Parameter as a Function of Percentage of Woven Fabric, Model L1 83

Figure 4.49 Maximum Longitudinal Stress as a Function of Percentage of Woven Fabric, Model L2 84

Figure 4.50 Maximum Transverse Stress as a Function of Percentage of Woven Fabric, Model L2 84

Figure 4.51 Maximum Radial Stress as a Function of Percentage of Woven Fabric, Model L2 85

Figure 4.52 Maximum Shear Stress S_{LR} as a Function of Percentage of Woven Fabric, Model L2 85

Figure 4.53 Maximum Shear Stress S_{TR} as a Function of Percentage of Woven Fabric, Model L2 86

Figure 4.54 Maximum Tsai-Wu Parameter as a Function of Percentage of Woven Fabric, Model L2 86

Figure 4.55 Maximum Longitudinal Stress as a Function of Longitudinal Bridge Width, Model L1 87

Figure 4.56 Maximum Transverse Stress as a Function of Longitudinal Bridge Width, Model L1 87

Figure 4.57 Maximum Radial Stress as a Function of Longitudinal Bridge Width, Model L1 88

Figure 4.58 Maximum Shear Stress S_{TR} as a Function of Longitudinal Bridge Width, Model L1 88

Figure 4.59 Maximum Tsai-Wu Parameter as a Function of Longitudinal Bridge Width, Model L1 89

Figure A3.1 Comprehensive Model 106

Figure A3.2 Contact Pressure at Contact Surface of Layer 2 of Comprehensive Model 107

Figure A3.3 Graph of Contact Pressure at A-A of Contact Surface of Layer 2 of Comprehensive Model 108
Figure A3.4 Graph of Contact Pressure at B-B of Contact Surface of Layer 2 of Comprehensive Model 108
Figure A3.5 Radial Displacement of Contact Surface Layer 1 of Comprehensive Model 109
Figure A3.6 Radial Displacement of Contact Surface of Layer 1, Model L1 . . 109
Figure A3.7 Two Layer Cross Bridge Finite Element Model 110
Figure A3.8 Graph of Contact Pressure of Two Layer Cross Bridge Finite Element Model 110
Figure A5.1 Variation of Maximum Longitudinal Stress with Mesh Refinement, Model L1 116
Figure A5.2 Variation of Maximum Transverse Stress with Mesh Refinement, Model L1 116
Figure A5.3 Variation of Maximum Radial Stress with Mesh Refinement, Model L1 117
Figure A5.4 Variation of Maximum Shear Stress S_{TR} with Mesh Refinement, Model L1 117
Figure A5.5 Variation of Maximum Tsai-Wu Parameter with Mesh Refinement 118
Figure A5.6 Final Mesh Density of Model L1 119
Figure A5.7 Variation of Maximum Longitudinal Stress with Mesh Refinement, Model L2 120
Figure A5.8 Variation of Maximum Transverse Stress with Mesh Refinement, Model L2 120
Figure A5.9 Variation of Maximum Radial Stress with Mesh Refinement, Model L2 121
Figure A5.10 Variation of Maximum Shear Stress S_{TR} with Mesh Refinement, Model L2 121
Figure A5.11 Variation of Maximum Shear Stress S_{TR} with Mesh Refinement, Model L2 122

Figure A5.12 Variation of Maximum Tsai-Wu Parameter with Mesh Refinement, Model L2 122

Figure A5.13 Final Mesh Density of Model L2 123

LIST OF TABLES

Table 4.1 Summary of Analysis 42
Table 4.2 Maximum Stresses and Tsai-Wu Failure Parameters for Model L1 44
Table 4.3 Maximum Stresses and Tsai-Wu Failure Parameters for Model L2 45
Table 4.4 Comparison of Reference Model with 100% Unidirectional Composite, Model L1 53
Table 4.5 Comparison of Reference Model with 100% Unidirectional Composite, Model L2 54
Table A2.1 Constituent Material Properties 99
Table A2.2 Unidirectionally Reinforced Material Properties 102
Table A2.3 Woven Fabric Reinforced Material Properties 103

LIST OF SYMBOLS

a	fibre radius
b	resin cylinder radius
c	fibre volume radius
C_{XY}, C_{XZ}, C_{YZ}	constants used in Tsai-Wu failure criterion interaction terms
c_i	radial gap between structural layers
E_R	radial tensile modulus of composite
E_L	longitudinal tensile modulus of composite
F_i	second rank tensor of Tsai-Wu failure criterion
F_{ij}	fourth rank tensor of Tsai-Wu failure criterion
F_{12}, F_{13}, F_{23}	interaction terms of Tsai-Wu failure criterion
F_L	axial force developed by one layer
F_E	external axial force required for equilibrium
G	shear modulus
K	bulk modulus
L	initial strip length of one pitch
dL	change in strip length
p	internal pressure
p_c	contact pressure
Δp_i	pressure drop through a layer
r	radius of layer
r_o	original radius of layer (pipe radius)
r_s	effective radius of composite strip
dr	radial strain
R	strength of composite in direction 12
S	strength of composite in direction 13
t	thickness of layer
t_e	thickness of helix layers
t_o	thickness of hoop layers
T	strength of composite in direction 23

T_L	torque developed by one layer
T_E	external torque required for equilibrium
u_i	radial displacement of layer i
X	strength of composite in direction 1
$\mathbf{X}$	definition of a point on a curve
Y	strength of composite in direction 2
z	length of one pitch
dz	change in pitch length
Z	strength of composite in direction 3
α	volume fraction of percentage of composite material in structural layers
α_e	volume fraction of percentage of composite material in helix layers
α_o	volume fraction of percentage of composite material in hoop layers
β	rotation per unit length of pipe
ϵ_L	longitudinal strain of composite strip
ϵ_{Le}	longitudinal strain of composite strips in helix structure
ϵ_{Lo}	longitudinal strain of composite strips in hoop structure
ϵ_z	axial strain of pipe
ϵ_Θ	circumferential strain of pipe
ϕ	helix angle of strips relative to axis of pipe
ϕ_e	helix angle of helix strips relative to axis of pipe
ϕ_o	helix angle of hoop strips relative to axis of pipe
κ	radius of curvature of helical composite strip
ν	Poisson's ratio
σ_L	longitudinal stress in composite strip
σ_{Le}	longitudinal stress in composite strip in helix structure
σ_{Lo}	longitudinal stress in composite strip in hoop structure
Θ	angle of rotation of composite strip

CHAPTER 1

INTRODUCTION

Flexible pipe has been employed in various forms for some time. Reinforced garden hose and hydraulic tubing are two common examples of helically wound, continuously constructed piping.

Large diameter, high pressure flexible tubing using steel as the structural material is widely used as risers for offshore oil platforms. However, this high pressure product develops large axial deformations which would be unsuitable for buried onshore use. Because of this, and the prohibitive price associated with materials and construction, this product has not been used for the onshore oil and gas industry.

A novel design has been developed employing mostly unidirectionally fibre-reinforced polymeric strips as the main load bearing members (Figure 1.1). The pipe is composed of a number of layers, each consisting of alternating independent fibre-reinforced composite strips and elastomeric polymer strips. The elastomeric strips are non-load bearing components, but perform two essential functions. Applied in each layer before the composite strips, they act as a mold during filament winding, maintaining alignment for the composite strips. Being low-modulus, they also allow limited and uniform movement between the composite strips, necessary for bending flexibility of the structure. The internal liner is a non-load bearing member, acting only as a bladder to contain the transported fluid. The cover is also non-structural, serving to protect the inner layers from external debris.

As the dominant loading in each composite strip is longitudinal, with relatively minor secondary stresses, the strongly anisotropic nature of unidirectionally reinforced materials allows efficient design of the structure. However, the unidirectional material is not effective for transverse or shear loading and additional transverse reinforcement is required in some layers that experience high secondary stresses. The purpose of this study is to model the secondary stresses and to design a composite structure able to withstand them.

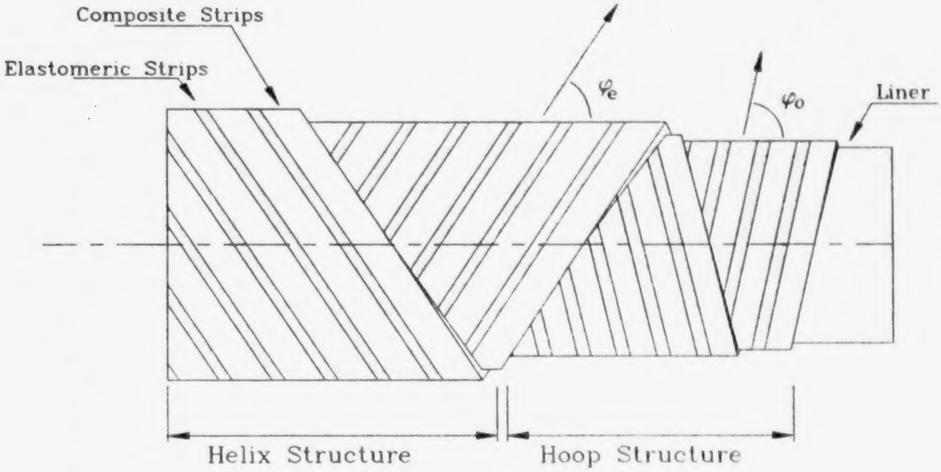

Figure 1.1 Schematic of Flexible Composite Pipe

CHAPTER 2
PRIMARY LOADING

2.1 Introduction

In order to fully understand the primary stresses that develop in the structural layers of the pipe, global models have been developed. These models deal simplistically with the stresses that develop in each composite strip in response to internal pressure and are used to predict the performance of the pipe in terms of axial force and torque (or growth and rotation for an axially and torsionally unrestrained pipe) that develop when internal pressure is applied. In the global models, longitudinal stresses are assumed uniform through the thickness of the composite strips in a layer, while radial stresses are assumed uniform throughout each layer. Given these assumptions, which are adequate for cases when significant transverse loading does not develop (for example, given low internal pressure), the global models have provided reasonably accurate predictions of pipe performance with regards to elongation and rotation of the pipe. However when transverse loading occurs (as internal pressure increases and contact pressures between successive layers increase), the additional stress levels in the composite strips can be significantly above those predicted.

2.2 Pipe Description

The four structural layers of the pipe can be seen in Figure 1.1. Each of the four layers is separated from the adjacent layers by a thin polyethylene film to allow relative movement. In actuality, the innermost layer is more complex than that shown in Figure 1.1, but this simple representation is used in the global models. The two innermost layers comprise the Hoop structure, which is wound at a high angle, allowing it to withstand large hoop loads. The Helix structure consists of the two outer layers, wound at a low angle to withstand axial loads. The following global model includes only the composite strips. The elastomeric strips, the liner and the cover are non-structural members and are not included.

2.3 Loading Conditions

Development of the pipe models requires consideration of numerous different loading conditions. Internal pressure applied to a specimen with one or both ends axially and rotationally unrestrained will result in axial growth and rotation, whereas if applied to specimen with full axial and rotational constraints at both ends, will result in an axial load and torque. This is significant when considering the deformation; the contact pressure between successive layers is considerably altered by variations in boundary conditions.

Restraint conditions applied in the laboratory are a combination of axial and rotational restraints applied to the ends of the specimen. In the fully restrained scenario, which consists of axial and rotational constraints at both ends, axial loading and torque are functions of internal pressure. In the unrestrained situation, axial growth and rotation are permitted, and are the parameters measured during the experiment or predicted by the global model.

In service, the pipe will be connected to flanges at both ends and buried, preventing any deformation, and will act as a fully restrained pipe. Given these conditions, the most realistic laboratory experiment would involve fully restrained specimens. However, as the pipe is normally bent during field use, lateral movement, which is essentially identical to axial elongation in this scenario, is impossible to restrict. Because of this, the test specimens are considered torsionally restrained and axially unrestrained.

Generally, pipe is designed to have zero axial growth and zero rotation, even under unrestrained conditions. Applying full constraints to this pipe would cause no axial load or torque. However, a perfectly axially and rotationally neutral pipe is difficult to manufacture, and even though it may be so designed, some deviation from the ideal is unavoidable.

The following analysis considers the case of the unrestrained condition, with some description of the restrained case. This is adequate to demonstrate the major components of the global model and the limitations with regard to secondary loading.

2.4 Single Radius Model

2.4.1 Introduction

The Single Radius Model (She, 1993) was the first attempt to predict pipe performance. This model is composed of four independent layers as is shown in Figure 1.1. However, it is assumed that the total thickness of all layers is very small relative to the radius of the pipe. In accordance with this assumption, any variation in radius between the layers is insignificant and all layers are assigned the same radius value. This greatly simplifies the equilibrium and deformation analyses by allowing axial symmetry in the model. In developing radial and axial equilibrium equations, the Hoop structure and the Helix structure (comprising two layers each) are treated as separate entities with the Hoop layers applying a single contact pressure on the Helix layers.

This requires that the two hoop layers must have identical geometries, as must the two helix layers. That is, the thicknesses t, and the percentages of composite material α in each layer must be identical, while the wrap angles ϕ must be identical but of opposite hand for each of the two layers in each structure.

The following discussion shows the development of the equations of the simple model and will explain the inherent limitations.

2.4.2 Strip Stress for the Unrestrained Case

From the free body diagram of Figure 2.1 showing radius r, internal pressure p and contact pressure p_c, radial equilibrium within the Hoop structure can be expressed as

$$2r(p-p_c) = 4t_o\alpha_o\sigma_{L_o}\sin^2\phi_o \tag{2.1}$$

where t is the layer thickness of each Hoop layer, α is the fraction of structural material in the layer, σ_L is the longitudinal stress in the composite strips and ϕ is the wind angle. The subscript $_o$ refers to the Hoop structure.

The Hoop strip stress can then be expressed as

$$\sigma_{L_o} = \frac{(p-p_c)r}{2\alpha_o t_o \sin^2\phi_o} \ . \tag{2.2}$$

Similarly, with internal pressure p = p_c and zero external pressure, the Helix strip stress can be expressed as

$$\sigma_{L_e} = \frac{p_c r}{2t_e\alpha_e\sin^2\phi_e} \ , \tag{2.3}$$

where the subscript $_e$ refers to the Helix structure.

It can be seen that the equations for stress assume a uniform pressure drop for the entire layer, and that the stress does not vary through the thickness.

2.4.3 Contact Pressure for the Unrestrained Case

Given the stress in each of the layers, the contact pressure between layers can be determined by considering the axial loads acting on the pipe. For an unrestrained specimen under internal pressure, the axial force equilibrium (see Figure 2.2) is

$$F_L = \pi r^2 p = 4\pi r t_o\alpha_o\sigma_{L_o}\cos^2\phi_o + 4\pi r t_e\alpha_e\sigma_{L_e}\cos^2\phi_e \ . \tag{2.4}$$

When Equation 2.4 is combined with Equations 2.2 and 2.3, the contact pressure between the Hoop and Helix layers for an unrestrained pipe is found to be

$$p_c = p\frac{\frac{1}{2} - \cot^2\phi_o}{\cot^2\phi_e - \cot^2\phi_o} \; . \tag{2.5}$$

As this is the contact pressure for an unrestrained specimen, pipe deformations are permitted. Thus this contact pressure will generally not be the same as that for a fully restrained pipe. With axial restraints, the axial strain is identically zero for all layers, and in the single radius model, circumferential strain will also be identical for all layers. The contact pressure for the restrained case can be developed from the general case, which follows.

2.4.4 Contact Pressure for the General Case

Radial and axial deformations of the pipe are now considered separately. Figure 2.3 shows one pitch of one strip, before deformation, mapped onto a plane with circumference $2\pi r$, wrap angle ϕ, strip length L and pitch length z. Figure 2.4 shows the effects of a change in axial length.

The initial length of the strip is

$$L = \frac{z}{\cos\phi} \; . \tag{2.6}$$

From Figure 2.4, the deflection of the composite strip is related to axial deformation of the pipe through

$$dL = dz\cos\phi \; .$$

Given the longitudinal strain of the composite strip ϵ_L = dL/L,

$$dz = \frac{dL}{\cos\phi} = \frac{\epsilon L}{\cos\phi} = \frac{\epsilon_L}{\cos\phi}\frac{z}{\cos\phi}$$

and

$$\frac{dz}{z} = \epsilon_z = \frac{\epsilon_L}{\cos^2\phi}$$

where ϵ_z is the axial strain of the pipe, or

$$\epsilon_L = \epsilon_z \cos^2\phi \ . \tag{2.7}$$

Figure 2.5 shows the effect of circumferential change only. The strain in the composite strip is related to circumferential strain through

$$dL = (2\pi dr)\sin\phi \ .$$

Given that

$$L = \frac{2\pi r}{\sin\phi}$$

it follows that

$$\frac{dL}{L} = \frac{(2\pi dr)\sin^2\phi}{2\pi r}$$

or

$$\epsilon_L = \epsilon_\theta \sin^2\phi \ . \tag{2.8}$$

where ϵ_θ is the circumferential strain of the pipe.

Combining equations 2.7 and 2.8, and assuming small strains, the total strain in the composite strip is thus

$$\epsilon_L = \epsilon_z \cos^2\phi + \epsilon_\theta \sin^2\phi \ . \tag{2.9}$$

Given Equations 2.2 and 2.3 for the stresses in the Hoop and Helix layers, the strains can be written as

$$\epsilon_{L_o} = \frac{\sigma_{L_o}}{E_o} = \frac{(p-p_c)r}{2t_o\alpha_o E_o \sin^2\phi_o} \tag{2.10}$$

and

$$\epsilon_{L_e} = \frac{p_c r}{2t_e\alpha_e E_e \sin^2\phi_e} . \tag{2.11}$$

Knowing that both ϵ_z and ϵ_θ are common for both the hoop and helix structures, Equation 2.9 can be rewritten as

$$\epsilon_{Lo} = \epsilon_z \cos^2\phi_o + \epsilon_\theta \sin^2\phi_o \tag{2.12}$$

and

$$\epsilon_{Le} = \epsilon_z \cos^2\phi_e + \epsilon_\theta \sin^2\phi_e \tag{2.13}$$

Inserting Equations 2.10 and 2.11 into Equations 2.12 and 2.13, the axial and circumferential strains of the pipe ϵ_z and ϵ_θ can be determined.

$$\epsilon_z = \frac{\dfrac{(p-p_c)r\sin^2\phi_e}{2t_o\alpha_o E_o \sin^2\phi_o} - \dfrac{p_c r \sin^2\phi_o}{2t_e\alpha_e E_e \sin^2\phi_e}}{\cos^2\phi_o \sin^2\phi_e - \cos^2\phi_e \sin^2\phi_o} \tag{2.14}$$

$$\epsilon_\theta = \frac{\dfrac{p_c r \cos^2\phi_o}{2t_e\alpha_e E_e \sin^2\phi_e} - \dfrac{(p-p_c)r\cos^2\phi_e}{2t_o\alpha_o E_o \sin^2\phi_o}}{\cos^2\phi_o \sin^2\phi_e - \cos^2\phi_e \sin^2\phi_o} . \tag{2.15}$$

By setting the numerator of Equation 2.12 to zero, and solving for the design variables, an axially neutral pipe can be developed. This is also used in the next section as the basis for fully restrained pipes with no axial elongation.

2.4.5 Contact Pressure for the Fully Restrained Case

The contact pressure for a fully restrained pipe can be calculated by setting the axial strain ϵ_z in Equation 2.12 to zero and solving for p_c:

$$p_c = \frac{p\sin^4\phi_e t_e \alpha_e E_e}{\sin^4\phi_o t_o \alpha_o E_o + \sin^4\phi_e t_e \alpha_e E_e} \tag{2.16}$$

Because Equations 2.2 and 2.3 for the strip stress are valid for any loading conditions, the stresses in the Hoop and Helix layers for a fully restrained pipe can be determined given the above contact pressure, for the general case, to be

$$\sigma_{L_o} = \frac{pr\sin^2\phi_o E_o}{2(\sin^4\phi_o t_o \alpha_o E_o + \sin^4\phi_e t_e \alpha_e E_e)} \tag{2.17}$$

$$\sigma_{L_e} = \frac{pr\sin^2\phi_e E_e}{2(\sin^4\phi_o t_o \alpha_o E_o + \sin^4\phi_e t_e \alpha_e E_e)} \; . \tag{2.18}$$

It can be shown that the contact pressures and the stresses are the same for an unrestrained pipe with zero axial growth as for a restrained pipe with zero axial load (She, 1993).

2.5 Multiple Radius Model

2.5.1 Introduction

This model incorporates several modifications to the single radius model (Budney, 1994). Most significant is the specification of individual radii r_i for each structural layer as can be seen in the schematic of Figure 2.6. Accordingly, each layer is assumed to act as a thin walled member with thickness t_i, as opposed to the entire structure, as was the case in the single radius model. A radial clearance, or gap c_i, has also been introduced between structural layers to account for observed and measured performance of test specimens. This gap represents a few different factors. The first and most obvious is the radial space between layers. The second is the compression of the polyethylene film which is applied between the layers. Being non-structural, this material was not included in the previous model, but affects the pipe performance and must be accounted for. Lastly, small resin-rich peaks of thermoset matrix material creating irregular surfaces will compress from radial loading, effectively behaving as an additional radial gap. Modifications made to account for these factors greatly complicate the solution, but provide a much more realistic model.

The dimensions of the multiple radius model are defined as in Figure 2.6. The internal radius of the structure is r, while r_1, r_2, r_3 and r_4 represent the mid-thickness radii of layers 1 to 4. The thicknesses t_1 to t_4 are the thickness values for each layer, and c_1, c_2 and c_3 represent the initial, as-manufactured radial gap between layers. These are estimated from experience and from the comparisons of predicted and measured performance.

The helix angles ϕ_1 to ϕ_4, measured relative to the axial direction of the pipe, represent the helix angles of layers 1 to 4.

Within each of the four structural layers, discrete helical strips of unidirectional composite material are separated by strips of low modulus, elastomeric polymer. Though these elastomeric strips are non load-bearing, they are used in order to maintain uniform separation of the composite strips during operation and to aid manufacturing by serving as a mold, guiding the placement of the composite. The constants α_1 to α_4 represent the volume fraction of composite within each layer, the remainder being occupied by the elastomeric polymer. The values of α are typically in the order of 75%.

The multiple radius model, because of its complexity, requires the solution of a system of equations to solve for the strip stress, axial load and torque. These include equations of compatibility and equilibrium, and constitutive relations.

Design of the pipe according to the multiple radius model is an iterative process. The strip stress, torque and axial loads, and radial displacement must all be determined in the process of formulating the required equations.

2.5.2 Material Properties for the Multiple Radius Model

The material properties are now defined for the load-bearing composite material. The elastomeric components do not contribute to the structural performance of the global model and are ignored.

Consider Figure 2.7, a representation of a composite strip, wound around the pipe at a helix angle of ϕ. The radial direction is represented by R, the fibre direction by L (the longitudinal direction of the strip) and the strip transverse direction by T. The material properties used in the model are elastic moduli in two directions, and Poisson's ratio in one plane. The nomenclature is E_L (the longitudinal modulus), E_R (the radial modulus) and ν_{LR} (Poisson's ratio governing transverse contraction due to longitudinal tension).

2.5.3 Development of Strip Stress, Torque and Axial Loads

An important concept used in the global model is that of contact pressures between layers, as illustrated in Figure 2.8. With internal pressure p, the contact pressure between the layers decreases by Δp_i through each layer i. Thus, the internal pressure acting on layer 4 is then the pipe internal pressure less the pressure drops occurring through each of layers 1, 2 and 3.

Given the pressures acting on each layer, the stress in those layers can also be defined. Consider Figure 2.9, a sketch of the first layer. Once again assuming that each layer is thin compared to the pipe radius, and that the stress is uniform through the thickness of the layer, hoop equilibrium can be used to determine the stress in each strip of the layer. This is similar to that developed for the single radius model, but is calculated for each individual layer instead of for the Hoop and Helix structures. The stress is

$$\sigma_{L_i} = \frac{\Delta p_i r_i}{2\,\alpha_i t_i \sin^2\phi_i} \; . \tag{2.19}$$

where $\Delta p_i = p_{i+1} - p_i$.

From the stress in the structural layers, the axial load and torque acting at each end of the pipe can be determined. This assumes that the pipe ends are capped, meaning that the strips are fixed at the ends, as in an end connection. In order to determine the torque developed, consider the free body diagram of Figure 2.10.

The torque T_{Li} in each layer i is

$$T_{L_i} = \sigma_{L_i} \cdot (2\pi r_i \alpha_i t_i \cos\phi_i)\sin\phi_i \cdot r_i$$

where $2\pi r_i \alpha_i t_i \cos\phi_i$ is the projection of the cross sectional area of the composite strips of one layer, or

$$T_{L_i} = \frac{\pi r_i^3 \Delta p_i}{\tan\phi_i} \tag{2.20}$$

Summing the torque of all layers, the net or external torque T_E is

$$\begin{aligned} T_E &= \frac{\pi r_1^3 \Delta p_1}{\tan\phi_1} + \frac{\pi r_2^3 \Delta p_2}{\tan\phi_2} + \frac{\pi r_3^3 \Delta p_3}{\tan\phi_3} \\ &+ \frac{\pi r_4^2 (p - \Delta p_1 - \Delta p_2 - \Delta p_3)}{\tan\phi_4} \; . \end{aligned} \tag{2.21}$$

This is the general case. If the pipe is torsionally unrestrained, there is no external torque, and Equation 2.19 is set to zero.

The axial load is determined in a similar fashion. Once again consider Figure 2.11. The axial load F_{Li} acting on each layer is

$$F_{L_i} = 2\pi r_i t_i \alpha_i \cdot \sigma_{L_i} \cos^2\phi_i$$

Then,

$$F_{L_i} = \frac{2\pi r_i^2 \Delta p_i}{\tan^2\phi_i} \tag{2.22}$$

Once again summing the loads of internal pressure and all four layers, the net or external axial load F_E is

$$F_E = p\pi r^2 - \frac{2\pi r_1^2 \Delta p_1}{\tan^2\phi_1} - \frac{2\pi r_2^2 \Delta p_2}{\tan^2\phi_2} - \frac{2\pi r_3^2 \Delta p_3}{\tan^2\phi_2} - \frac{2\pi r_4^2 (p - \Delta p_1 - \Delta p_2 - \Delta p_3}{\tan^2\phi_4} \tag{2.23}$$

This is valid for the general case. With unrestrained ends, F is equal to zero.

The torque and axial load developed due to internal pressure have thus been developed. The deformations of the pipe are now determined.

2.5.4 Strip Displacements Due to Pipe Deformations

The displacements of the strips are considered in terms of radial, circumferential and axial displacements.

Radial displacement is caused by two factors: Poisson's ratio contraction and radial compression. These cause changes in the radius of each layer. Radial displacement is also caused by axial and circumferential displacements, relating to elongation and relative rotation respectively. Each of these factors will be studied as follows.

With regards to radial deformation due to strip stress, there are two factors. Thicknesses of the strips are altered when radial loads are applied, the resulting contact pressures compressing the layers. Poisson's ratio contraction from strip tension will further reduce the difference between radius values of adjacent structural layers. Radial compression and Poisson's ratio contraction are related to strip stress by

$$\epsilon_R = \frac{\sigma_R}{E_R} - \frac{\nu_{LR}\sigma_L}{E_L} . \tag{2.24}$$

Now consider the relationship between axial growth and radial displacement (see Figure 2.11). In this case, an elongation of the pipe will cause a radial contraction of the pipe. A single strip, of radius r, wound at an angle ϕ with a pitch z, grows axially an amount dz, this growth corresponding to a radial deformation of 2πdr.

With regards to original dimensions,

$$\tan\phi = \frac{2\pi r}{z} ,$$

and

$$\frac{2\pi r}{z\tan\phi} = 1 \tag{2.25}$$

Assuming small deformations,

$$\tan\phi = \frac{-dz}{2\pi dr} \tag{2.26}$$

Relating Equations 2.23 and 2.24,

$$dr = -\frac{dz}{2\pi\tan\phi}$$

$$dr = \frac{-dz}{2\pi\tan\phi} \cdot \frac{2\pi r}{z\tan\phi}$$

and

$$dr = -\frac{dz}{z} \cdot \frac{r}{\tan^2\phi} \tag{2.27}$$

Thus, in the case of two strips,

$$dr_1 - dr_2 = -\frac{dz}{z}\left(\frac{r_1}{\tan^2\phi_1} - \frac{r_2}{\tan^2\phi_2}\right) \tag{2.28}$$

where $dr_1 - dr_2$ is the relative displacement of the strips and dz/z is the unit change in length.

Now consider the relationship between rotation and radial displacement as represented in see Figure 2.12). As with axial growth, a rotation of one end of the pipe relative to the other will cause a radial expansion or contraction. A single strip of radius r, wound at an angle ϕ with a pitch z, expands radially an amount dr. The strip length remains unchanged, as does the length of the pipe, but the circumference of the enclosed area will change and the length of the strip no longer corresponds to one pitch. Given the rotation per unit length ß, one end will rotate and cause an overlap of angle ßz relative to the other end.

In order to determine the overlap, the original and deformed circumferences are equated.

$$2\pi r = (2\pi + \beta z)(r + dr)$$

Ignoring higher order elements,

$$\begin{aligned} 2\pi dr &= -\beta z r \\ dr &= \frac{-\beta z r}{2\pi} \end{aligned} \tag{2.29}$$

Given that

$$\tan\phi = \frac{2\pi r}{z},$$

$$z = \frac{2\pi r}{\tan\phi} \tag{2.30}$$

which can be substituted into Equation 2.27. Then

$$dr = -\beta \frac{r^2}{\tan\phi} \tag{2.31}$$

For two adjacent layers,

$$dr_1 - dr_2 = -\beta\left(\frac{r_1^2}{\tan\phi_1} - \frac{r_2^2}{\tan\phi_2}\right) \tag{2.32}$$

Thus, Equations 2.26 and 2.29 relate radial displacement of adjacent layers ($dr_1 - dr_2$) to rotation (ß) and axial growth (dz).

Next, consider the effects of strip strain. If there is no axial strain, as defined earlier for the case of purely radial and circumferential deformations, Equation 2.9 can be reduced to

$$\epsilon_L = \epsilon_\theta \sin^2\phi \tag{2.33}$$

Given that

$$\epsilon_L = \frac{\sigma_L}{E_L} \tag{2.34}$$

the circumferential strain, ϵ_θ can be written as

$$\epsilon_\theta = \frac{\epsilon_L}{\sin^2\phi} \tag{2.35}$$

or

$$\epsilon_\theta = \frac{\sigma_L}{E_L \sin^2\phi} \tag{2.36}$$

or

$$\epsilon_\theta = \frac{\Delta p r}{E_L \alpha t \sin^2\phi} \tag{2.37}$$

Defining the radial displacement u = dr, and noting that

$$\epsilon_\theta = \frac{(2\pi dr)}{2\pi r} = \frac{dr}{r} = \frac{u}{r}$$

Equations 2.33 and 2.34 can be used to define u in terms of strip stress or internal pressure,

$$u = \frac{\sigma_L r}{E_L \sin^2\phi} \tag{2.38}$$

$$u = \frac{\Delta p r^2}{E_L \alpha t \sin^4\phi} \tag{2.39}$$

All of the fundamental equations necessary to determine the deformation of the pipe have now been developed. At this point, they are assembled to allow solution.

2.5.5 System of Equations

If layer 1 has stress σ_1 and pressure drop Δp_1 and layer 2 has stress σ_2 and pressure drop Δp_2, the relative radial displacement between layers 1 and 2 is

$$u_1 - u_2 = \frac{\sigma_{L_1} r_1}{E_1 \sin^2\phi_1} - \frac{\sigma_{L_2} r_2}{E_2 \sin^2\phi_2} \tag{2.40}$$

or

$$u_1 - u_2 = \frac{\Delta p_1 r_1^2}{E_1 \alpha_1 t_1 \sin^4\phi_1} - \frac{\Delta p_2 r_2^2}{E_2 \alpha_2 t_2 \sin^4\phi_2} \tag{2.41}$$

Combining these radial displacements with the effects of axial elongation and rotation, the compatibility equation is developed:

$$\begin{aligned} c_1 &= u_1 - u_2 \\ &= \Delta p_1 \frac{r_1^2}{E_1 \alpha_1 t_1 \sin^4\phi_1} - \Delta p_2 \frac{r_2^2}{E_2 \alpha_2 t_2 \sin^4\phi_2} \\ &\quad - \frac{dz}{z}\left(\frac{r_1}{\tan^2\phi_1}\right) - \beta\left(\frac{r_1^2}{\tan\phi_1} - \frac{r_2^2}{\tan\phi_2}\right) \end{aligned} \tag{2.42}$$

where c_1 is the radial gap between layers 1 and 2. This equation is developed in an identical manner for each of the remaining layers of the pipe.

Equilibrium equations for the pipe are also developed, setting torsional and axial loads to zero:

$$\frac{\pi r_1^3 \Delta p_1}{\tan\phi_1} + \frac{\pi r_2^3 \Delta p_2}{\tan\phi_2} + \frac{\pi r_3^3 \Delta p_3}{\tan\phi_3} + \frac{\pi r_4^2 (p - \Delta p_1 - \Delta p_2 - \Delta p_3)}{\tan\phi_4} = 0. \tag{2.43}$$

$$p \pi r^2 - \frac{2\pi r_1^2 \Delta p_1}{\tan^2\phi_1} - \frac{2\pi r_2^2 \Delta p_2}{\tan^2\phi_2} - \frac{2\pi r_3^2 \Delta p_3}{\tan^2\phi_2} - \frac{2\pi r_4^2 (p - \Delta p_1 - \Delta p_2 - \Delta p_3}{\tan^2\phi_4} = 0. \tag{2.44}$$

Using an iterative method to solve these compatibility and equilibrium equations, the 'performance' of the pipe can be determined on the basis of axial elongation and rotation. This is significant when knowledge of the behaviour of the pipe under service conditions is required.

Another output of the above solution is the pressure drop through each layer. Although not an output for pipe performance, the pressure drop through a layer is significant when the secondary stresses are determined. Assumed to be constant within each layer for the global model, in reality, the pressure drops vary throughout the layer and cause stress gradients in the composite strips.

The above equations can also be used to determine the absolute radial displacement of each layer for an unrestrained pipe. This value is used later in this study as one of the boundary conditions for the finite element model used. For a restrained pipe, the displacements θ and dz/z are set to zero, and the torque T_T and axial load F_T needed for equilibrium are then calculated. Laboratory tests of bent pipe are modelled as torsionally restrained and axially unrestrained pipes.

2.6 Inherent Limitations to the Global Model

It should be noted that there are a number of limitations to the models defined thus far. The major limitation, with regards to secondary stresses, is that neither the single radius or multiple radius model models defines how many composite and elastomeric strips are incorporated into each layer. Thus the width of each composite and elastomeric strip, values important for later determination of secondary stresses, are also not defined. The required number of strips is determined by manufacturing constraints, and analysis of secondary stresses, using the results generated in this thesis.

Also, non-uniformity of strip stress and contact pressures will be shown to cause secondary bending of the composite strips. These two factors are not considered in the global model.

Notwithstanding the above limitations of the global model, it has been shown through testing to effectively model the elongation and rotation of the pipe when subjected to internal pressure.

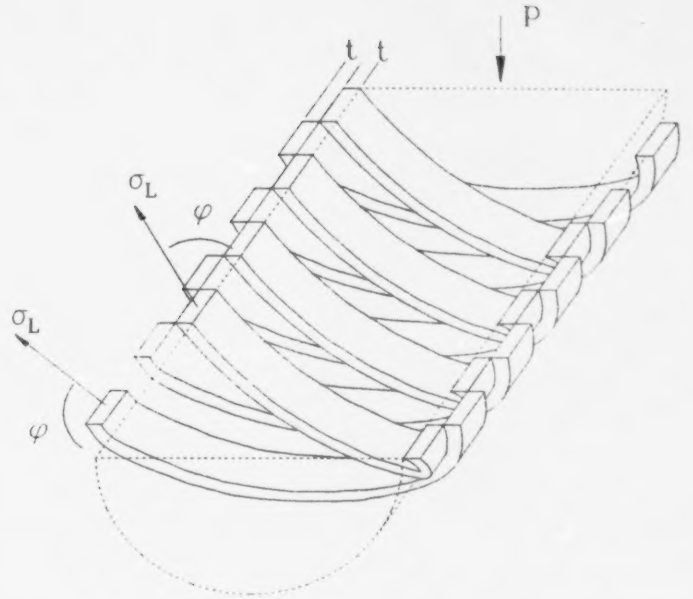

Figure 2.1 Radial Equilibrium of Hoop and Helix Structures

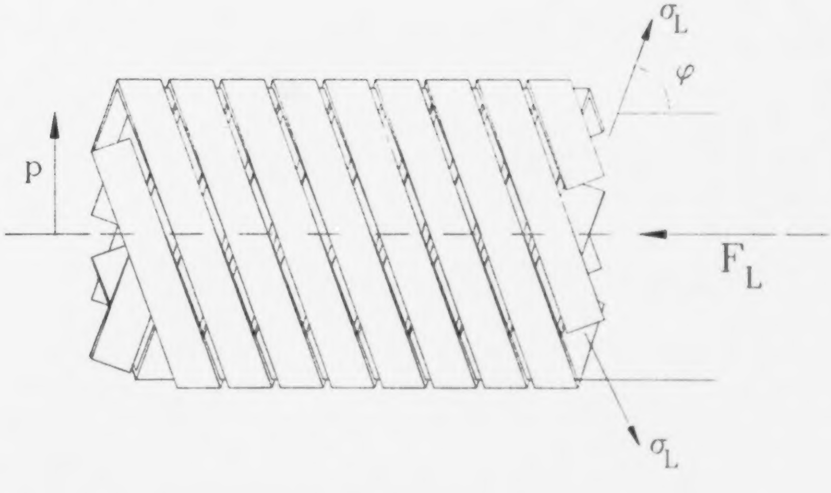

Figure 2.2 Axial Equilibrium of Hoop and Helix Structures

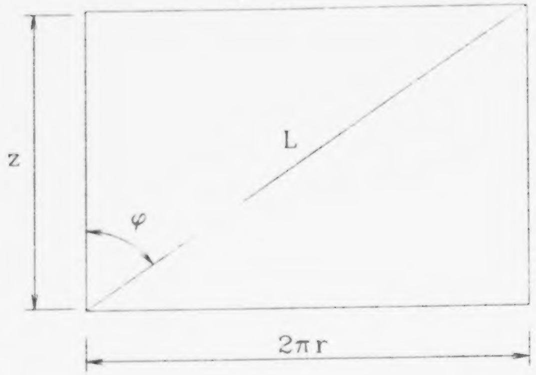

Figure 2.3 One Pitch of Pipe Mapped onto a Plane

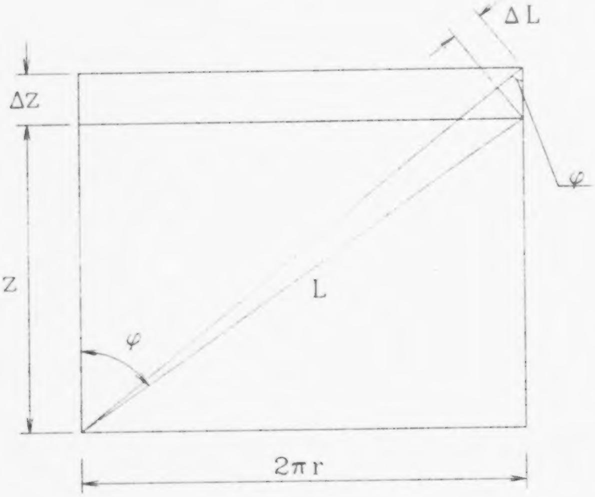

Figure 2.4 Axial and Radial Deflections

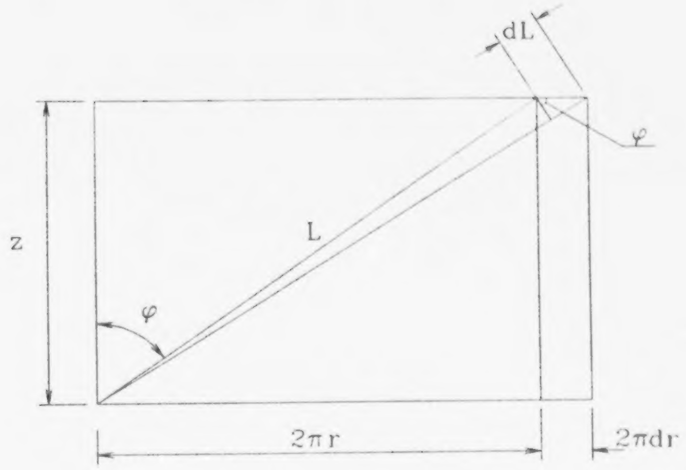

Figure 2.5 Circumferential and Radial Deflections

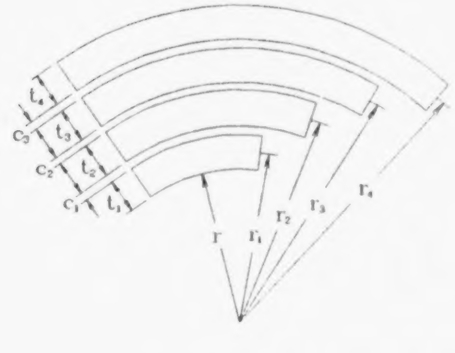

Figure 2.6 Schematic of Multiple Radius Model

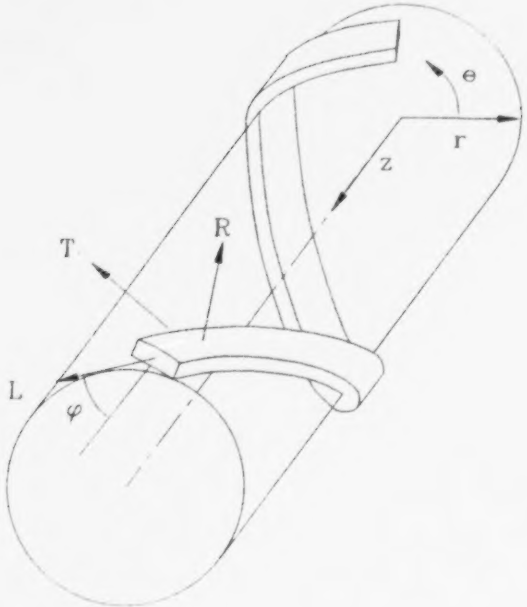

Figure 2.7 Composite Strip Coordinate System

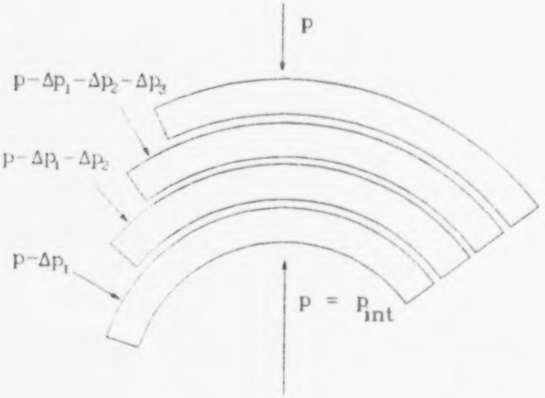

Figure 2.8 Schematic of Contact Pressures

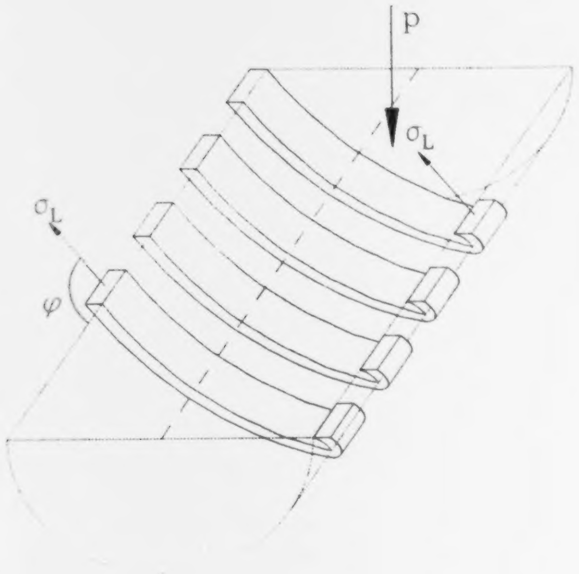

Figure 2.9 Radial Equilibrium of One Layer

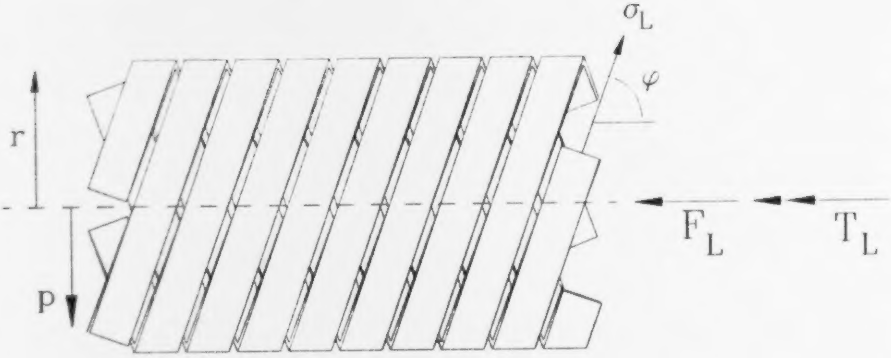

Figure 2.10 Axial and Rotational Equilibrium in One Layer

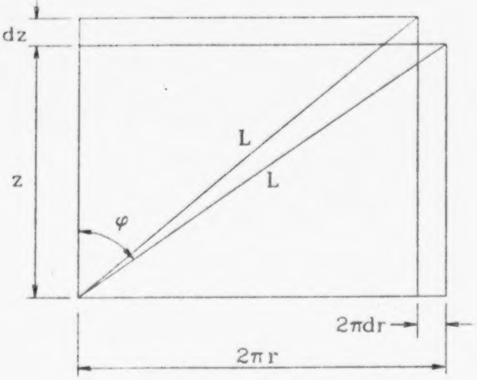

Figure 2.11 Axial Growth and Radial Deflection

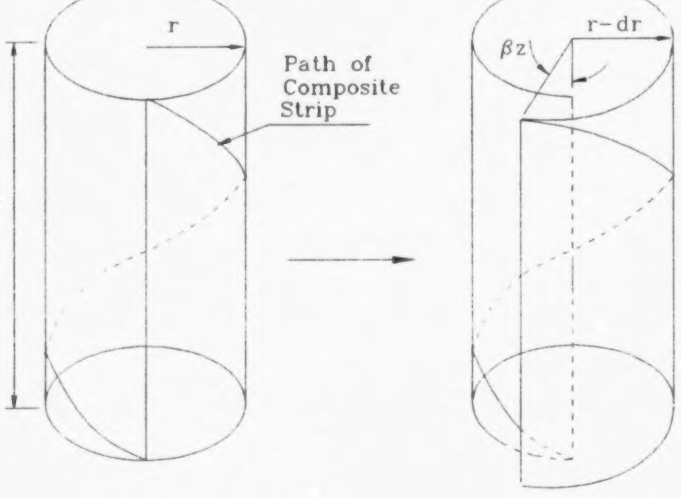

Figure 2.12 Rotation and Radial Deflection

CHAPTER 3

SECONDARY STRESSES

3.1 Description of Secondary Stresses

3.1.1 Introduction

As has been explained in the previous chapter, the global models deal simplistically with the stresses caused by internal pressure. Consequently, when irregularities in contact pressures caused by the presence of nonstructural components within each layer are taken into account, it is found that additional stresses are induced by bending. These are referred to as secondary stresses. These include transverse tensile and shear stresses, stresses for which the unidirectionally reinforced material is not ideally suited.

Experimental evidence of secondary stresses was found during high pressure burst tests. Upon examination of burst specimens, it was found that the composite strips in the innermost layer near the failure site suffered severe longitudinal cracking and cross-fibre shearing. These observations indicated secondary loading of the composite strips not accounted for by the global model. The causes of these secondary effects can be understood by a thorough examination of the innermost layer itself.

3.1.2 Inner Hoop Layer

Given that the elastomeric strips and the liner are low modulus and non-structural, it is essential that there be no path from the pressurized fluid to the exterior of the pipe consisting only of elastomer and liner. That is, there must be an overlapping mechanism by which the liner and elastomeric strips are completely contained by composite strips. This mechanism has been introduced into the innermost layer. Consider Figure 3.1, a schematic of the inner and outer hoop. Note that the elastomeric strips have not been included, leaving empty regions between the composite strips. It can been seen that the inner most layer has been separated into two interlocking layers and that there is no radial path through the layer consisting only of elastomeric strips. In this thesis, the two individual layers of the inner hoop are designated layer 1 and layer 2. The protuberance of the 'T'-strip serves to retain the position of the strips relative to each other when bending of the pipe occurs.

3.1.3 Observations and Causes of Secondary Stresses

As mentioned above, several observations were made upon completion of burst testing of pipe specimens. Upon comparison of several specimens, it was clear that there was a common mode of failure. There was significant damage to the inner hoop (layers 1 and 2) and a subsequent rupture path existed through the remainder of the structural layers. There was limited damage to the outer hoop, while there was only a shifting of elastomers in the helix layers. Before failure, strain gauge data indicated that the inner hoop structure experienced the highest levels of strain of all the layers. Visual analysis substantiated these readings.

Though some details of the inner hoop failures differed between specimens, there was one common factor. All failures appeared to involve, to some degree, bending and shearing of composite strips into the regions occupied by elastomer above them. This indicated loss of radial support of elastomeric strips that had been pushed out of position, requiring the composite strips to bridge the gap left by the elastomer. This occurred in the hoop structure wherever an elastomeric strip crossed a composite strip. This region was generically referred to as a bridge region. This behaviour was observed to occur most frequently in the inner hoop structure, to a limited degree in the outer hoop, and not at all in the helix layers.

3.1.4 Bridge Regions

There are two distinct bridge regions within the hoop structure. Both are apparent from Figure 3.1. Given internal pressure, layer 1 strips will be forced into the region occupied by the elastomer above them and will experience transverse bending and shear. For the purpose of this thesis, it is assumed that the elastomeric strips provide no radial support to the strips beneath them. This region is referred to as the longitudinal-bridge, as the bridge follows the longitudinal axis of the strip.

However, the constraints of the outer hoop also affect the inner hoop layers. As can be seen in Figure 3.1, the elastomeric strip of the outer hoop creates additional bridge regions into which the strips of layers 1 and 2 are forced. There is bending in this region and, as layers 1 and 2 are not orthogonal, additional out-of-plane bending and shear occurs. These regions are referred to as cross-bridges because the elastomer crosses over the composite strip at some angle.

The following study will include a detailed analysis of these two bridge regions.

3.2 Critical Stress Regions

3.2.1 Introduction

Analysis of the secondary stresses must take into account the behaviour of all of the strips involved. As stated above, the most significant secondary loading occurs within layers 1 and 2. Thus this investigation will include these strips of the inner hoop structure, with the effects of the outer layers accounted for by the use of appropriate boundary conditions.

3.2.2 Longitudinal Bridge

Consider the longitudinal-bridge affecting the layer 1 strips. In addition to the longitudinal stresses induced by internal pressure, the strip experiences bending around the longitudinal axis. This introduces transverse-tensile stresses at the top of the strip and transverse-compressive at the bottom. Because of the radial constraints of the layer 2 strips, shear also occurs along the bridge. Thus the strip experiences transverse-tensile stress and shear stresses, both of which depend largely on the strength of the matrix material in a unidirectional material.

3.2.3 Cross Bridge

Next consider the cross bridge, with the greatest effect experienced in the strips of layer 2. Under internal pressure, the inner hoop 2 strip, in addition to experiencing longitudinal stress, expands into the elastomeric regions of the outer hoop. This bending results in additional longitudinal tensile and shear stresses.

The analysis of the inner hoop 2 cross bridges is complicated by the fact that the strips may not be subjected to a uniform internal pressure. The composite and elastomeric strips of layer 1 transfer the pressure to layer 2 in different ways. In contrast to the elastomer of the outer layers, the elastomer of layer 1 is fully contained by the composite strips of layers 1 and 2 and simply transmits the internal pressure. The composite strips of layer 1, however, are stressed longitudinally and therefore transfer a lower pressure to the next layer. These two effects result in non-uniform longitudinal stress distribution and secondary stresses in the layer 2 strips. This non-uniformity must be accounted for by the use of appropriate boundary conditions for the analysis.

3.3 Modelling of Critical Stress Regions

3.3.1 Introduction

It is clear that an extremely complex phenomenon is occurring. The unidirectional material experiences secondary loading for which it is not suited. In order to understand the effects and possible solutions to this phenomenon, and as it is not known which of the bridge regions experiences the greatest stresses, the two bridge regions within the inner hoop are considered.

Given the complexities of the system, it was decided to use finite element methods to model the bridge regions. As the ANSYS finite element package had the capability to use composite materials and was readily available, it was deemed suitable for the purposes of the following analysis.

A finite element model of each of the two bridge regions has been constructed. Geometric complexity and limited computer resources prevented a more encompassing model.

3.3.2 Helical Approximation

In order to simplify modelling of the structure, the helical geometry of the composite strips has been approximated by a purely cylindrical model, with an effective radius taking into account the helical angle. However, the radius of the helical strips at any point on their path is much larger than the radius of the pipe. The effective strip radius r_s is related to the true pipe radius r_o and the wrap angle ϕ through the equation

$$r_s = \frac{r_o}{\sin^2\phi} \tag{3.1}$$

Development of this equation is described in Appendix 1. This effective radius, along with the original layer thicknesses and strip dimensions is used to determine the geometry of the model in a purely cylindrical orientation.

The only difference between the helical and cylindrical models of a composite strip is the slight twist that the cylindrical model does not account for. However, the relationship between any two layers is not changed by making this assumption, and the twist is thus neglected for this study.

3.3.3 Material Properties

Characterization of the material properties of the composite forms being used involves a combination of experimental testing and theoretical approximations. There were two composite forms used, both of which use a DOW Derekane vinyl ester resin as matrix and continuous E-glass fibre as the reinforcing material. Each composite strip combined a unidirectionally-reinforced core with layers of a woven fabric-reinforced composite at the top and bottom. The woven fabric consists of E-glass yarns woven together to produce a cloth-like tape. The glass is woven in a 0°-90° orientation and has roughly the same number of yarns per inch in both the longitudinal and transverse directions. The woven fabric was added to improve the transverse properties of the composite, and it will be shown that this fabric adds transverse tensile and shear strength without seriously diminishing the longitudinal strength of the composite strip.

Appendix 2 details the material properties used in the finite element model.

Non-linear material properties have not been considered to date. While the properties of unidirectional composite material are very linear in the direction of the fibres, transverse and shear loading may cause non-linear deformations in the material. However, consideration of non-linear properties involves a complex analytical or numerical solution. The goal of this study was thus limited to investigation in the elastic region.

3.3.4 Model Geometries

The element type used was a 8 node 3-D layered structural solid, numbered 46 of the ANSYS library. This element was chosen because it supported the Tsai-Wu failure criterion as well as anisotropic material properties. Though it also supported internal layering, several elements were instead built up to provide the required thickness.

The geometry of the models was carefully determined to provide the most realistic scenario while minimizing computational requirements. From observations, it was clear that massive structural failure was occurring in both layers 1 and 2. Thus, both of these layers were considered. While a model encompassing both layers was desirable, computational capacity limited this to a very simple model. A more effective solution was to generate two separate models, one for each layer. Performing this double analysis ensured that both layers of the inner hoop were adequately studied. The two models along with the displacement constraints, shown in Figures 3.2 and 3.3, have been designated Model L1 and Model L2 respectively, representing layers one and two.

Comparing the sizes of Models L1 and L2 and the comprehensive model highlights the computing requirements of both types of models. While Models L1 and L2 consisted of approximately 5000 elements, the comprehensive model included about 14000 elements.

3.3.5 Boundary Conditions

The boundary conditions were carefully selected to provide the most realistic loading scenario while minimizing computational requirements. For loading and constraint determination, an internal pressure of 7000 psi was utilized. This represented a typical burst pressure for pipe specimens previously tested.

Some of the boundary conditions applied to the two models were generated through use of a comprehensive finite element model encompassing both layers of the inner hoop. This model was used to determine the pattern of contact pressures acting between layers 1 and 2. The comprehensive model was not used extensively, as use of the facilities required to complete the large analysis was very limited.

The comprehensive model generated about 40000 degrees of freedom. The two smaller models generated only about 17000 degrees of freedom, a significant reduction in the computing resources required.

The contact pressures at the contact surface, determined with this comprehensive model were then approximated by pressure gradients and applied to the contact surface of Model L2. Appendix 3 details the process by which the applied pressure gradients were determined.

3.3.5.i *Model L2*

The circumferential and axial constraints were identical for the models of both layers. Circumferential constraints were applied to both ends of all strips, inducing a longitudinal stress in the fibre direction as radial expansion occurs. Axial constraints were applied to two nodes of the central strip. The locations of these two nodes were selected as having low displacement in the axial direction, so as to minimize stress concentrations about those points. The displacement constraints for Model L2 are as shown in Figure 3.2.

The key to modelling the bridge regions was the development of the radial constraints. While applying a nominal radial displacement to induce the correct longitudinal stress, variations in radial displacement must be permitted in order to simulate the deformations occurring at the bridges.

The radial constraints for Model L2 consisted of a fixed radial displacement constraint applied to the outer surface of layer 2. This constraint simulated the radial displacement of the outer hoop at a given internal pressure, and was determined through use of the global model. For an internal pressure of 7000 psi, a nominal longitudinal stress of 43160 psi was determined by the global model to be experienced in the strip. This was related to a fixed radial displacement through

$$dr = \frac{\sigma_L r_{2o}}{E_L}$$

where r_{2o} was the radius at the outer surface of layer 2.

It was assumed that the elastomer of the outer hoop provides no radial support; the radial constraints were applied to inner hoop 2 in the region of outer hoop composite only, with no constraints applied in the region of outer hoop elastomer. Because the outer hoop crosses the inner hoop at some angle, this region of radial constraint was set at the appropriate angle between these two layers in an actual pipe. In order to maintain equilibrium, the circumferential ends of the composite strips were also formed at this angle.

Internal pressure was applied to Model L2 in two ways. Where internal pressure acted on this layer directly, a value of 7000 psi was applied. This included the inner surface as well as the surface overtop of the layer 1 elastomer, where it was assumed that the elastomer, being completely contained, simply transmits radial pressure to the composite above it. Where layer 1 contacted layer 2, a pressure gradient was applied which was determined through limited use of the comprehensive model as noted above.

3.3.5.ii *Model L1*

The radial constraints were determined in a different manner for Model L1. Figure 3.3 shows the displacement constraints applied to Model L1. Because the effects of the longitudinal bridge and the cross bridge are cumulative as they act on inner hoop 1, a uniform radial displacement field cannot be applied to Model L1 as it was to Model L2. Some allowance must be given to the radial expansion of layer 1 into the cross bridge region. In order to apply the appropriate displacement field at the contact surface between layers 1 and 2, pressure gradients were applied to the outer surface instead of radial displacement constraints. The pressure gradients have been manipulated to give the contact surface of Model L1 a displacement field identical to that of Model L2. Appendix 2 details the development of the displacement fields.

The internal pressure of 7000 psi applied to Model L1 was applied to the inner surface.

3.3.6 Failure Criteria

In order to compare the effects of material and geometric variations of the model, a number of possible failure criteria are available. In this study, two such criteria were employed. Appendix 4 details the development of the two failure criteria used. The Maximum Stress Theory (Nahas, 1986), by considering the component stresses, indicates the dominant mode of failure, but does not allow for interaction between the stresses and is thus not a reliable indicator of point of failure. The Tsai-Wu Criterion (Tsai and Wu, 1971) includes interaction between the stresses but does not indicate mode of failure. Both failure criteria will be used in the following analysis, as shown below.

The constants required for the Tsai-Wu Criterion include the material strengths as detailed in Appendix 3 along with interaction factors approximated as detailed in Appendix 4.

3.3.7 Mesh Refinement

Given the geometry, the material properties, the loads, and the boundary conditions, the appropriate mesh refinement was determined. This was accomplished for each of the two models by performing the analysis with three different meshes, each more refined than the last.

Appendix 5 details the process by which the final mesh density was determined for each model and shows the final mesh generated for each model.

3.4 Analysis

The goal of this study was to understand the nature of the stresses occurring within the composite strips and how small design changes affect the magnitudes of the stresses. When analyzing the results of the finite element model, both of the previously explained failure criteria were used.

The analysis consisted of three components.

First, a strip of each of layers 1 and 2 were modelled given typical design parameters. These two models were then compared to each other in order to determine the critical layer in future pipe design considerations.

Subsequently, several design parameters were altered slightly and the results were compared to the reference model. This allowed determination of the effects of small changes on component stresses.

Additionally, in order to determine the effectiveness of the transverse reinforcement, the layers of woven fabric were eliminated, creating completely unidirectional composite strips. These were also compared to the reference models.

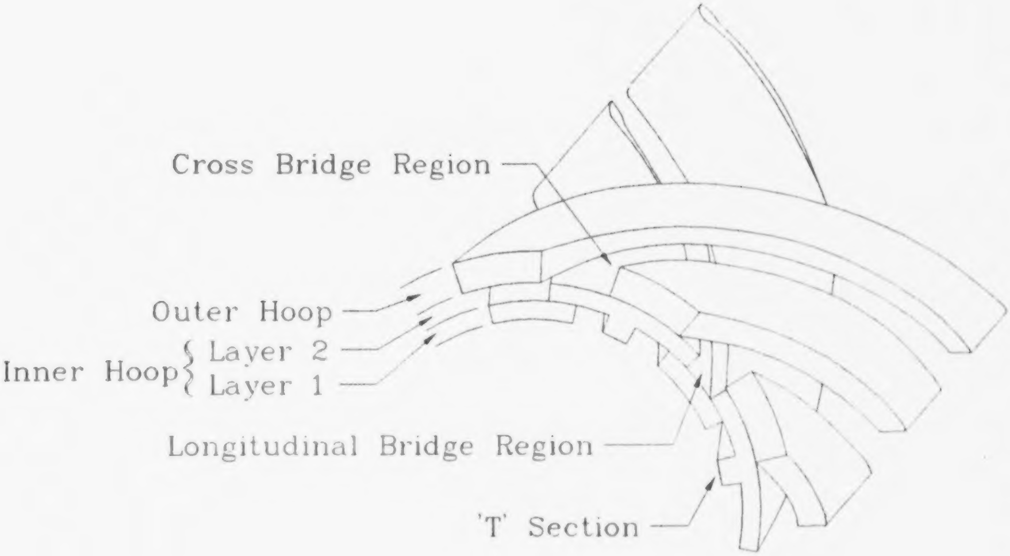

Figure 3.1 Schematic of Inner and Outer Hoop Layers

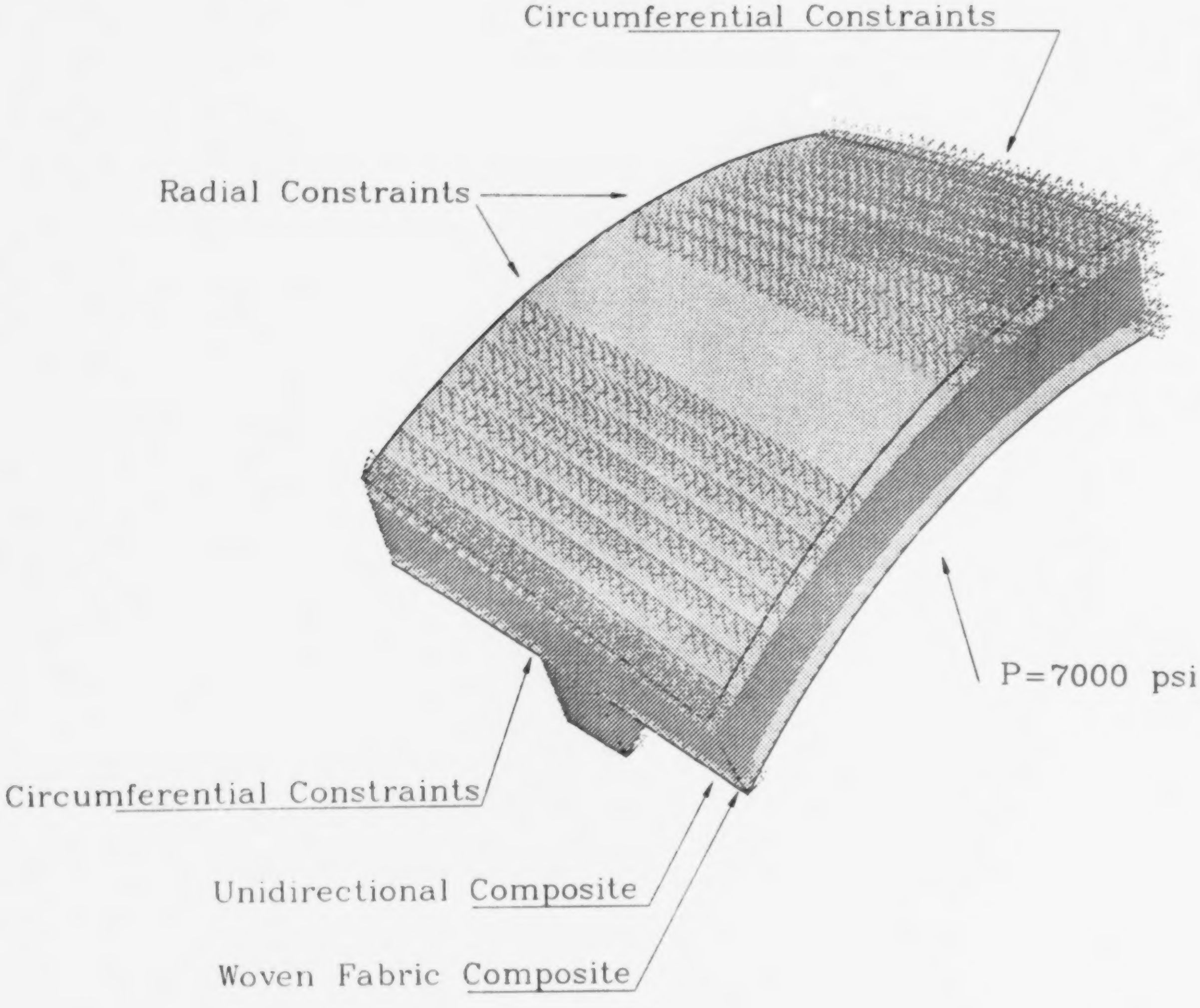

Figure 3.2 Sketch of Model L2, Showing Displacement Constraints

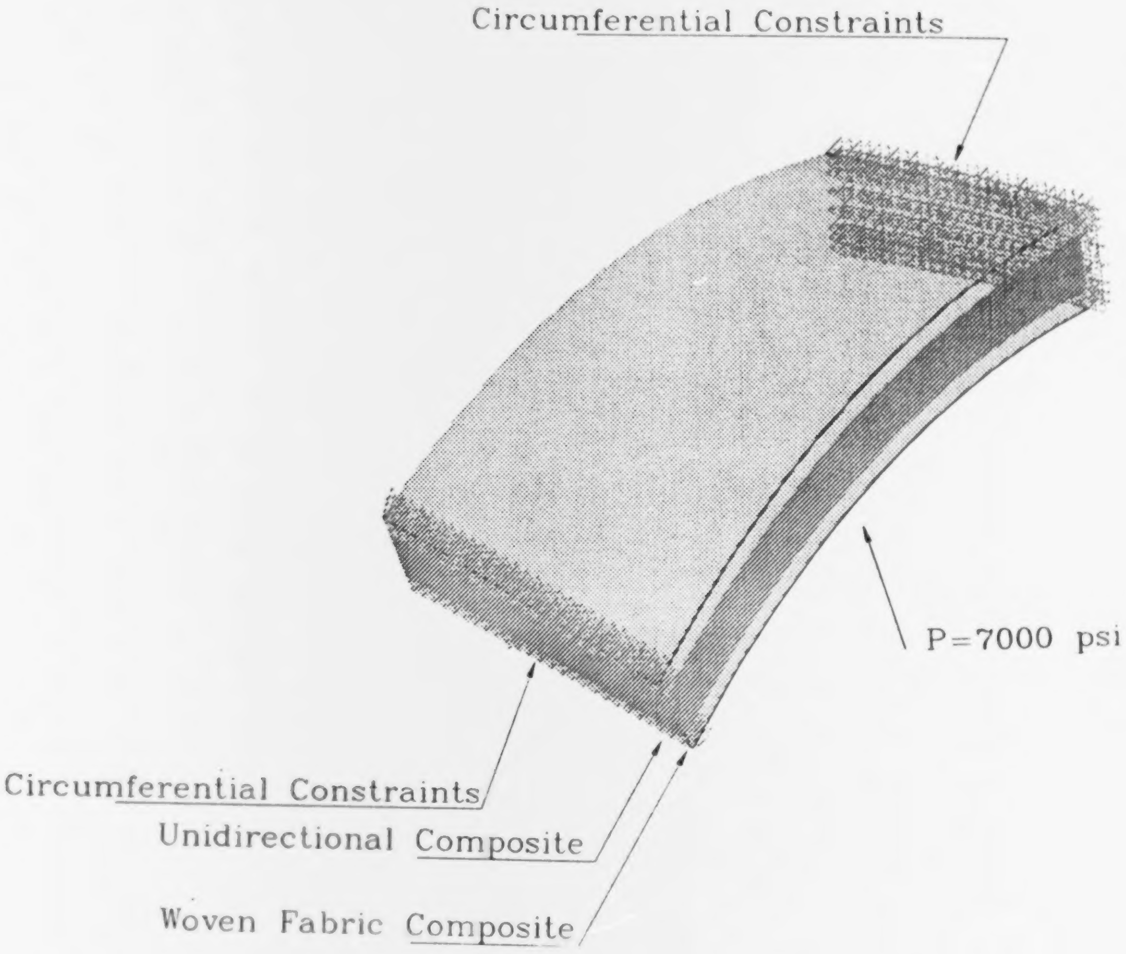

Figure 3.3 Sketch of Model L1, Showing Displacement Constraints

CHAPTER 4
RESULTS

4.1 Introduction

Two critical stress regions were modelled. Based on a typical pipe design, the initial analysis details the locations and nature of the stresses in each bridge region developed under internal pressure, and shows the strengths and weaknesses of the present design with regards to these stresses. Output of the finite element analysis in the form of stress distribution plots are included with this section to clarify the explanations.

Given this analysis, slight parametric variations were then introduced in order to determine the effects of variations of the critical variables on the composite stresses. The most significant design variables included the width of the longitudinal bridge (width of layer 2 elastomer), the width of the cross bridge (width of outer hoop elastomer), the percentage of woven fabric and the angle of the cross bridge. All of these parameters had the potential to significantly alter the stress states occurring in the bridge regions. Study of these parametric variations allowed greater understanding of the sensitivity of the design. Included with this section are graphs of component stresses as functions of the modified parameter.

Finally, in order to demonstrate the effectiveness of the woven fabric, both models L1 and L2 were analyzed with 100% unidirectional composite and compared with the reference model.

The analyses performed are summarized in Table 4.1.

As many of the companies for whom this project holds relevance are American, and who use imperical units more often than metric, the results of this thesis are presented in imperical units.

Table 4.1 Summary of Analysis

Model L1	Model L2
i. Reference design	i. Reference design
ii. Cross bridge width	ii. Cross bridge width
iii. Cross bridge angle	iii. Cross bridge angle
iv. Percentage of woven fabric	iv. Percentage of woven fabric
v. Longitudinal bridge width	
vi. 100% unidirectional composite	v. 100% unidirectional composite

The results of the above analyses are presented in terms of component stresses (averaged at the nodes) and Tsai-Wu parameters. Because nodal stress averaging is invalid at the boundaries between material types, the results are given separately for the unidirectional and woven fabric composites. Model L2 results for the unidirectional material are further subdivided into the unidirectional 'core' of the main section of the strip, and the unidirectional 'T' section. These two regions experience different levels of stress and are considered separately.

In terms of both failure criteria, failure of the pipe is considered to have occurred when any single component (unidirectional or woven fabric layers) exceeds the respective criteria. Though the pipe may still be able to withstand internal pressure, the long term capacity may be seriously damaged at this point.

4.2 Analysis of Reference Model

4.2.1 Model L1

Layer 1 experienced significant radial expansion into the longitudinal bridge region and subsequent bending about the longitudinal axis of the pipe. This deformation can be understood by consideration of Figure 3.1.

As there was increased radial expansion in this region, the longitudinal stress was higher than nominal at the top surface. Figures 4.1 and 4.2. display the longitudinal stress distribution for the unidirectional and woven fabric composites respectively. The difference between the minimum and maximum stresses should be noted.

Bending of the strip about the longitudinal axis caused high transverse tensile stresses at the top and high transverse compressive stresses at the bottom of the strip, as was to be expected with this deformation. Figures 4.3 and 4.4 show the stress distribution for the two composites. As the transverse strength of the unidirectional material is only 4,870 psi, it can be seen that the transverse strength has been exceeded at this pressure.

The radial stresses acting at the edges of the longitudinal bridge were also significant. Figures 4.5 and 4.6 show the distribution of radial stress, showing that in some places, these values are significantly higher than the internal pressure.

Shear stress S_{TR} was highest along the edges of the bridge as shown in Figures 4.7 and 4.8. Given shear strengths of 9,700 psi and 20,100 psi for the unidirectional and woven fabric respectively, these shear stresses were significant in the unidirectional material.

The two additional shear stresses S_{LR} and S_{LT} were both lower than 500 psi and were neglected in the study of Model L1. This was not unexpected, as there is no loading to cause shear in these planes.

The Tsai-Wu parameters for the two materials are shown in Figures 4.9 and 4.10. As expected considering the component stresses, the highest value for the unidirectional material was in the centre of the bridge, where bending caused high transverse tensile stresses. In the woven fabric, which had high transverse strength, the highest value is found at the edges of the bridge, where the radial stress and shear stress S_{TR} were both high.

Because the normal compressive material strengths are much higher than the tensile strengths, compressive stresses were not considered significant for most cases, apart from radial stresses.

The maximum stresses and Tsai-Wu parameters for Model L1 are summarized in Table 4.2, along with the component strengths.

Table 4.2 Maximum Stresses and Tsai-Wu Failure Parameters for Model L1

Stress Component	Maximum Stresses (psi)		Material Strengths (psi)	
	Unidirectional	Woven Fabric	Unidirectional	Woven Fabric
Longitudinal Stress	57789	26485	125000	36000
Transverse Stress	5306	15829	4870	36000
Radial Stress	-10312	-14000	-18700	-18700
Shear Stress STR	4175	4225	9700	20100
Tsai Wu Parameter	.882	.838	1	1

4.2.2 Model L2

In contrast to Model L1, the composite strip of Model L2 experienced bending about the transverse axis, accompanied by radial expansion into the cross bridge region. This manifested itself in higher longitudinal and radial normal stresses and higher shear stress S_{LR}.

The distribution of longitudinal stress in Model L2 is shown in Figures 4.11 to 4.13. The longitudinal stress increased in the region of the cross bridge for all three components as shown. Considering Figures 4.11 and 4.12, it can be seen that there was a significant difference in the longitudinal stress through the thickness of the strip. This indicates that some error may be introduced into the global model, which assumes uniform stress through the thickness of the strip, in accordance with thin cylinder theory.

The transverse stresses within Model L2 were not as significant as those in Model L1. Figures 4.14 to 4.16 display the transverse stresses in each component. Figure 4.16 is viewed from the bottom of the strip to show the high stresses developed at the inner radius.

Once again, there were also high radial stresses at the edge of the cross bridge. Figures 4.17 to 4.19 show the stress distribution.

Because of the orientation of the cross bridge, the shear stress S_{LR} was much higher in Model L2 than Model L1. The high shear stresses were found at the edges of the bridge, as can be seen in Figures 4.20 to 4.22.

The shear stress S_{TR}, though much lower than in Model L1, was not insignificant. The stress distribution is shown in Figures 4.23 to 4.25.

The Tsai-Wu failure parameters are shown in Figures 4.26 to 4.29. The bottom layer of the woven fabric has been displayed independently in Figure 4.29, to show the high values at the edge of the strip.

The maximum stresses and Tsai-Wu parameters experienced in Model L2 are summarized in Table 4.3, along with the appropriate material strengths.

Table 4.3 Maximum Stresses and Tsai-Wu Failure Parameters for Model L2

Stress Component	Maximum Stresses (psi)			Material Strengths (psi)	
	Unidirectional		Woven Fabric	Unidirectional	Woven Fabric
	Core	'T'			
Longitudinal Stress	47128	52880	28419	125000	36000
Transverse Stress	1760	1983	5057	4870	36000
Radial Stress	-8326	-6900	-11586	-18700	-18700
Shear Stress S_{LR}	1863	2056	1917	20100	20100
Shear Stress S_{TR}	1390	1106	1650	9700	20100
Tsai Wu Parameter	.211	.297	.784	1	1

4.2.3 Discussion

It can be seen that Model L1 experienced higher stresses than Model L2. This is especially noticeable in the transverse stress and the shear stress S_{TR}. This was due to the transverse bending of layer 1 that occurred in the longitudinal bridge region, which was to be expected.

It should be noted that while the maximum transverse stress in the unidirectional composite in Model L1 reached 5306 psi and the transverse strength for this material was only 4870 psi, the Tsai-Wu failure parameters for this region was only 0.882. This low value is due to finite element discretization. While the nodal stresses are extrapolated to the surface of the element, the Tsai-Wu parameters are determined from the stresses at the integration points of the element. When bending of the element occurs, introducing tensile stress at the top and compressive stresses at the bottom, the stress at the centre of the element is significantly reduced from that at the surfaces. Thus the Tsai-Wu criteria gives an artificially low value. Despite this discrepancy, the Tsai-Wu criteria can be used to compare the results between similar models, given the parametric analysis.

The extremely high value of the transverse stress in the unidirectional composite revealed a discrepancy between the finite element model and experimental work. The finite element model predicted failure before 7000 psi, while several pipe specimens subjected to short term pressure tests burst at pressures greater than 7000 psi. There are two explanations for this difference. First of all, the transverse stress in the unidirectional composite would cause transverse failure in the unidirectional material, which does not necessitate failure of the strip. Given the shear strength of the woven fabric, the structure could withstand a greater load before failure.

Another reason for the difference is due to the assumption that the elastomeric strips forming the bridges provide no radial support. In reality, as contact pressure between layers is increased, the elastomeric material is effectively confined, providing limited radial support for short term loading, increasing the short term pressure capacity. Essentially, the bridge deformations would not be as severe as if there were no elastomer present. However, for long term situations, this radial support may not be dependable, as the elastomer may creep under load and eventually lose pressure-transmitting capability.

4.3 Cross Bridge Width

The width of the cross bridge is a function of the width of the outer hoop elastomer. This dimension is determined through design and manufacturing limitations. A certain percentage of elastomeric material is required in each layer, roughly 20-30%, in order to maintain structural flexibility. The elastomeric strips should be narrow enough to prevent severe damage at the cross bridge sites but not so narrow as to cause instability during manufacture. Generally, strips that are narrower than they are thick are undesirable.

Because layer 2 was directly affected by the cross bridge, this layer is considered first.

4.3.1 Model L2

As was noted in section 4.2, layer 2 experienced radial expansion in the region of the cross bridge, causing high longitudinal stresses at the centre of the bridge, and high radial and shear stresses at the edges.

As was to be expected, increases in the width of the cross bridge exacerbated the problems of high stresses. This was noticeable mostly with shear stress S_{LR}, along the edges of the bridge. For the variations considered, a 40% change in cross bridge width caused close to a 100% increase in shear stress, as can be seen in Figure 4.30.

The longitudinal and transverse stresses increased only slightly as the cross bridge width increased, in both the unidirectional and woven fabric material, as shown in Figures 4.31 and 4.32. The radial stress, however, increased significantly in the woven fabric as can be seen in Figure 4.33. This high radial stress occurred at the edge of the bridge.

The shear stress S_{TR} also increased slightly as bridge width increased as seen in Figure 4.34. The end result can be seen in Figure 4.35 in which the Maximum Tsai-Wu parameter is plotted against cross bridge width. A 40% change in cross bridge width caused a roughly 40% increase in this value.

4.3.2 Model L1

Layer 1 strips are insulated from the severe effects of the cross bridge by layer 2. This resulted in negligible changes in all stresses when the cross bridge width was altered. The plot of Tsai-Wu criteria demonstrates this in Figure 4.36.

4.3.3 Discussion

Variations in cross bridge width had a greater impact on layer 2 than on layer 1. The increase in shear stress S_{LR} was the greatest factor, directly affecting the Tsai-Wu parameters. As would be expected, increasing the width of the cross bridge increased all the component stresses.

4.4 Cross Bridge Angle

The cross bridge angle is not a direct design variable, rather the result of the choices of wrap angle for the inner and outer hoop structures. The affect of the cross bridge angle was studied to determine the effect of angle changes on the shear stresses acting along the edge of the bridge. Once again, Model L2 is considered first.

4.4.1 Model L2

As cross bridge angle increased, approaching 90°, there was a general decrease in stress levels in layer 2.

The exception to this was the longitudinal stress in the woven fabric, which increased slightly, as can be seen in Figure 4.37. All other normal and shear stresses, shown in Figures 4.38 to 4.41, experienced small but noticeable decreases with increasing angle. The exception is the radial stress in the woven fabric which decreased dramatically as the angle increased.

Figure 4.42 shows the maximum Tsai-Wu parameters, which decreased the most in the woven fabric, about 20% as the angle increased 30°. The Tsai-Wu parameters in the other components experienced a less significant change.

4.4.2 Model L1

As with the effects of varying cross bridge width, changes in cross bridge angle caused only negligible differences in layer 1 stresses. Figure 4.43 shows the Maximum Tsai-Wu parameters for this parametric change, demonstrating minimal variation.

4.4.3 Discussion

As stated above, variations in cross bridge angle caused small changes only in layer 2. Layer 1 was not affected significantly by this parameter. It can be concluded that the parameter has little direct impact on the component stresses.

4.5 Percentage of Woven Fabric

The volume fraction of woven fabric was varied from 30 to 50% of the composite strip. The thicknesses at top and bottom were equal, and the total thickness of the strip was kept constant. The thickness of the fabric was varied, changing the thickness of the unidirectional layer.

4.5.1 Model L1

Increases in the amount of woven fabric did not greatly affect the longitudinal stresses in the unidirectional or the woven fabric composites, as can be seen in Figure 4.44. However, as more fabric was added, with higher transverse modulus, the transverse stress was greatly reduced in the unidirectional composite, and slightly increased in the woven fabric, as is shown in Figure 4.45.

The remaining stresses are not changed as significantly, as is shown in Figures 4.46 and 4.47, but given that the transverse stress in the unidirectional material is close to the strength of the material, any decreases in this stress clearly improves the performance of the composite strip, as shown with the maximum Tsai-Wu parameters in Figure 4.47.

4.5.2 Model L2

The effects of the percentage of woven fabric are not as significant in layer 2 as they are in layer 1. In general, there is a slight increase in most stresses as the amount of fabric increases. This is due to the reduced effective longitudinal modulus of the strip allowing greater longitudinal strain and greater expansion into the cross bridge region.

Figures 4.49 to 4.53 show the variations in stress as the amount of woven fabric changes. Figure 4.54 shows that there is little change in maximum Tsai-Wu parameter for this layer.

4.5.3 Discussion

It has been shown that a certain amount of woven fabric is critical in layer 1. High transverse and shear stresses demand a material with high transverse strength and shear strength S_{TR}, located at the top and bottom of the strip, and this can be achieved with woven fabric. By increasing the amount of woven fabric, the transverse stress in the unidirectional material is reduced, while increasing the stress in the woven fabric only slightly. However, this must be balanced with the fact that large amounts of woven fabric substantially reduce the longitudinal modulus of the strip, and may affect the elongation and rotation of the pipe.

Woven fabric is not as critical in layer 2 and in fact according to this study, causes greater cross bridge effects due to the reduced longitudinal modulus. Given that the unidirectional and woven fabric have similar shear strengths in plane LR, additional woven fabric will not increase the strength of layer 2 in the cross bridge region.

However, it must also be noted that the transverse stresses acting in the unidirectional material are not insignificant. As stress acting in this direction tends to cause matrix-related creep, some transverse reinforcement is still necessary.

4.6 Longitudinal Bridge

The width of the longitudinal bridge is a function of the width of the layer 2 elastomer. As with the outer hoop elastomer, this dimension is dictated by design and manufacturing considerations. An additional factor is the amount of overlap generated between layer 1 and 2 strips, which is dependent on the widths of the composite and elastomeric strips. As this dimension decreases, the possibility increases that bending of the pipe will lead to severe shifting of the strips relative to each other and loss of this overlap.

The width of the longitudinal bridge does not directly affect the secondary stresses in layer 2. Thus only Model L1 is considered in this study.

4.6.1 Model L1

As was to be expected, a wider longitudinal bridge allowed greater radial expansion, causing greater stresses. Figures 4.55 to 4.58 show that all significant stresses increased dramatically as the bridge width was increased. Once again, because of the low transverse strength of the unidirectional material, the changes in maximum Tsai-Wu parameters are most significant in the unidirectional material as is seen in Figure 4.59.

4.6.2 Discussion

As noted above, transverse stresses are critical in the unidirectional material, and as the bridge width was increased, these stresses became even more severe. It is clear when considering the Tsai-Wu values that any significant increase in longitudinal bridge width will cause problems related to transverse stresses in the unidirectional material. It should be noted that longitudinal cracking of the unidirectional material may not cause immediate failure. The presence of these cracks does not seriously affect the longitudinal strength of the material. However, once the transverse strength is exceeded, the possibility of further radial expansion is increased, which may lead to longitudinal failure.

4.7 Comparison with 100% Unidirectional Composite

In order to demonstrate the benefits of woven fabric in the composite, both Models L1 and L2 have been analyzed as completely unidirectional components.

4.7.1 Model L1

The woven fabric of layer 1 provided transverse and shear strength in the longitudinal bridge region. When this fabric was removed and replaced with unidirectional material, the stresses were not dramatically altered, but given the much lower transverse strengths of the unidirectional material (4870 psi as compared to 36000 psi), the maximum Tsai-Wu parameters were much higher for the completely unidirectional composite. The stresses in the two models were tabulated in Table 4.4. The data was divided into the 'core' material and the 'surface' material. The woven fabric was also included.

Table 4.4 Comparison of Reference Model with 100% Unidirectional Composite, Model L1

Stress Component	Unidirectional/ Woven Composite Stresses (psi)		100% Unidirectional Composite Stresses (psi)	
	Core	Surface	Core	Surface
Composite Type	Uni	Fabric	Uni	Uni
Longitudinal Stress	58406	26610	57589	57569
Transverse Stress	5275	15605	5249	11507
Radial Stress	- 10191	-13796	- 9105	- 11654
Shear Stress S_{TR}	4115	4173	3694	3176
Tsai-Wu Parameter	.877	.828	.868	2.653

4.7.2 Model L2

The introduction of woven fabric into layer 2 did not benefit the composite as it did in layer 1. In fact, with the reduced longitudinal modulus and greater radial expansion, the woven fabric reduces the short term effectiveness of the layer 2 composite strip. The stresses developed in the strip were compared with those of a completely unidirectional material and the results are tabulated in Table 4.5. The composite has been divided into the core of the main strip, the surface layers where woven fabric occurs in the unidirectional/fabric composite, and the unidirectional 'T'.

Table 4.5 Comparison of Reference Model with 100% Unidirectional Composite, Model L2

Stress Component	Stress in Unidirectional/ Woven Composite (psi)			Stress in Unidirectional Composite (psi)		
Location	Core	'T'	Surface	Core	'T'	Surface
Composite Type	Uni	Uni	Fabric	Uni	Uni	Uni
Longitudinal Stress	47128	52880	28419	46850	52299	48828
Transverse Stress	1763	1983	5057	1053	937	3177
Radial Stress	-8326	-6900	-11586	-8053	-6881	-9714
Shear Stress S_{LR}	1863	1917	1917	1503	1354	1593
Shear Stress S_{TR}	1390	1650	1650	1394	730	1398
Tsai-Wu Parameter	.211	.297	.784	.062	.070	.71

4.7.3 Discussion

It can be seen that for layer 1, removal of the transverse reinforcement would be catastrophic. The transverse loading was far too extreme for the 100% unidirectional composite. If woven fabric were removed, a significant reduction in the width of the longitudinal bridge would be required in order to reduce the transverse loading.

However, the woven fabric seems to worsen the situation of layer 2. As the secondary loading largely consists of increased longitudinal stress and shear stress S_{LR}, the woven fabric adds little by way of transverse strength and actually decreases the longitudinal strength and modulus of the composite. This would seem to indicate removal of the woven fabric is in order. However, one must consider the loading at the surface of the strip. With a transverse stress of almost 3200 psi, and a maximum Tsai-Wu parameter of 0.7, the long term transverse strength of the composite must be retained. Considering this, removal of the woven fabric may improve short term strength of the composite, but greatly reduce the long term capacity.

4.8 Experimental Results

Though experimentation was not a significant part of this thesis, prototype testing was performed simultaneously, with preliminary results from this study used for optimization. The following explains three successive prototype tests which demonstrate the effectiveness of the finite element analysis.

Initial finite element modelling determined that there were high transverse and shear stresses occurring at the top and bottom surfaces of Layer 1 in the longitudinal bridge region. This led to the reduction of bridge widths and the introduction of woven fabric into layer 1. Subsequent testing demonstrated the benefits of these improvements as is explained below.

Initial tests were performed on a pipe designated P1 with large bridge widths and purely unidirectional material. Designed with the global model to burst at 7000 psi internal pressure, it burst at 5000 psi internal pressure, at ambient temperature. A subsequent iteration P2 which reduced the bridge widths and introduced woven fabric into Layer 1 was designed to burst at 9000 psi internal pressure and burst at 8375 psi in a short term test at ambient temperature. This clearly demonstrated the benefits of these initial improvements. A later iteration P3 was designed for a lower short term pressure capacity of 7500 psi but higher long term capacity with additional fabric in Layer 2. Subjected to short term loading, this prototype burst at 7300 psi internal pressure, but the subsequent prototype contained pressure for over 1000 hours at 6300 psi. This demonstrated the long term high pressure capacity of the pipe. (Bouey and Freiheit, 1995)

It can be seen that improvements, based on finite element analysis and supplemented by visual analysis and documentation of failure modes, were able to significantly improve the pressure capacity of the pipe.

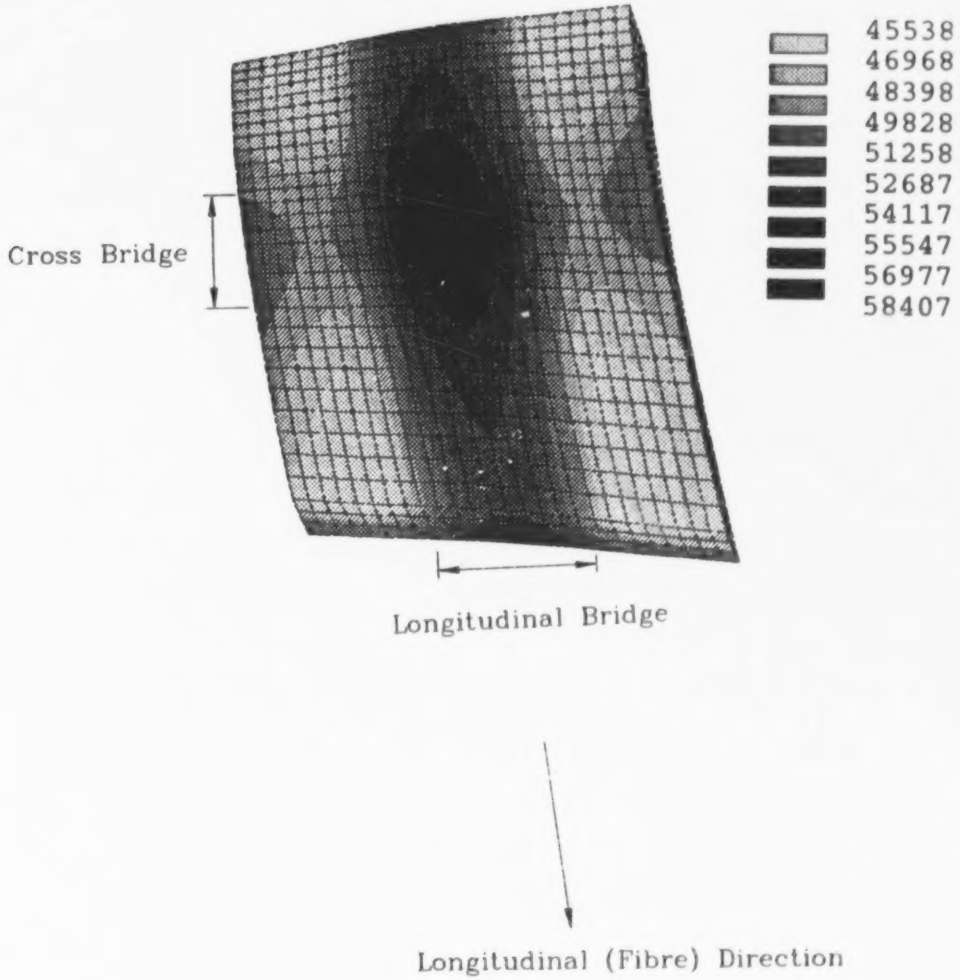

Figure 4.1 Longitudinal Stress in Unidirectional Composite (psi), Model L1, with Bridge Regions Identified

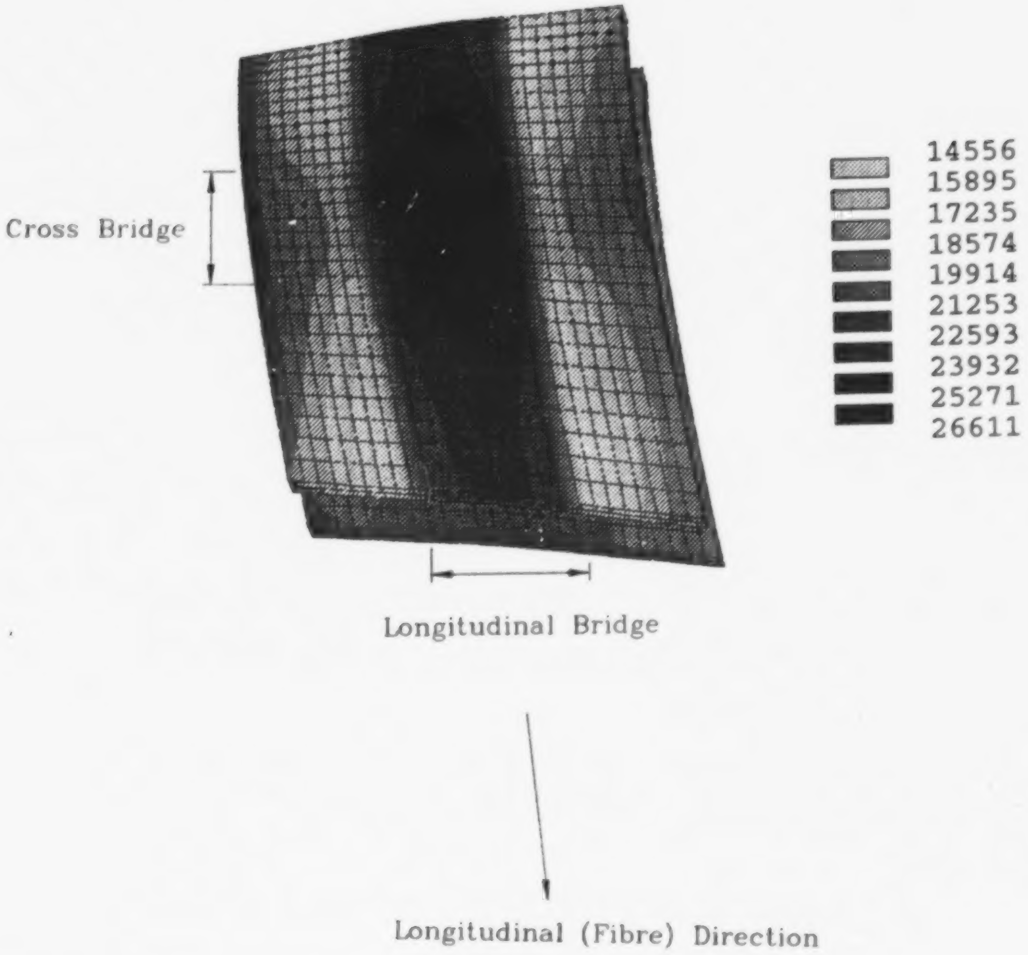

Figure 4.2 Longitudinal Stress in Woven Fabric Composite, Model L1, with Bridges Identified

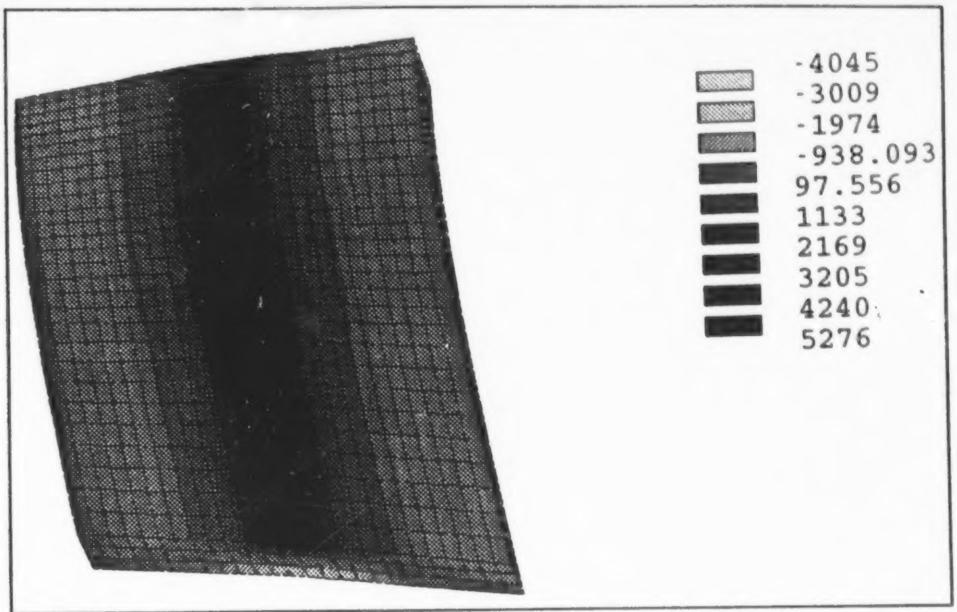

Figure 4.3 Transverse Stress in Unidirectional Composite (psi), Model L1

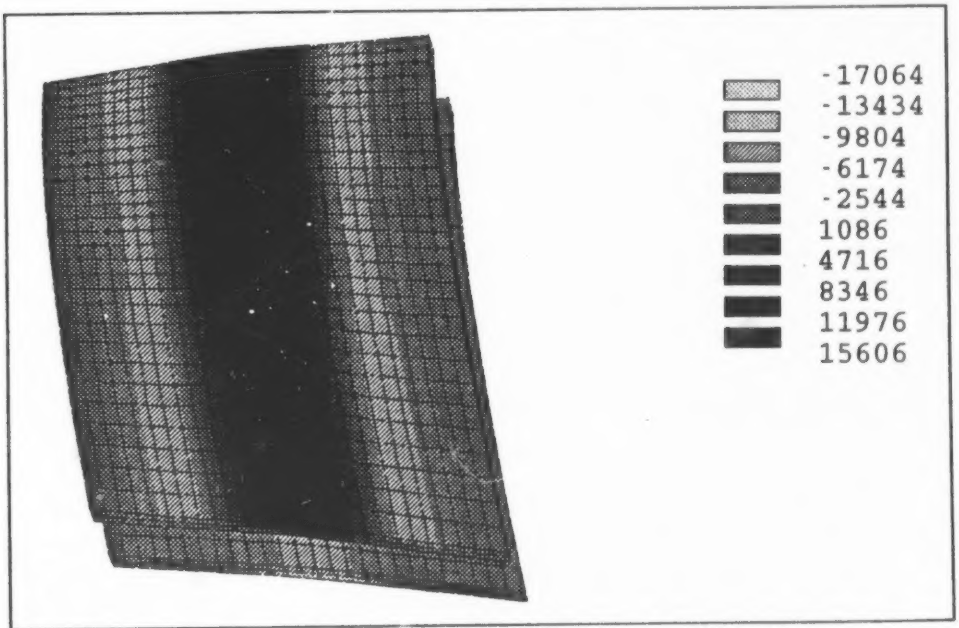

Figure 4.4 Transverse Stress in Woven Fabric Composite (psi), Model L1

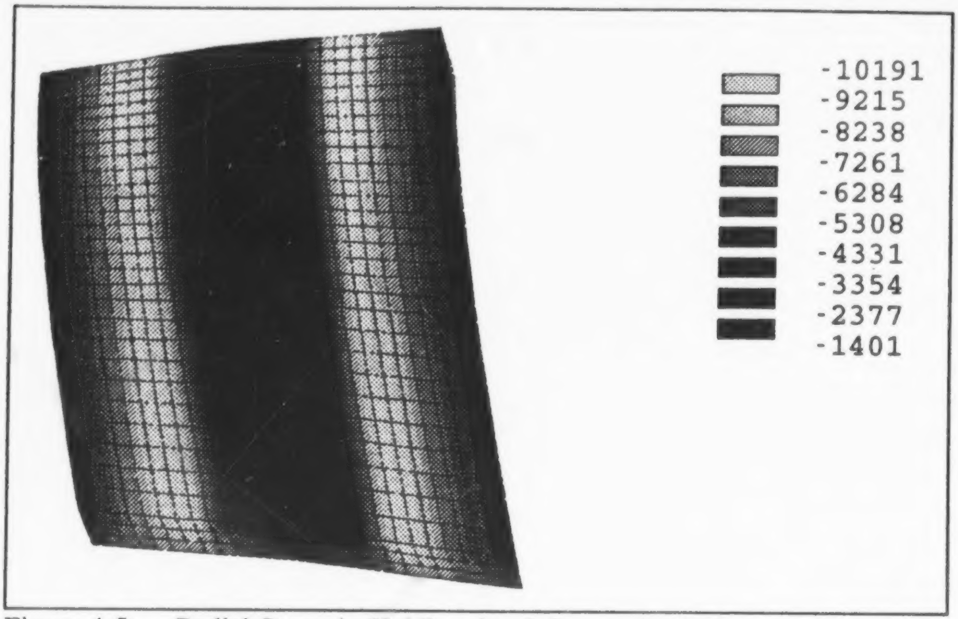

Figure 4.5 Radial Stress in Unidirectional Composite (psi), Model L1

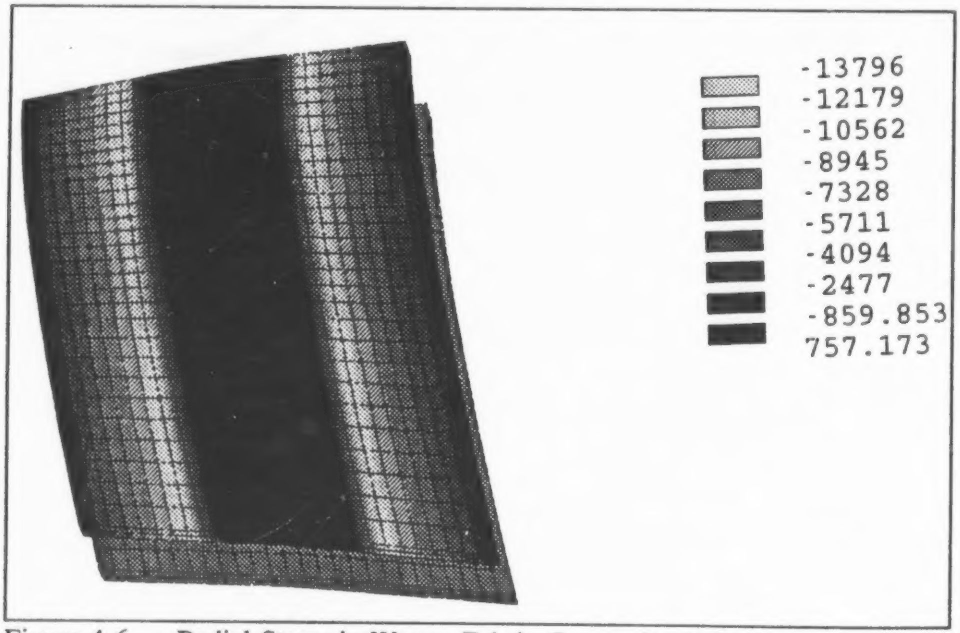

Figure 4.6 Radial Stress in Woven Fabric Composite (psi), Model L1

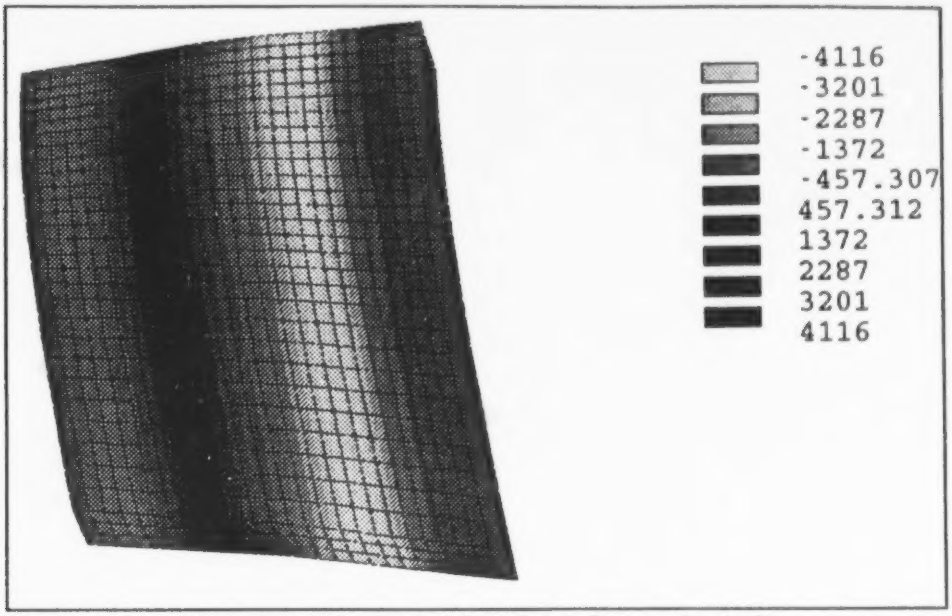

Figure 4.7 Shear Stress S_{TR} in Unidirectional Composite (psi), Model L1

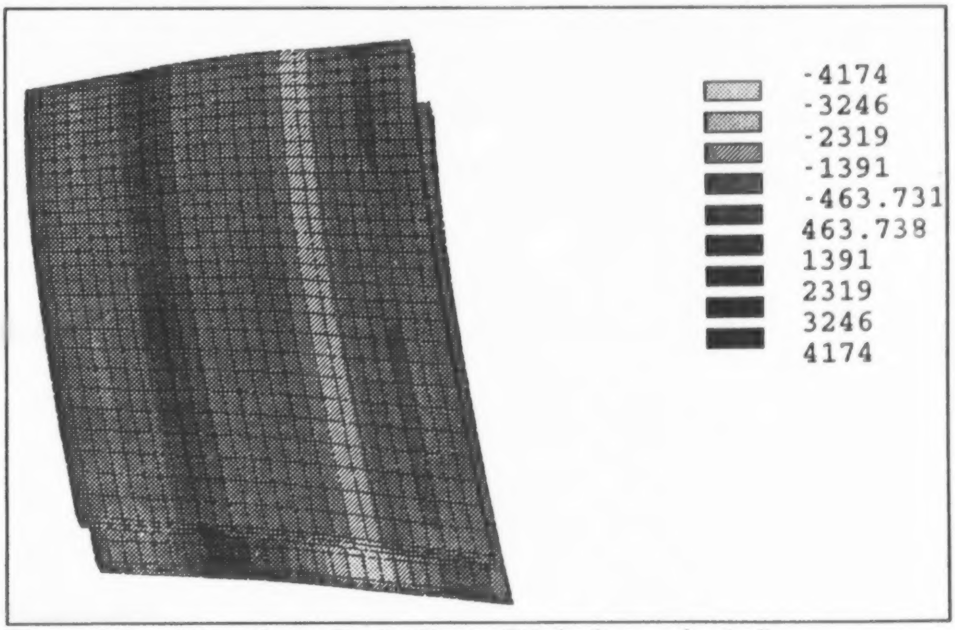

Figure 4.8 Shear Stress S_{TR} in Woven Fabric Composite (psi), Model L1

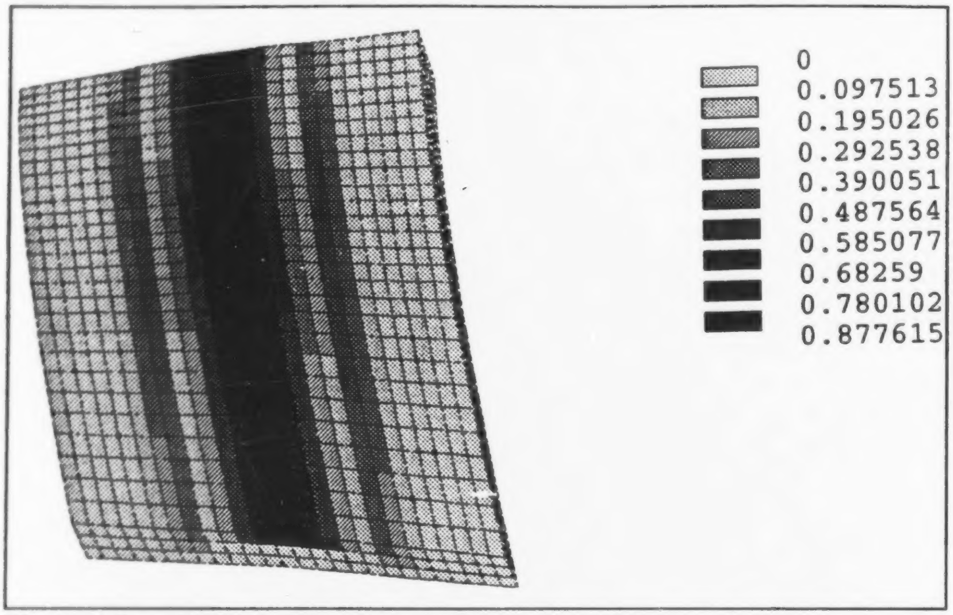

Figure 4.9 Tsai-Wu Parameters in Unidirectional Composite Model L1

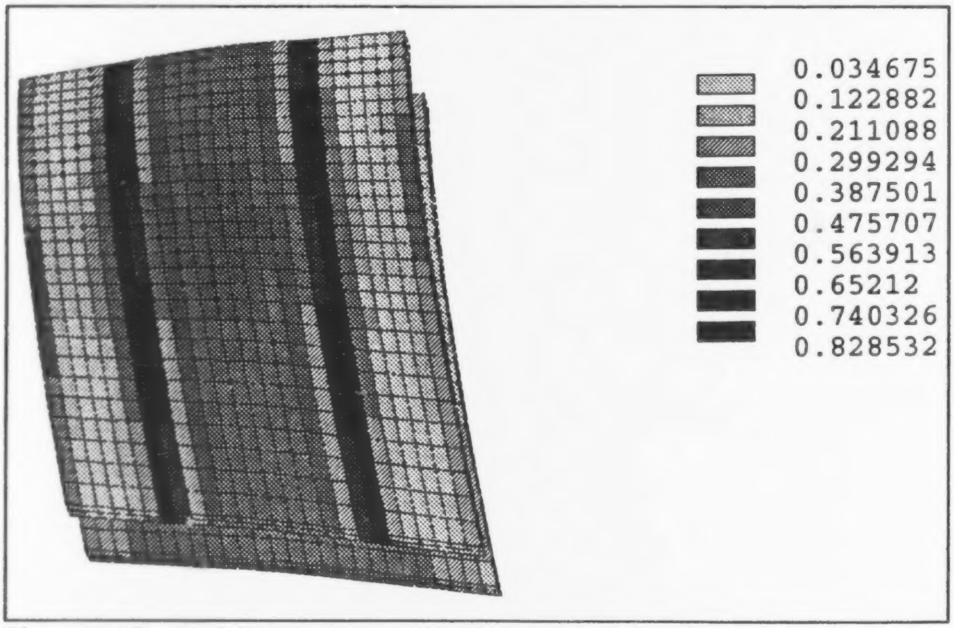

Figure 4.10 Tsai-Wu Parameters in Woven Fabric Composite Model L1

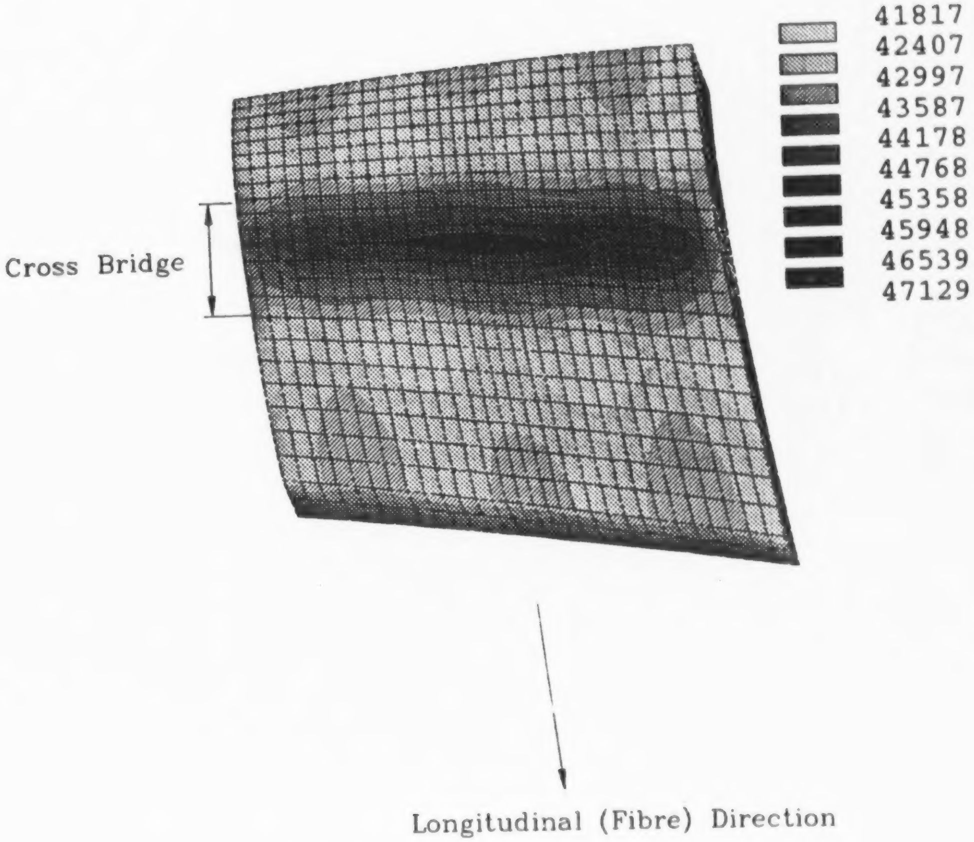

Figure 4.11 Longitudinal Stress in Unidirectional Composite (psi), Model L2, with Cross Bridge Region Identified

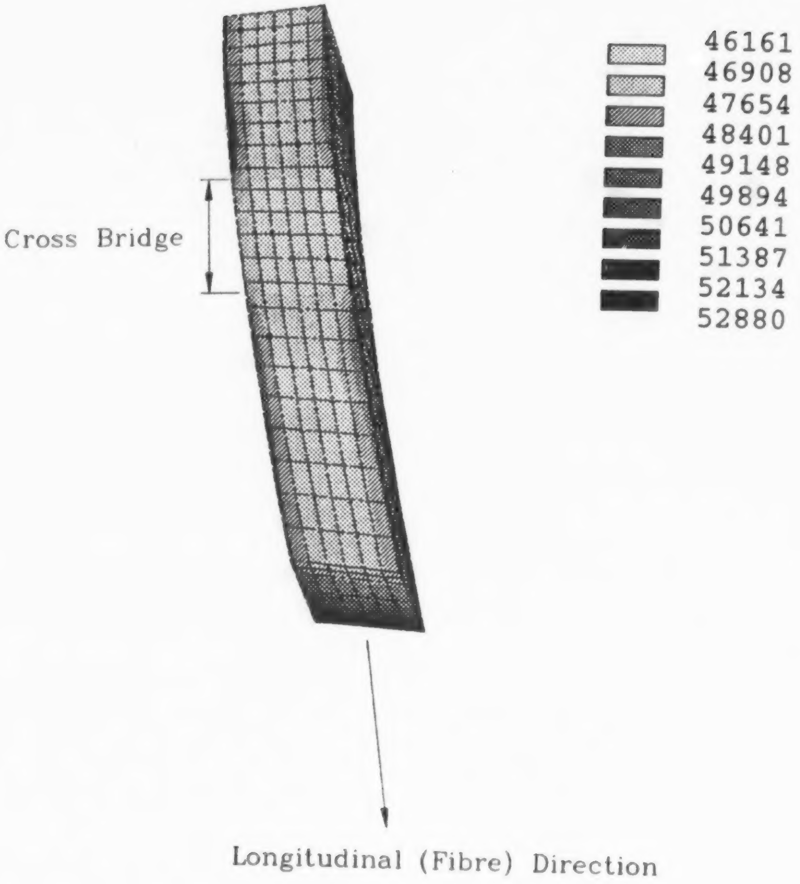

Figure 4.12 Longitudinal Stress in Unidirectional Composite 'T' (psi), Model L2, with Cross Bridge Region Identified

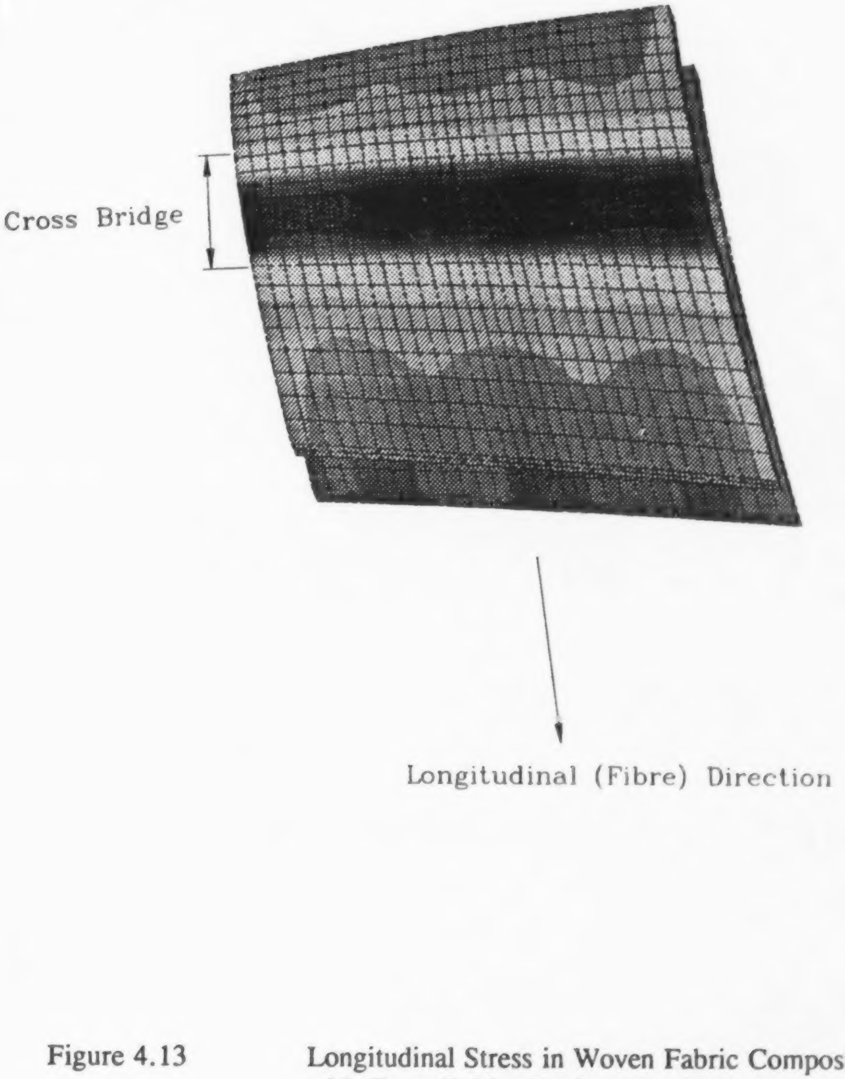

Figure 4.13 Longitudinal Stress in Woven Fabric Composite (psi), Model L2, with Cross Bridge Region Identified

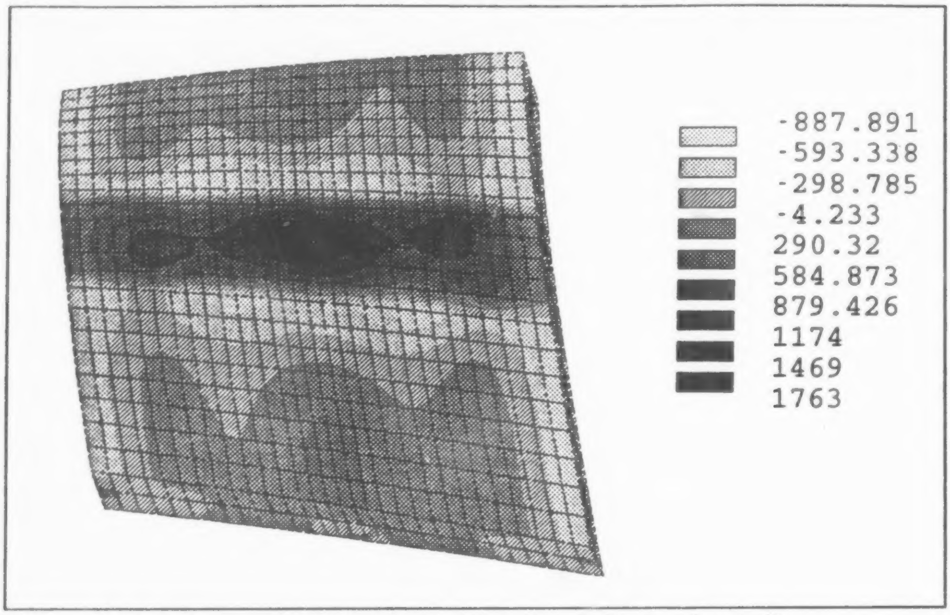

Figure 4.14 Transverse Stress in Unidirectional Composite (psi), Model L2

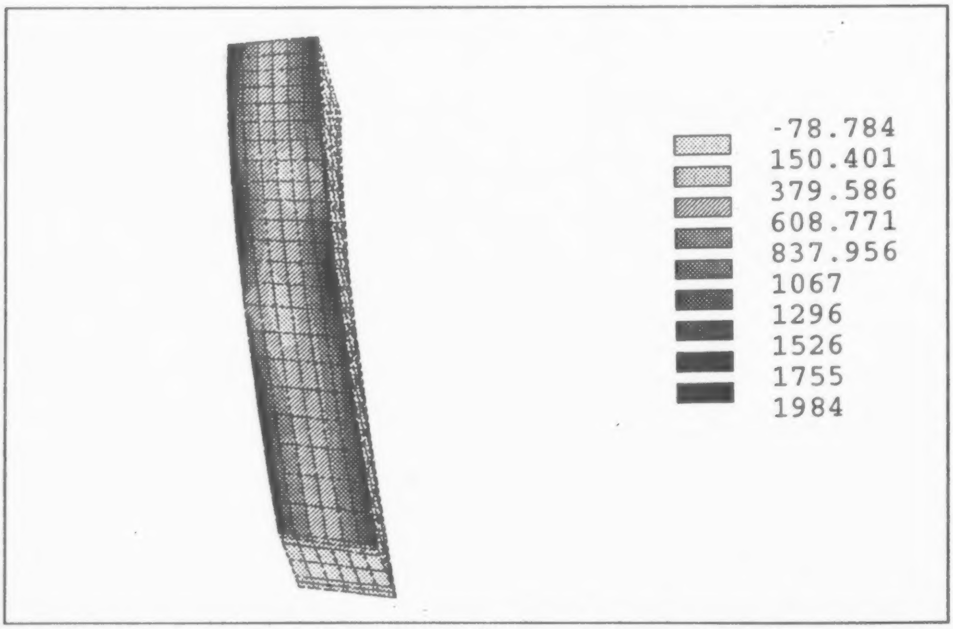

Figure 4.15 Transverse Stress in Unidirectional Composite (psi), Model L2, 'T' Section

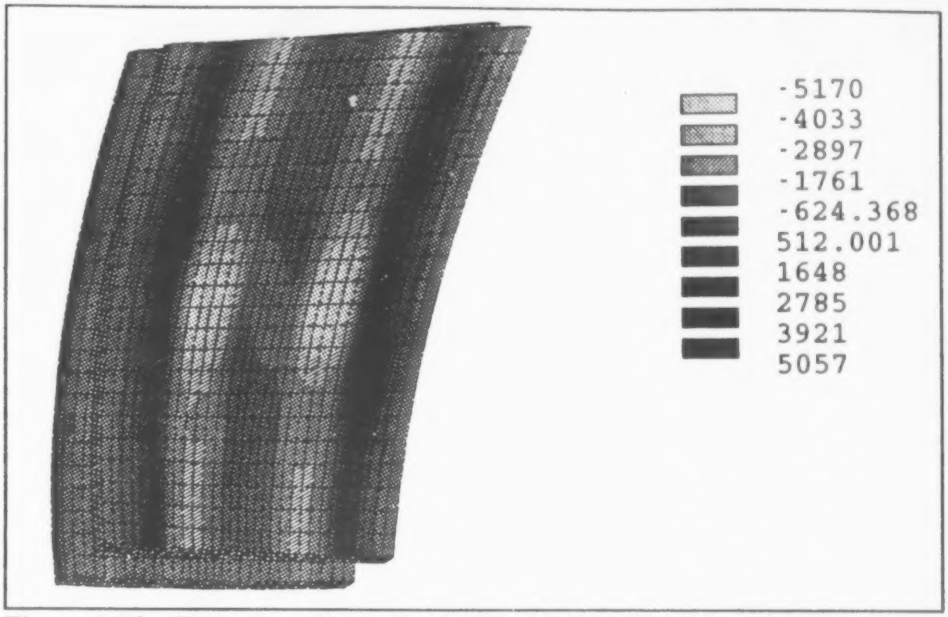

Figure 4.16 Transverse Stress in Woven Fabric Composite (psi), Model L2

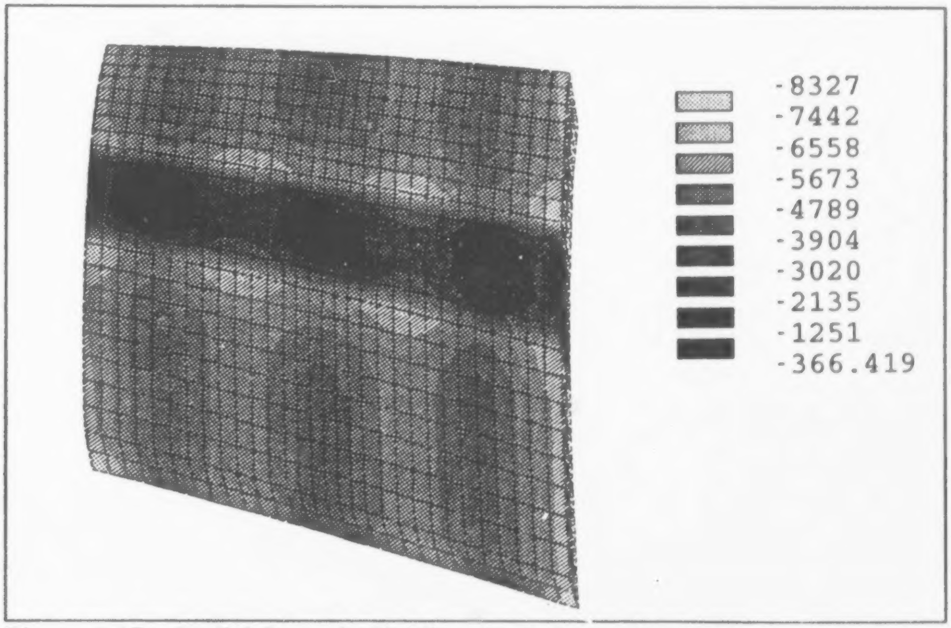

Figure 4.17 Radial Stress in Unidirectional Composite (psi), Model L2

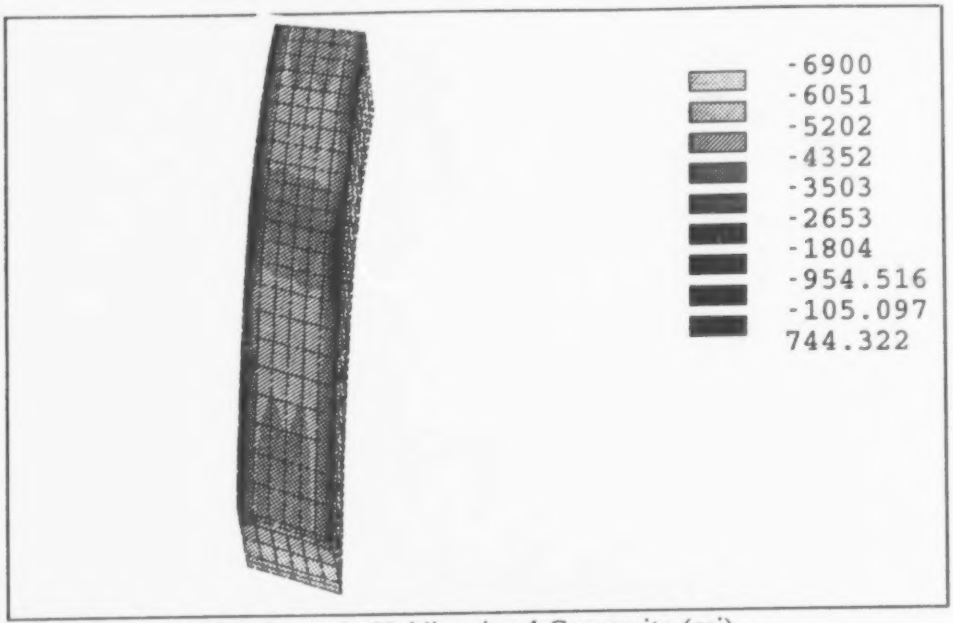

Figure 4.18 Radial Stress in Unidirectional Composite (psi), Model L2, 'T' Section

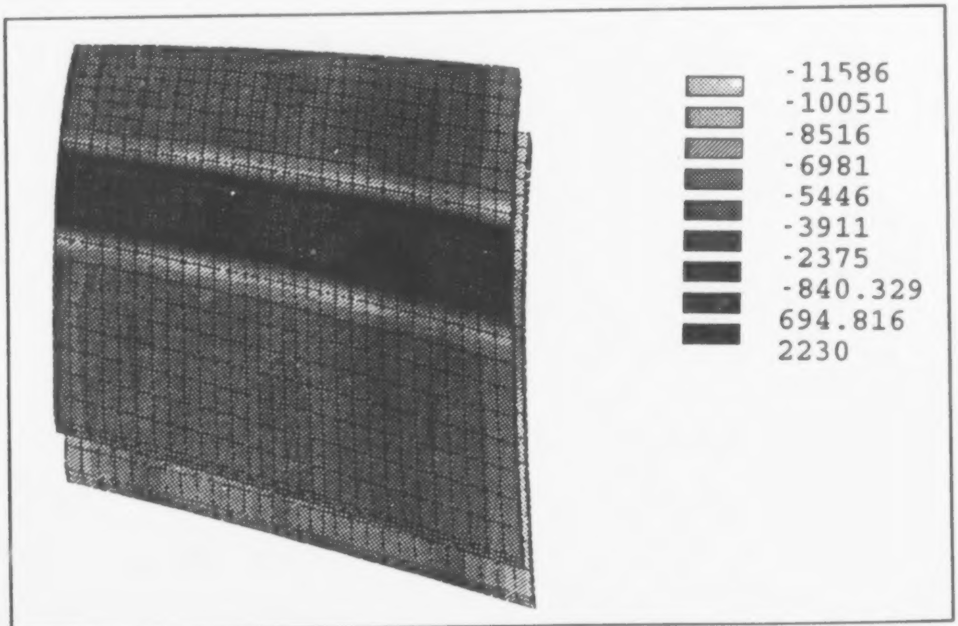

Figure 4.19 Radial Stress in Woven Fabric Composite (psi), Model L2

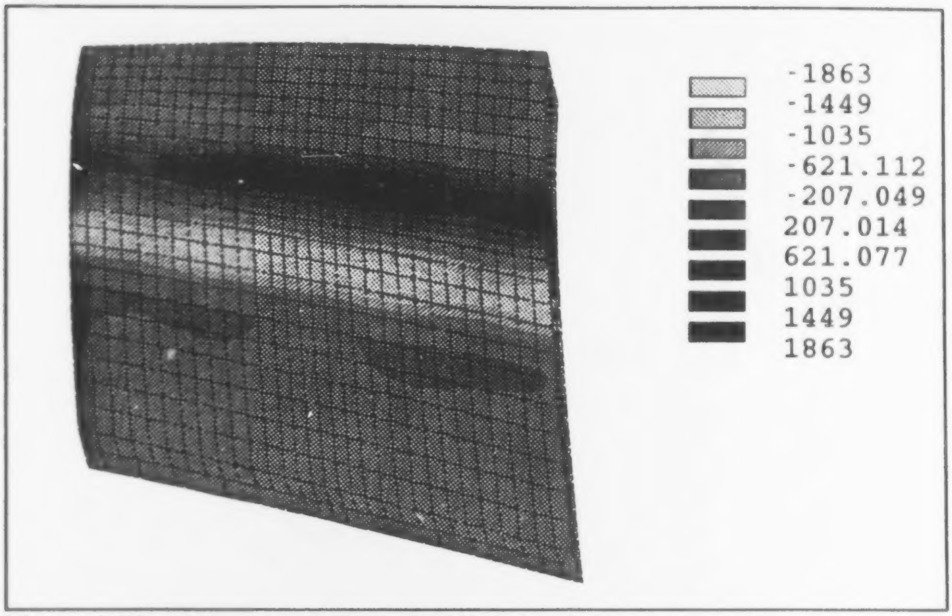

Figure 4.20 Shear Stress S_{LR} in Unidirectional Composite (psi), Model L2

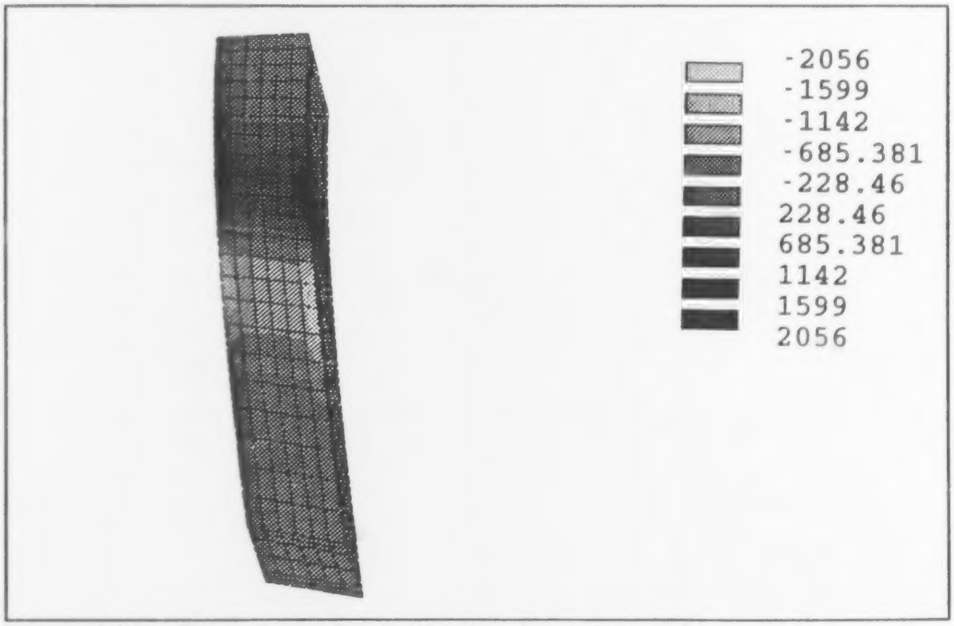

Figure 4.21 Shear Stress S_{LR} in Unidirectional Composite Model L2, 'T' Section

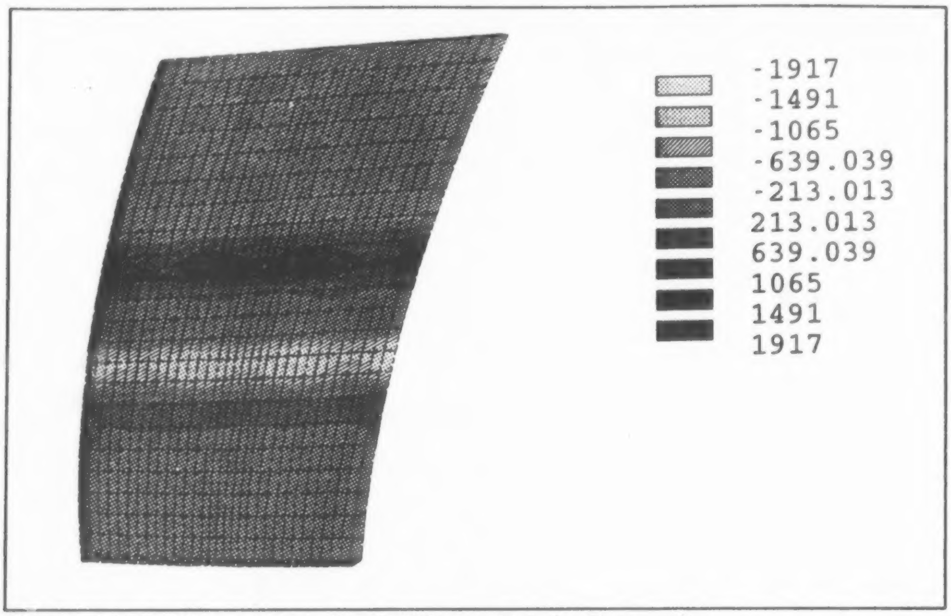

Figure 4.22 Shear Stress S_{LR} in Woven Fabric Composite Model L2

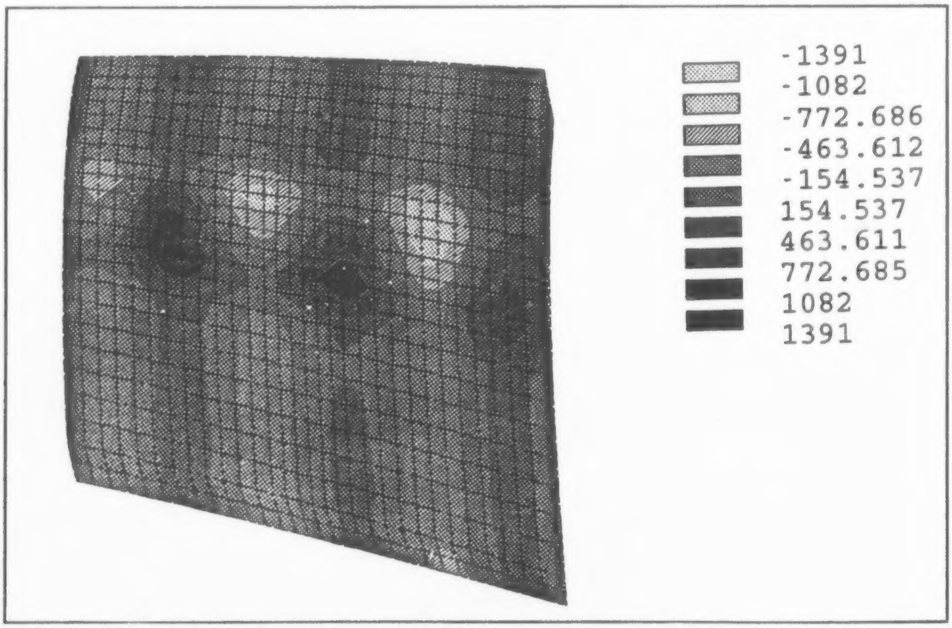

Figure 4.23 Shear Stress S_{TR} in Unidirectional Composite (psi), Model L2

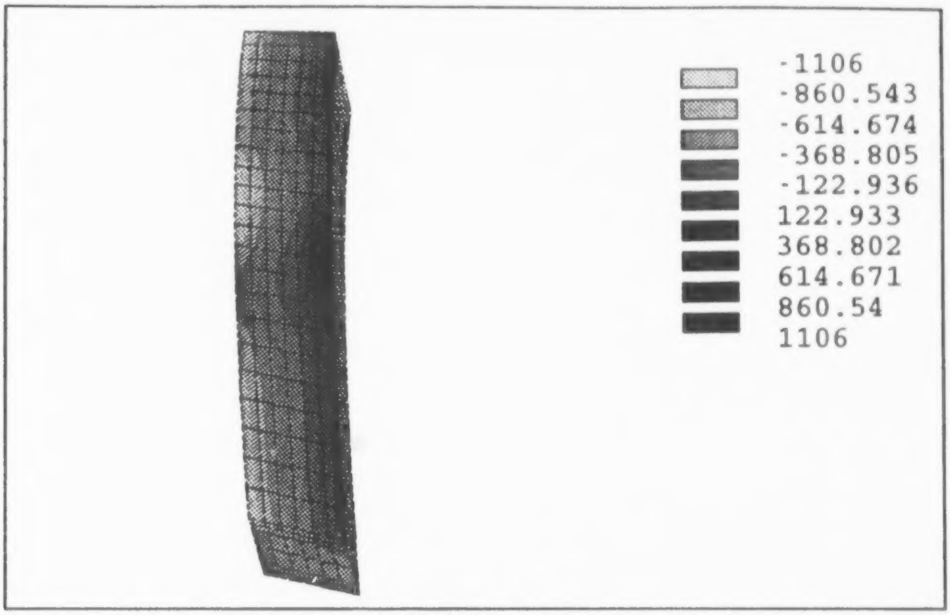

Figure 4.24 Shear Stress S_{TR} in Unidirectional Composite Model L2, 'T' Section

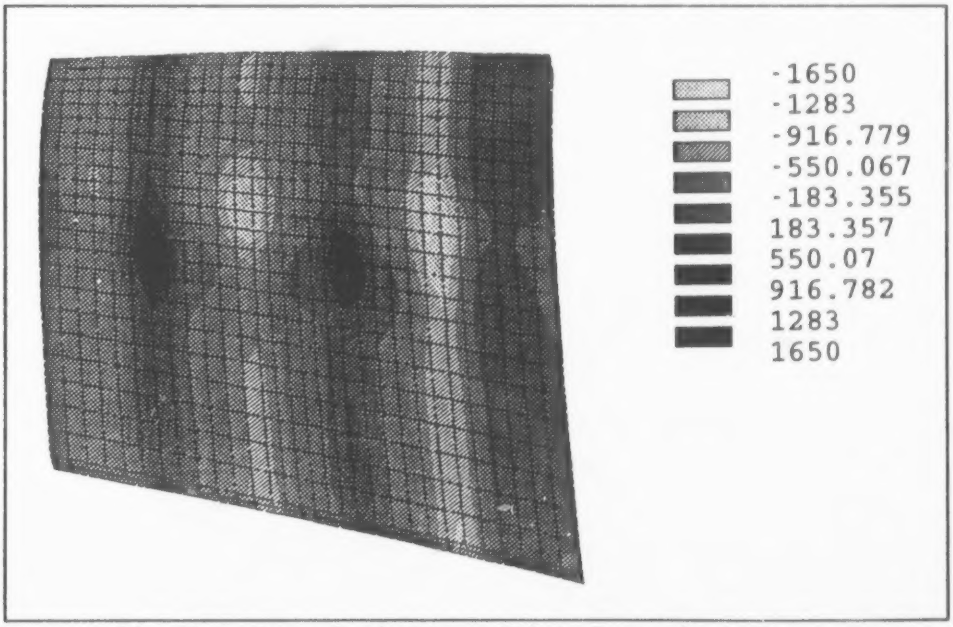

Figure 4.25 Shear Stress S_{TR} in Woven Fabric Composite (psi), Model L2, View of Top of Bottom Layer of Fabric

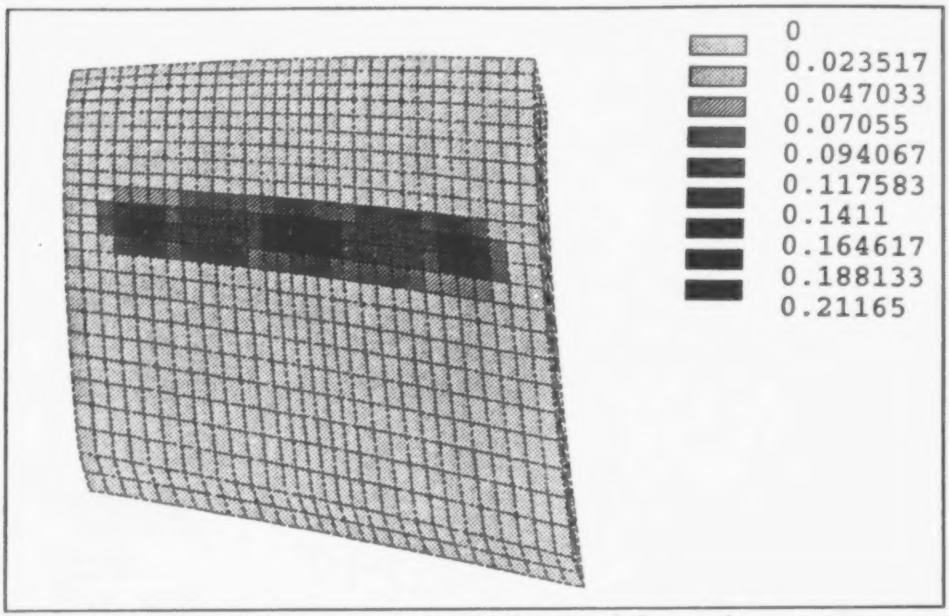

Figure 4.26 Tsai-Wu Parameters in Unidirectional Composite Model L2

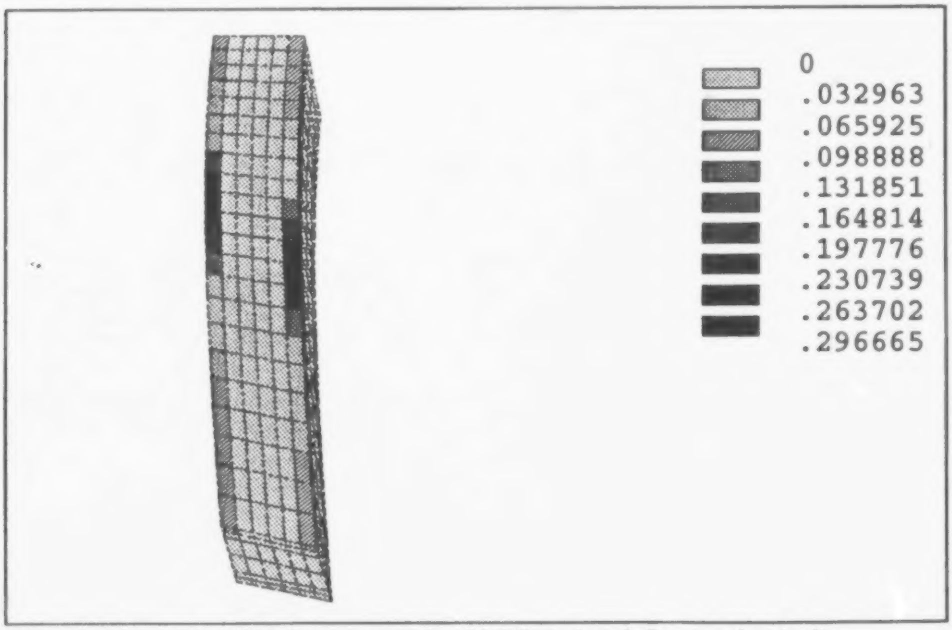

Figure 4.27 Tsai-Wu Parameters in Unidirectional Composite (psi), Model L2, 'T' Section

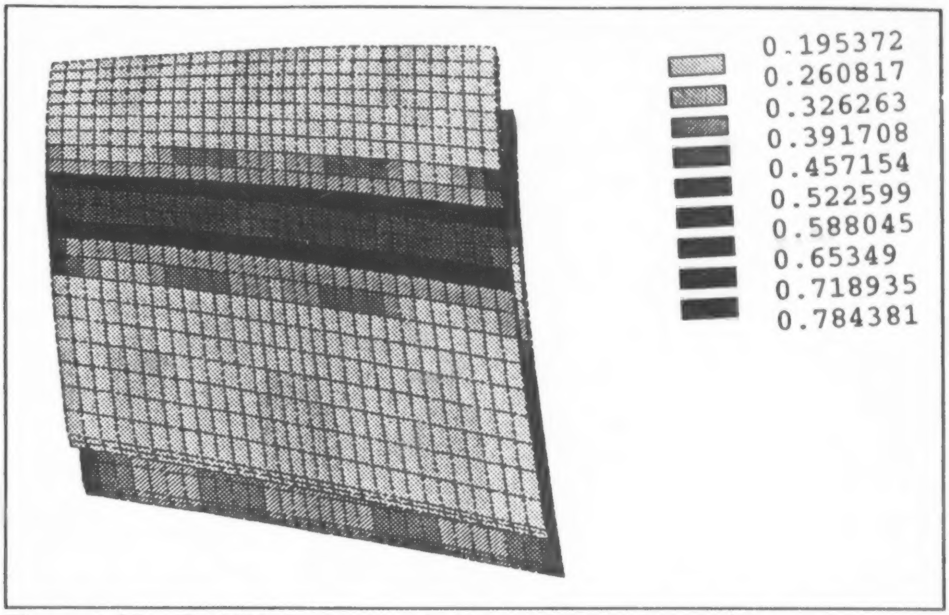

Figure 4.28 Tsai-Wu Parameters in Woven Fabric Composite Model L2

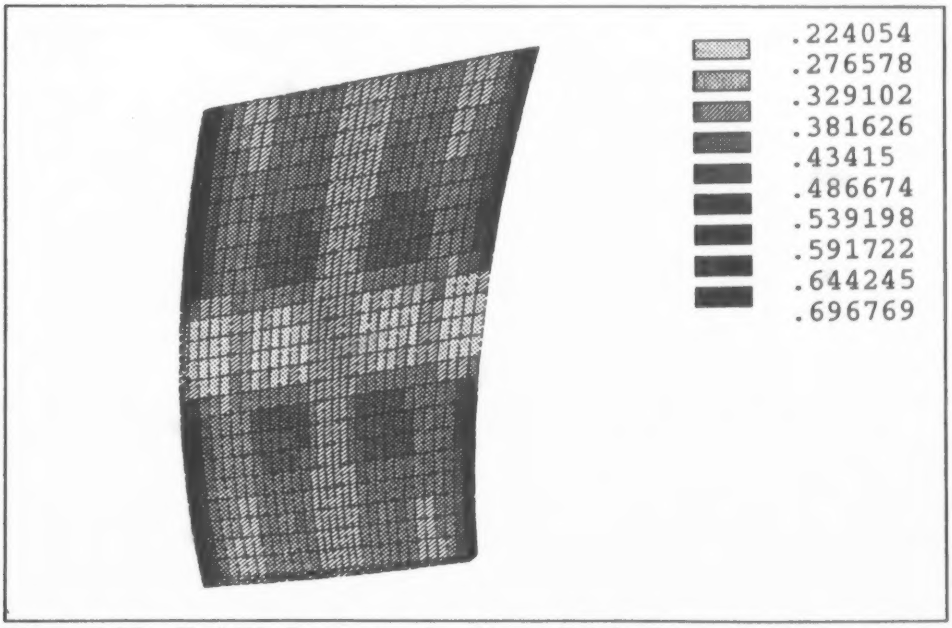

Figure 4.29 Tsai-Wu Parameters in Woven Fabric Composite, Model L2

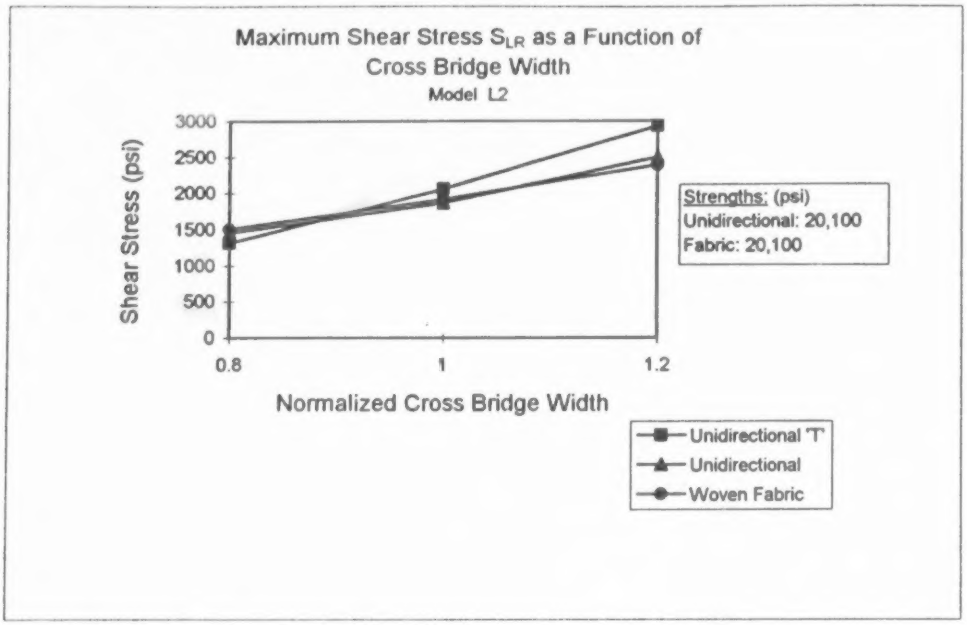

Figure 4.30 Maximum Shear Stress S_{LR} as a Function of Cross Bridge Width, Model L2

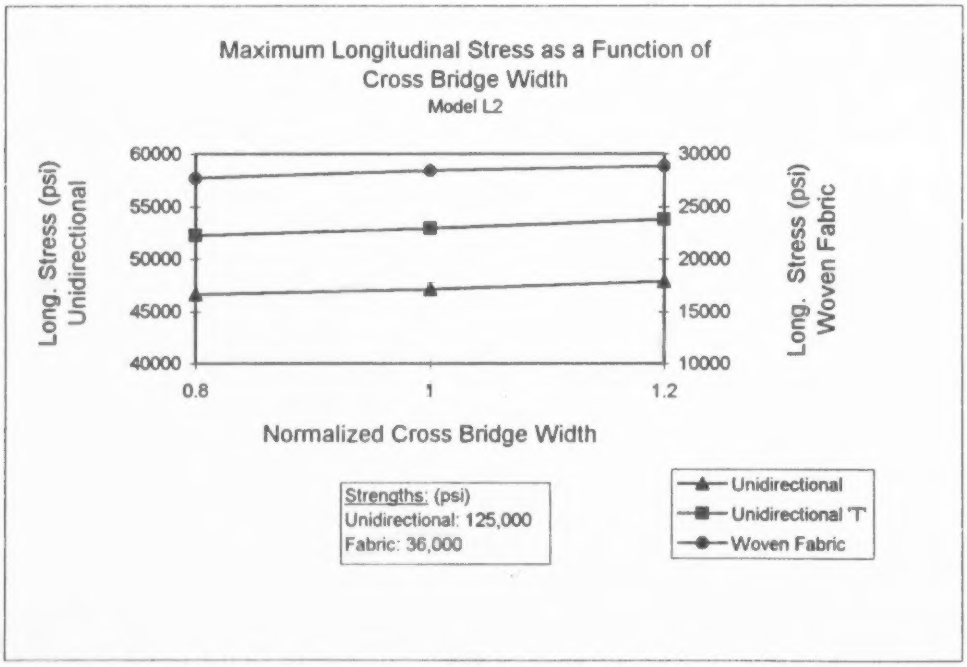

Figure 4.31 Maximum Longitudinal Stress as a Function of Cross Bridge Width, Model L2

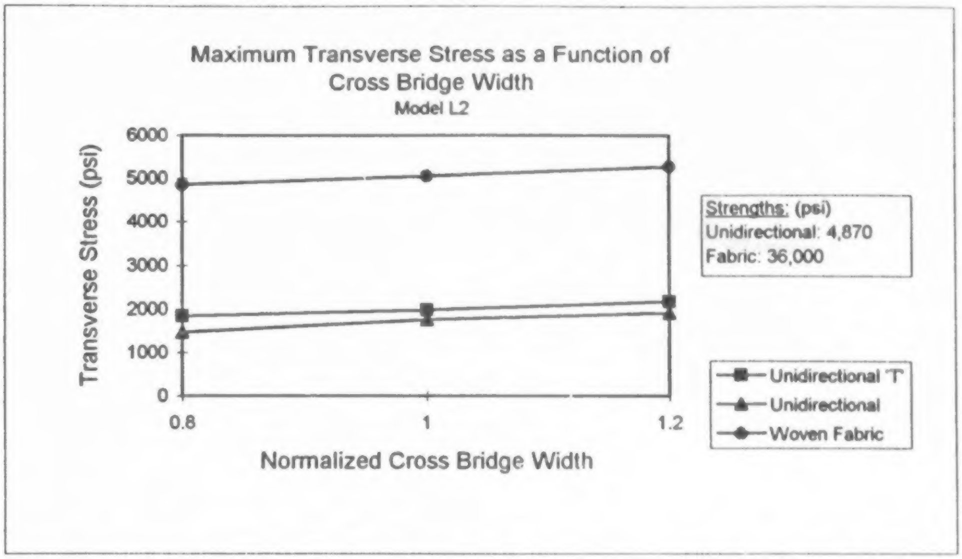

Figure 4.32 Maximum Transverse Stress as a Function of Cross Bridge Width, Model L2

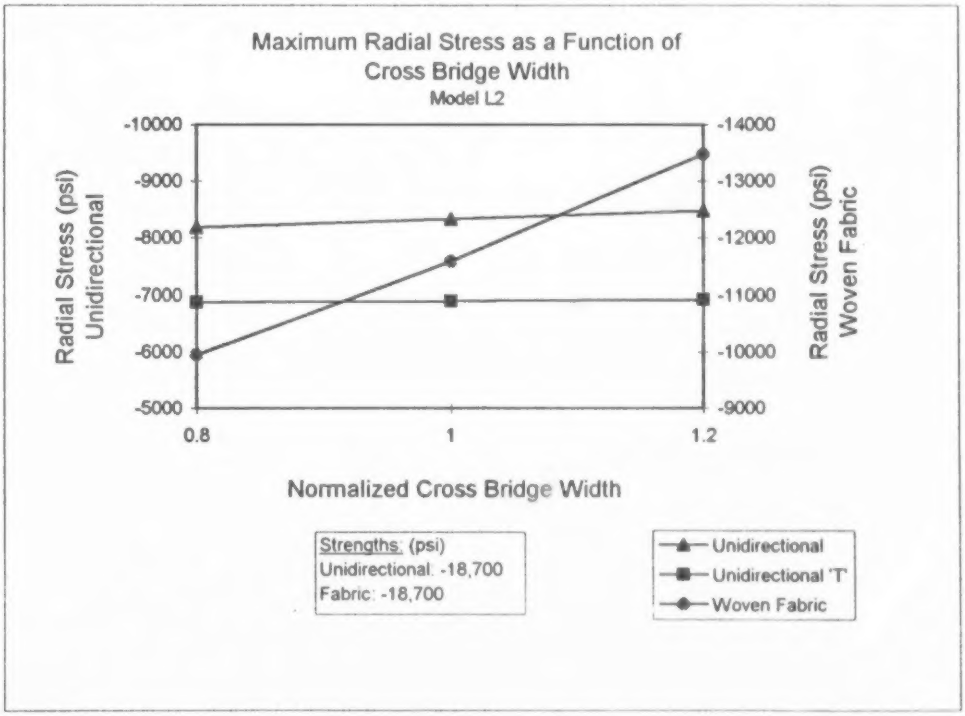

Figure 4.33 Maximum Radial Stress as a Function of Cross Bridge Width, Model L2

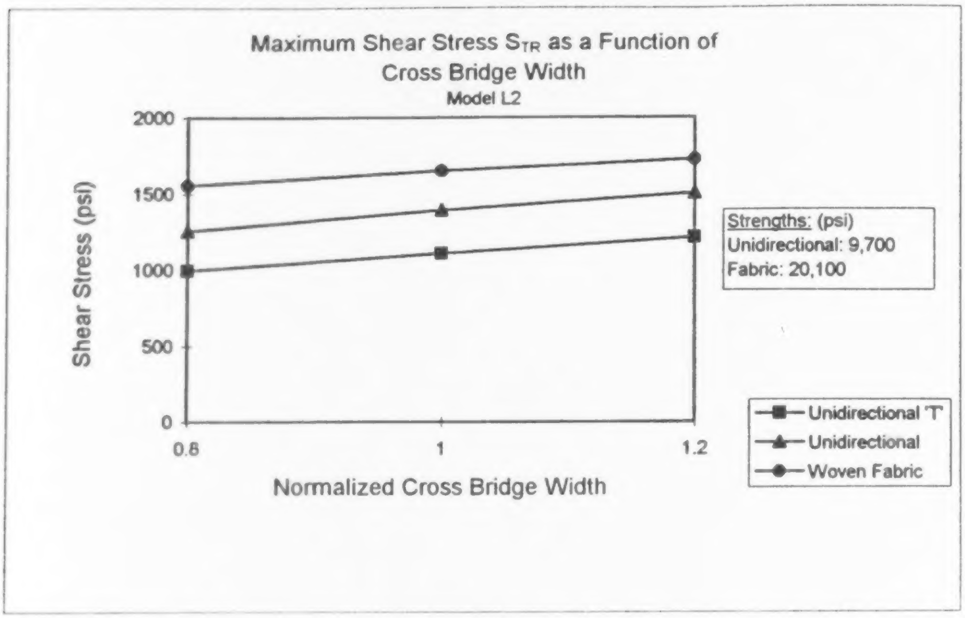

Figure 4.34 Maximum Shear Stress S_{TR} as a Function of Cross Bridge Width, Model L2

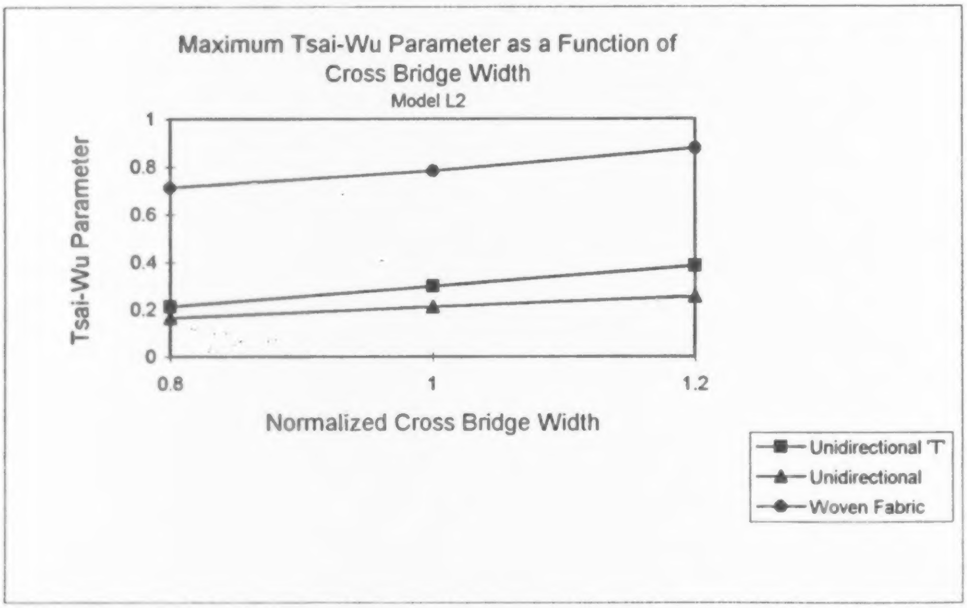

Figure 4.35 Maximum Tsai-Wu Parameter as a Function of Cross Bridge Width, Model L2

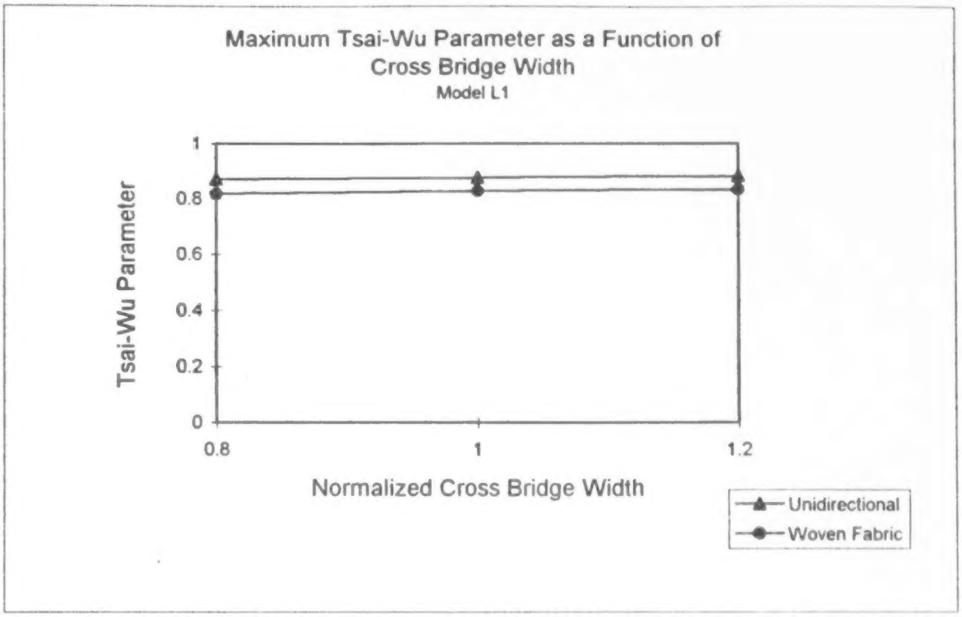

Figure 4.36 Maximum Tsai-Wu Parameter as a Function of Cross Bridge Width, Model L1

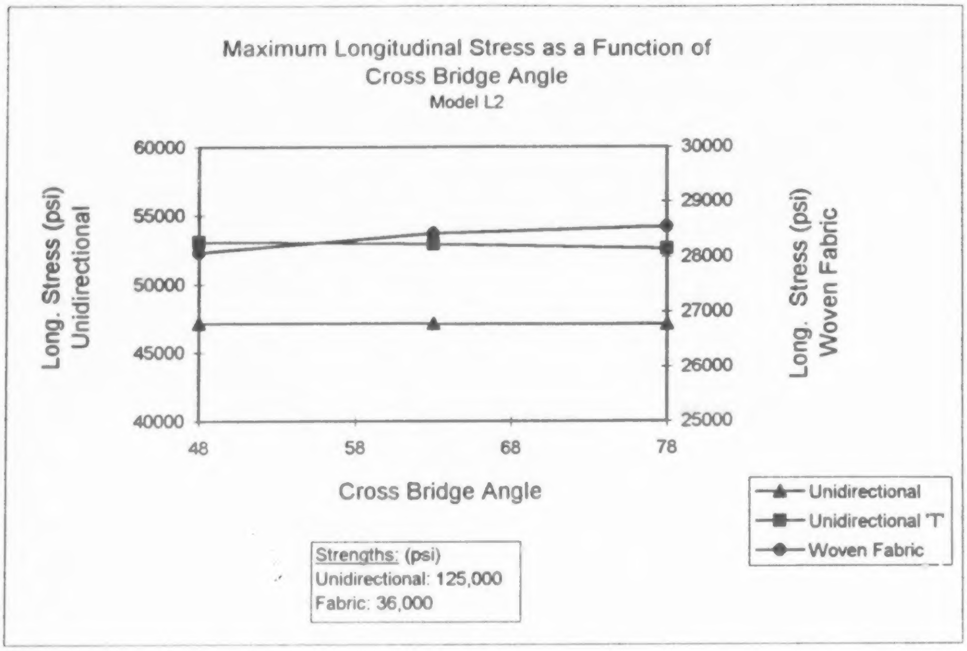

Figure 4.37 Maximum Longitudinal Stress as a Function of Cross Bridge Angle, Model L2

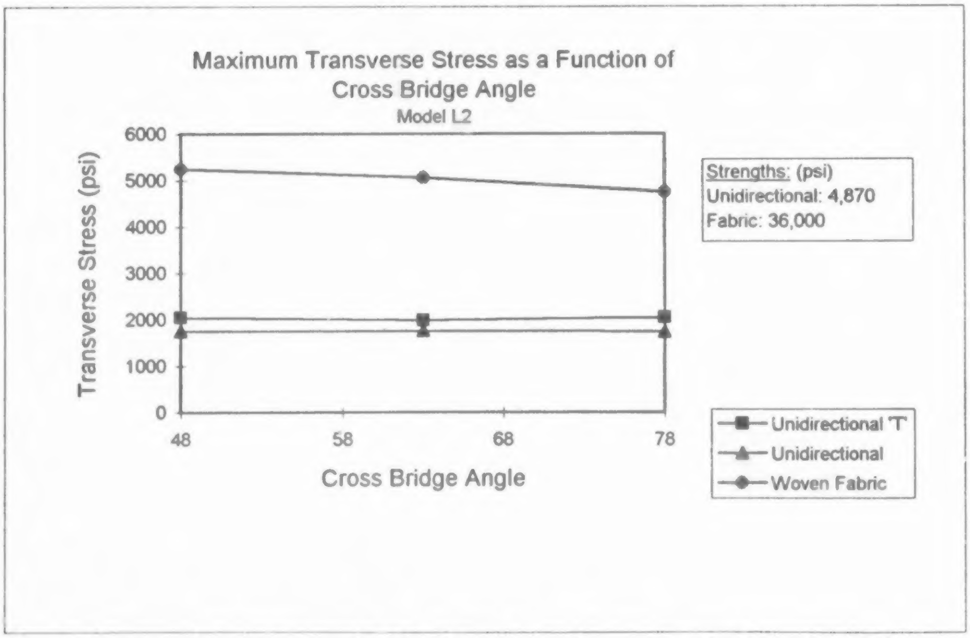

Figure 4.38 Maximum Transverse Stress as a Function of Cross Bridge Angle, Model L2

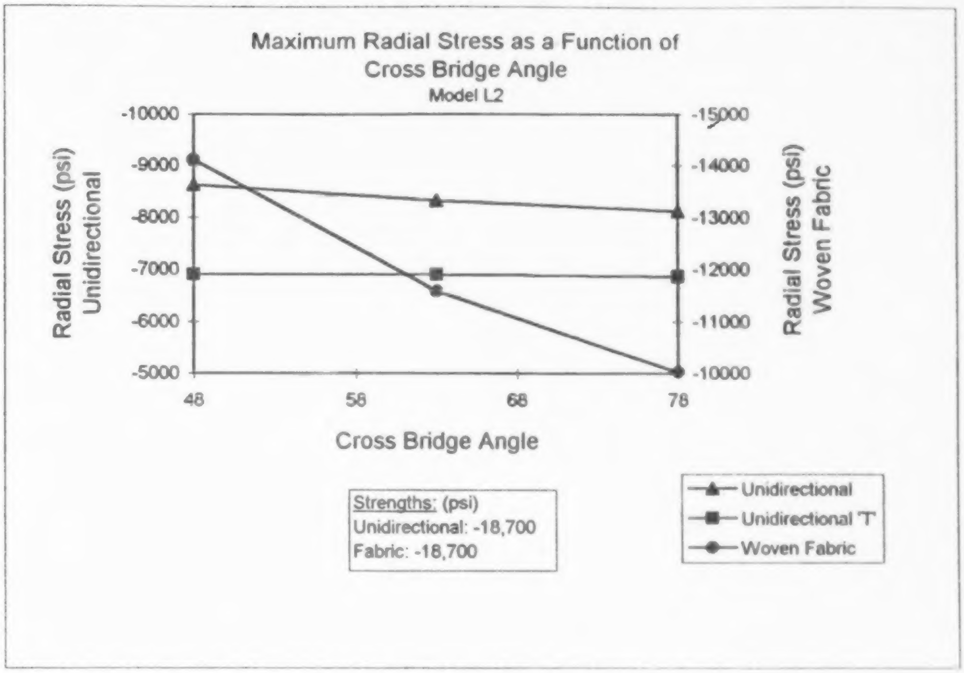

Figure 4.39 Maximum Radial Stress as a Function of Cross Bridge Angle, Model L2

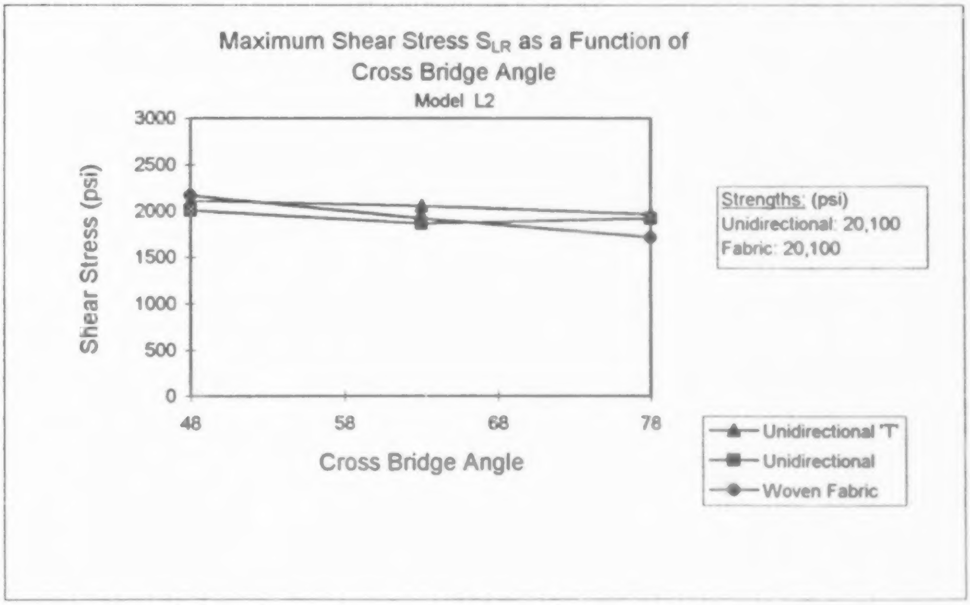

Figure 4.40 Maximum Shear Stress S_{LR} as a Function of Cross Bridge Angle, Model L2

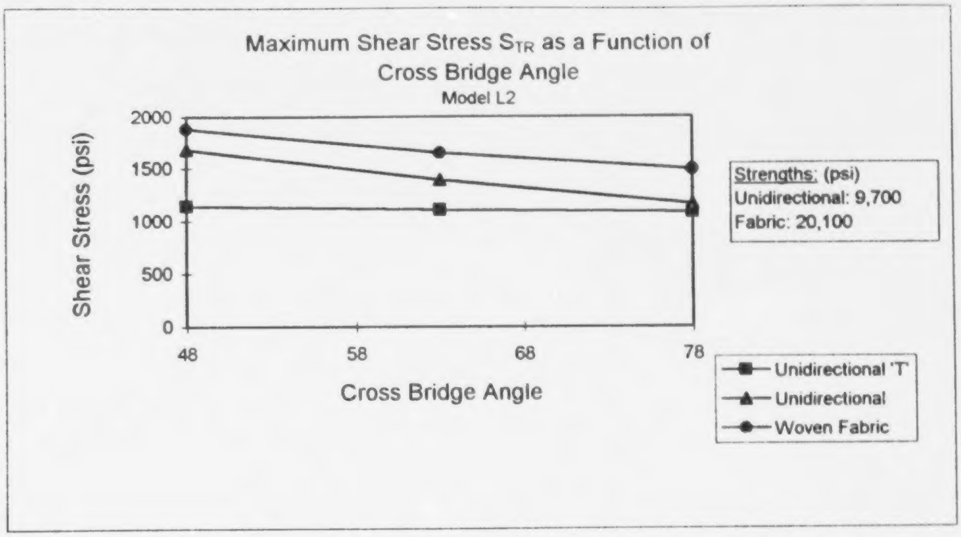

Figure 4.41 Maximum Shear Stress S_{TR} as a Function of Cross Bridge Angle, Model L2

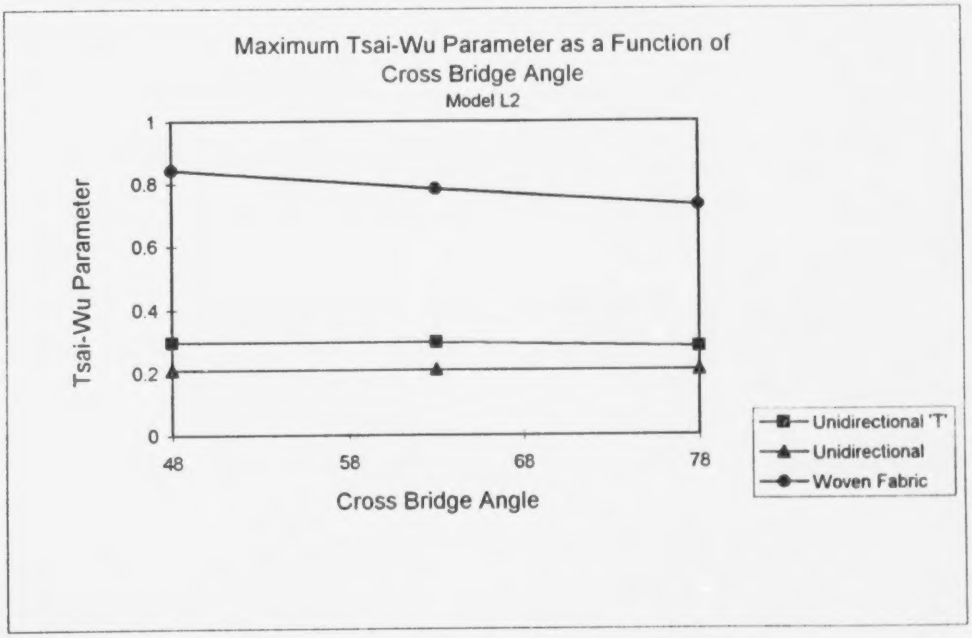

Figure 4.42 Maximum Tsai-Wu Parameter as a Function of Cross Bridge Angle, Model L2

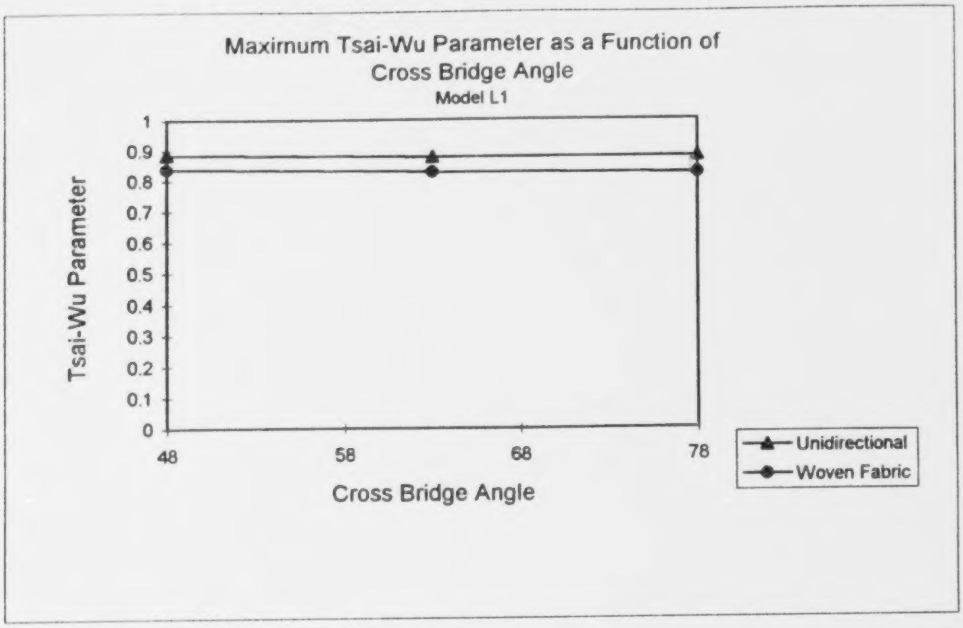

Figure 4.43 Maximum Tsai-Wu Parameter as a Function of Cross Bridge Angle, Model L1

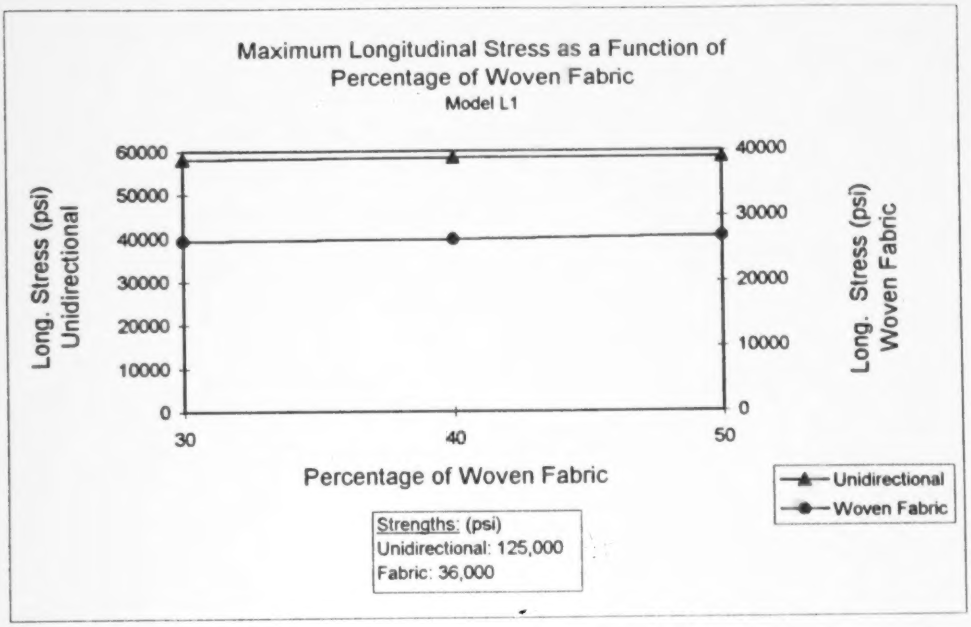

Figure 4.44 Maximum Longitudinal Stress as a Function of Percentage of Woven Fabric, Model L1

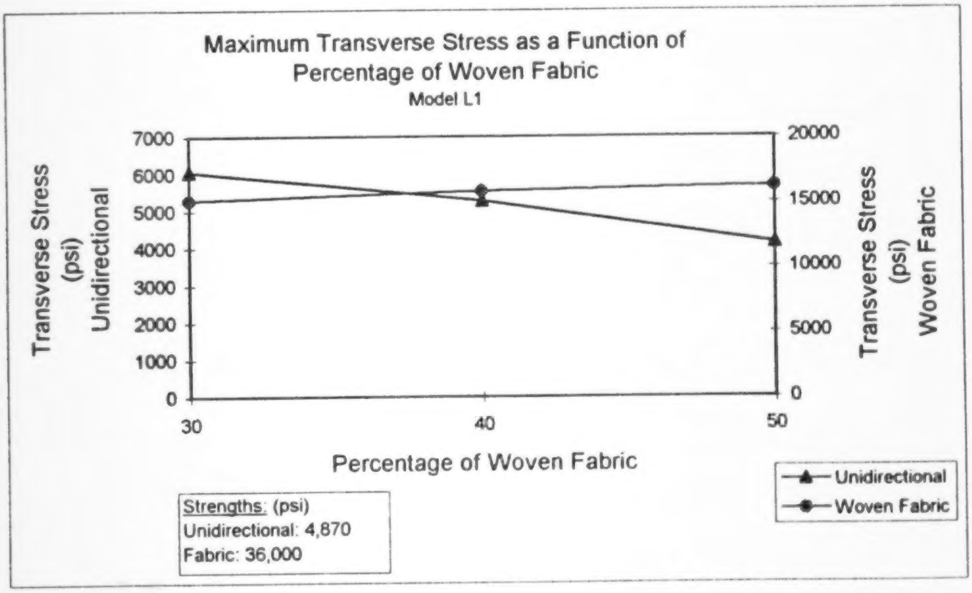

Figure 4.45 Maximum Transverse Stress as a Function of Percentage of Woven Fabric, Model L1

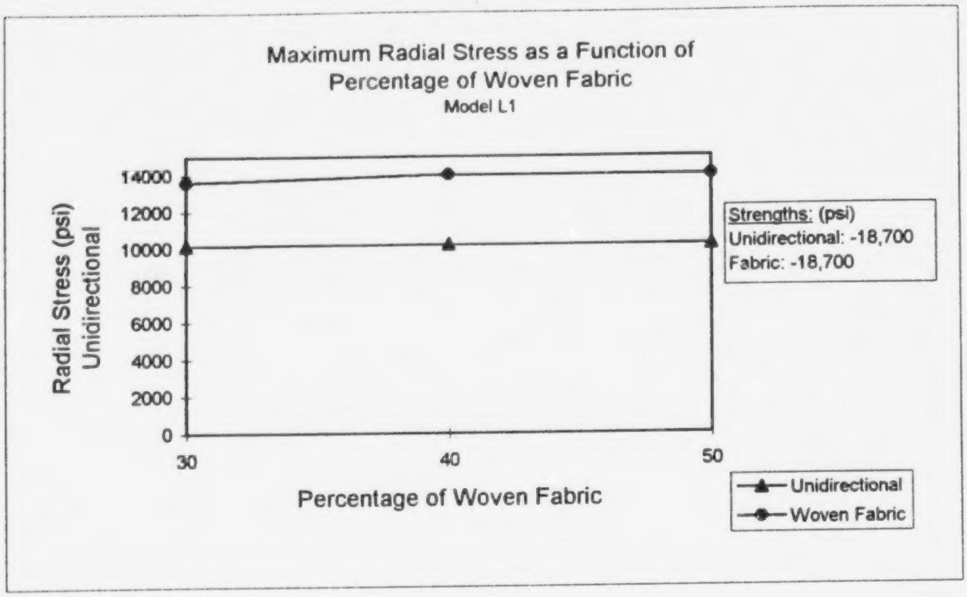

Figure 4.46 Maximum Radial Stress as a Function of Percentage of Woven Fabric, Model L1

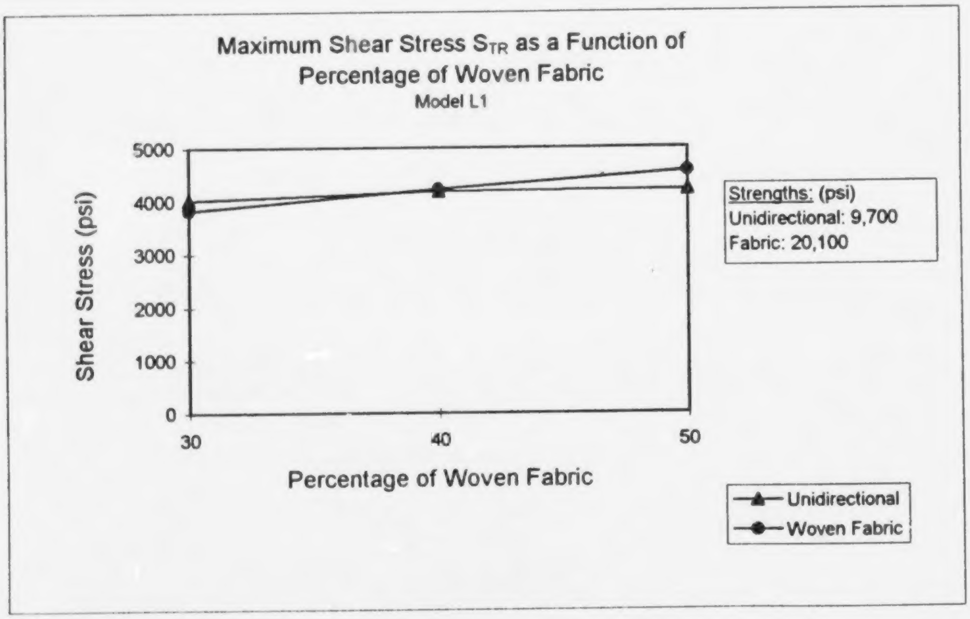

Figure 4.47 Maximum Shear Stress S_{TR} as a Function of Percentage of Woven Fabric, Model L1

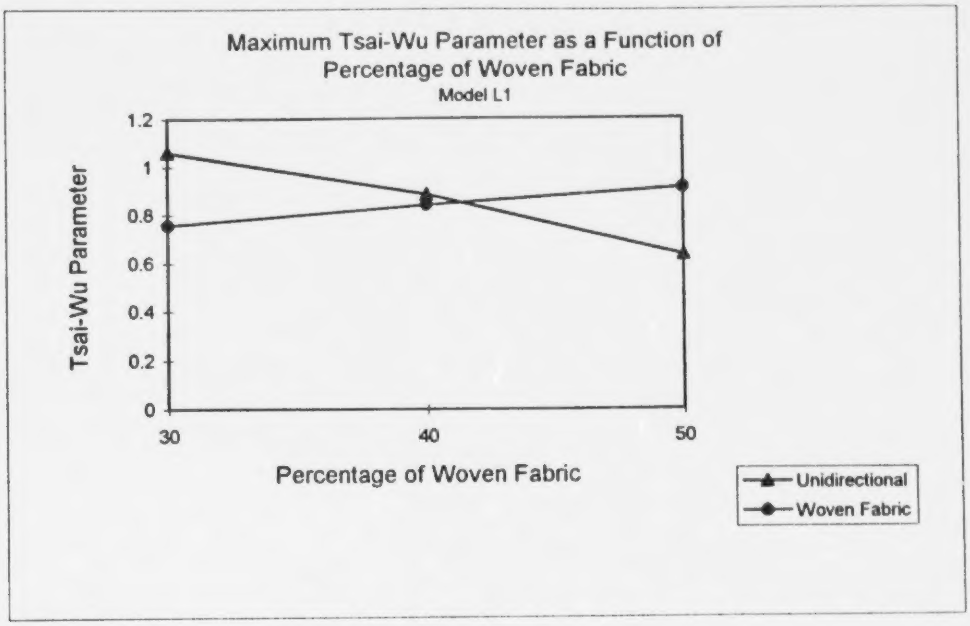

Figure 4.48 Maximum Tsai-Wu Parameter as a Function of Percentage of Woven Fabric, Model L1

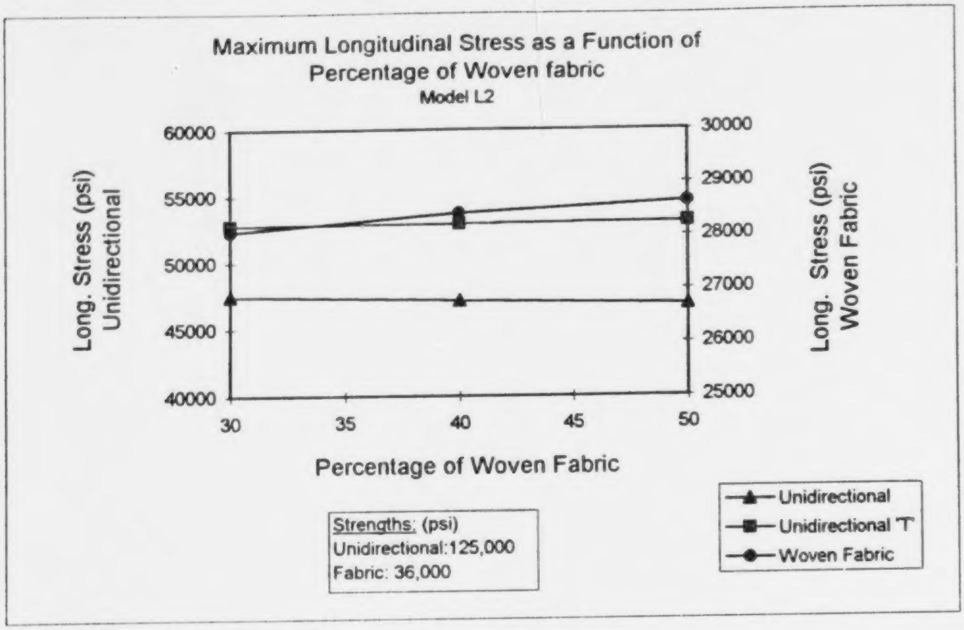

Figure 4.49 Maximum Longitudinal Stress as a Function of Percentage of Woven Fabric, Model L2

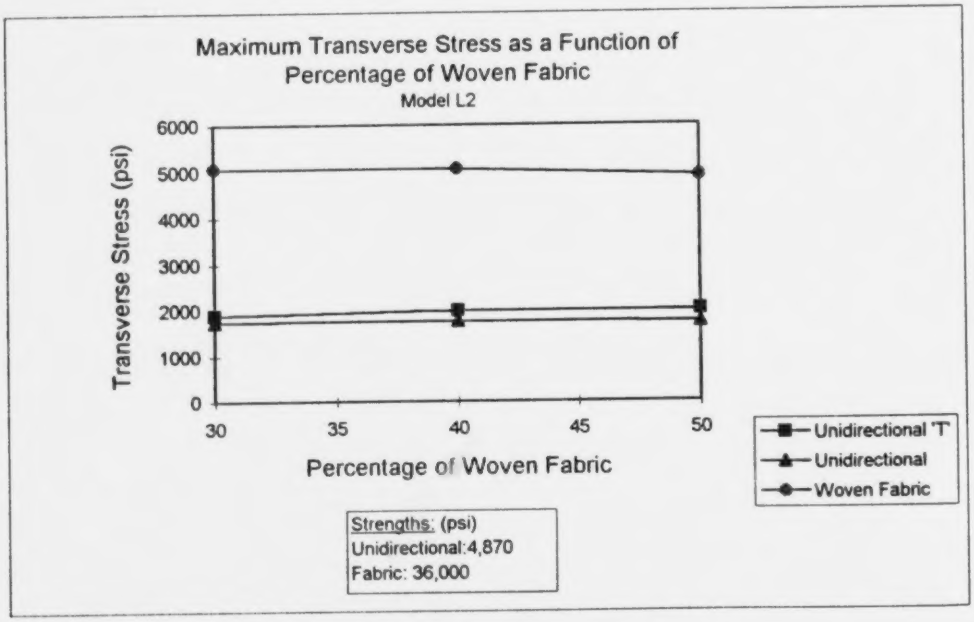

Figure 4.50 Maximum Transverse Stress as a Function of Percentage of Woven Fabric, Model L2

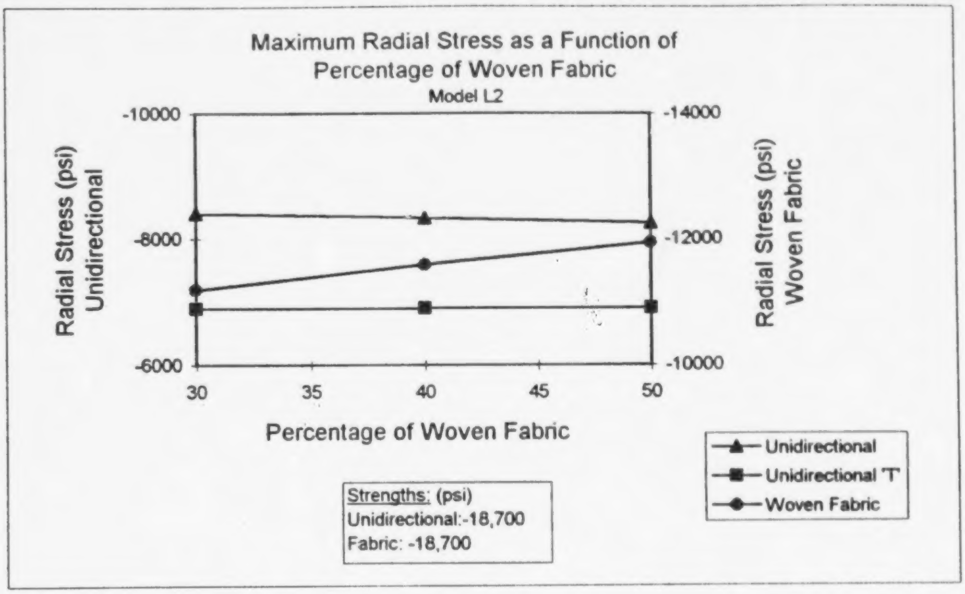

Figure 4.51 Maximum Radial Stress as a Function of Percentage of Woven Fabric, Model L1

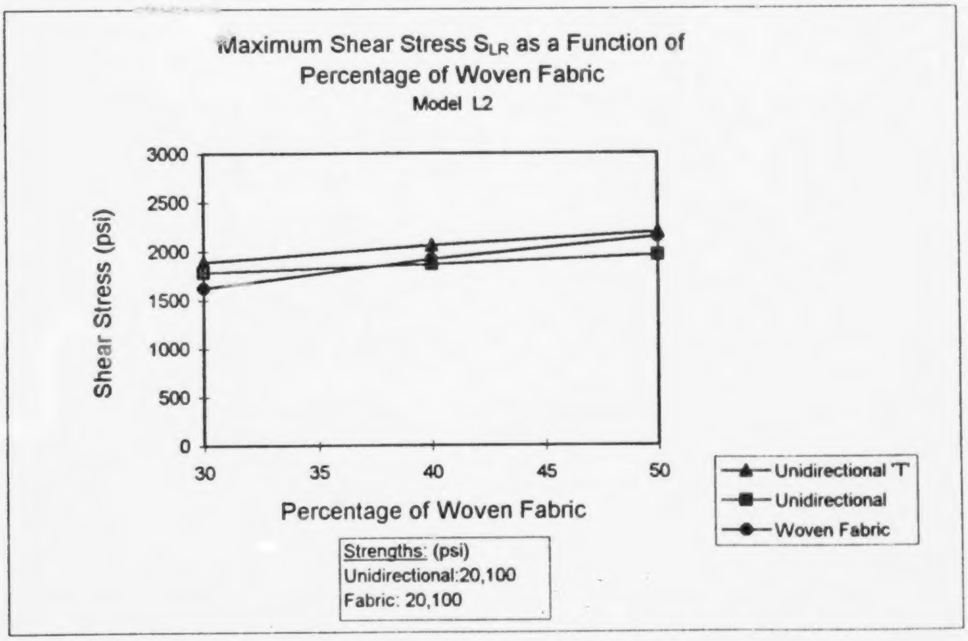

Figure 4.52 Maximum Shear Stress S_{LR} as a Function of Percentage of Woven Fabric, Model L2

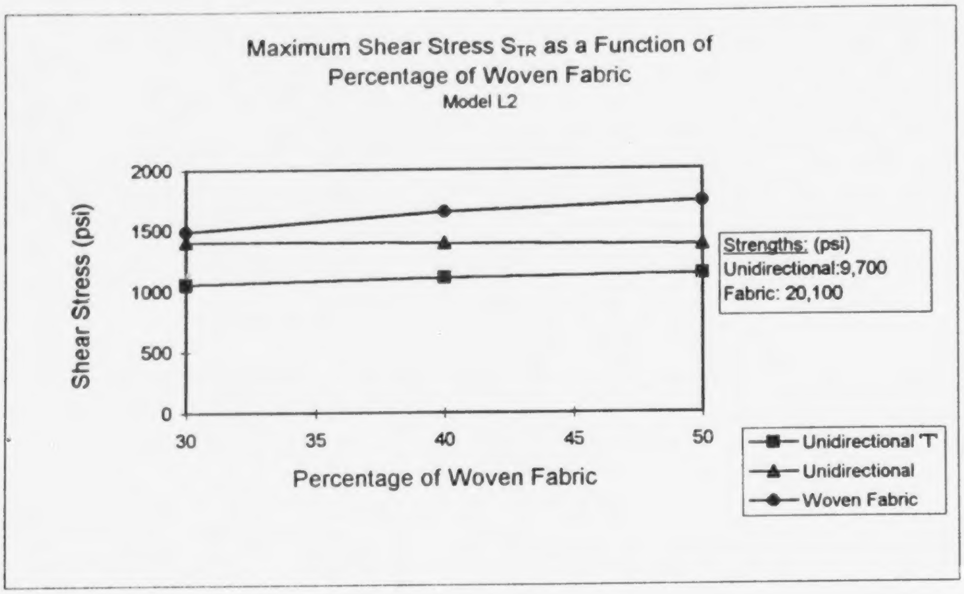

Figure 4.53 Maximum Shear Stress S_{TR} as a Function of Percentage of Woven Fabric, Model L2

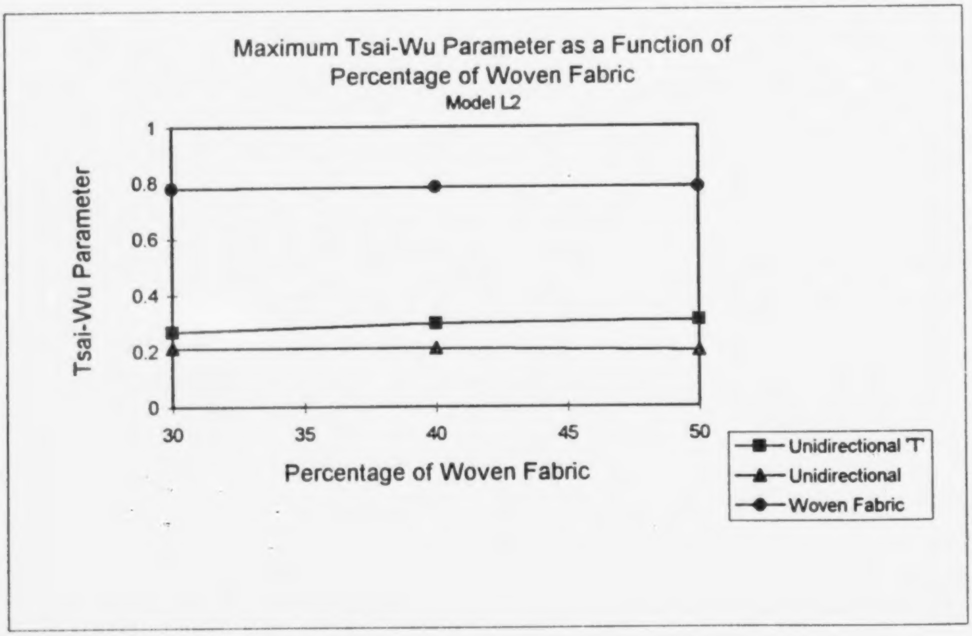

Figure 4.54 Maximum Tsai-Wu Parameter as a Function of Percentage of Woven Fabric, Model L2

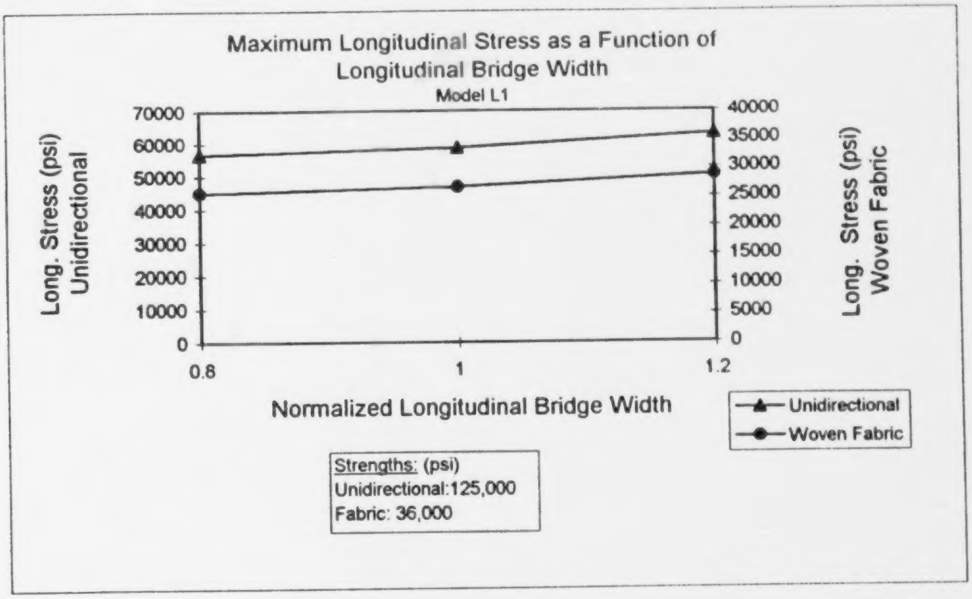

Figure 4.55 Maximum Longitudinal Stress as a Function of Longitudinal Bridge Width, Model L1

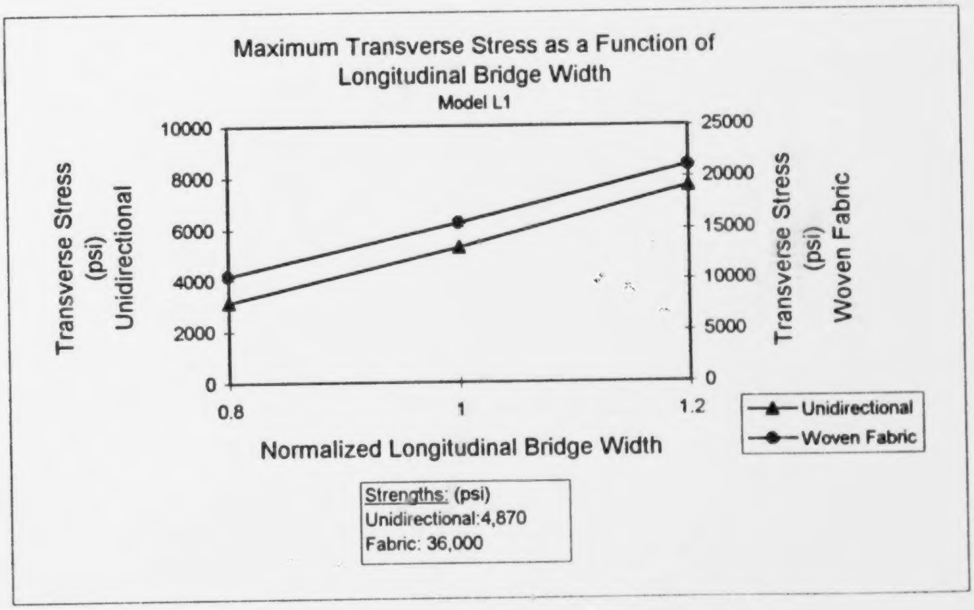

Figure 4.56 Maximum Transverse Stress as a Function of Longitudinal Bridge Width, Model L1

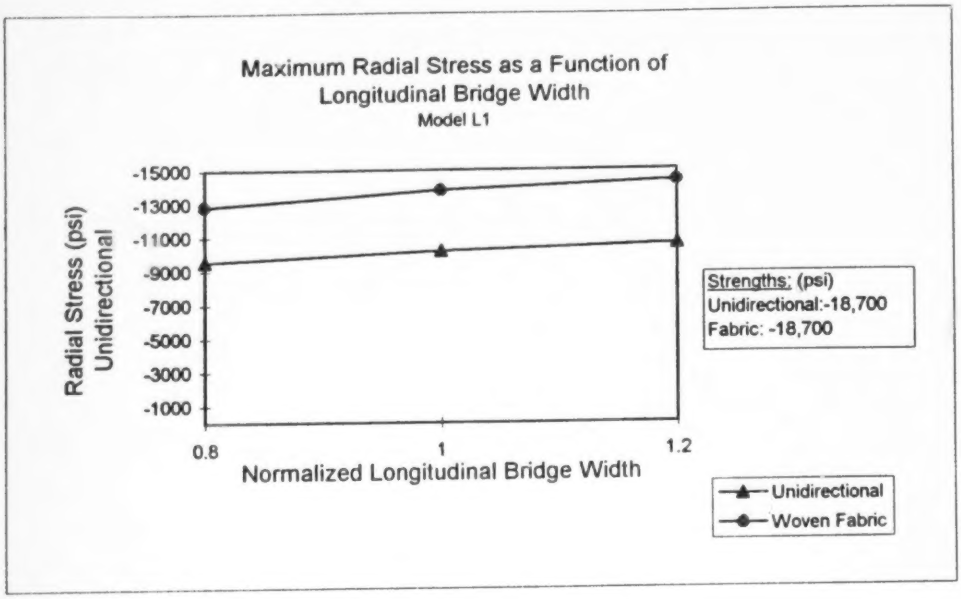

Figure 4.57 Maximum Radial Stress as a Function of Longitudinal Bridge Width, Model L1

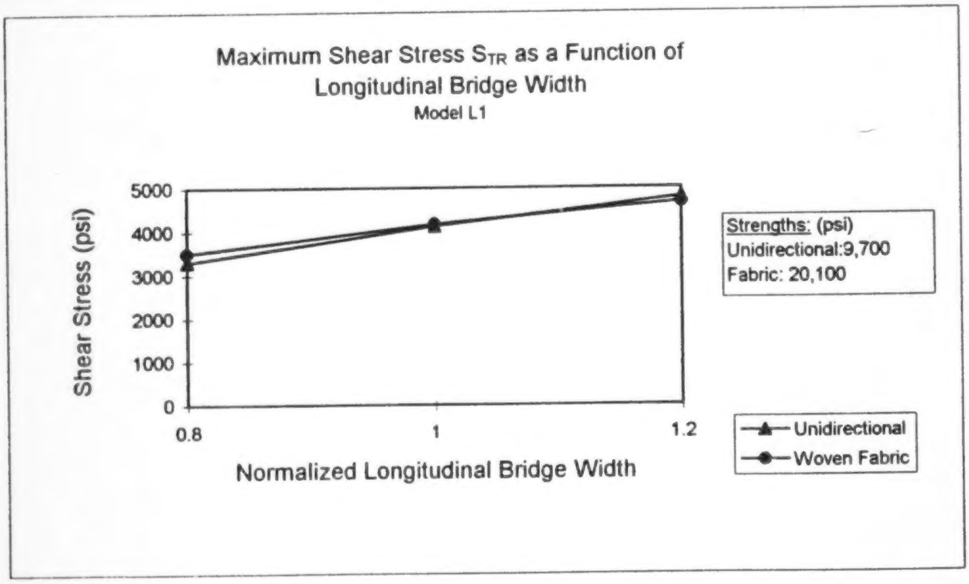

Figure 4.58 Maximum Shear Stress STR as a Function of Longitudinal Bridge Width, Model L1

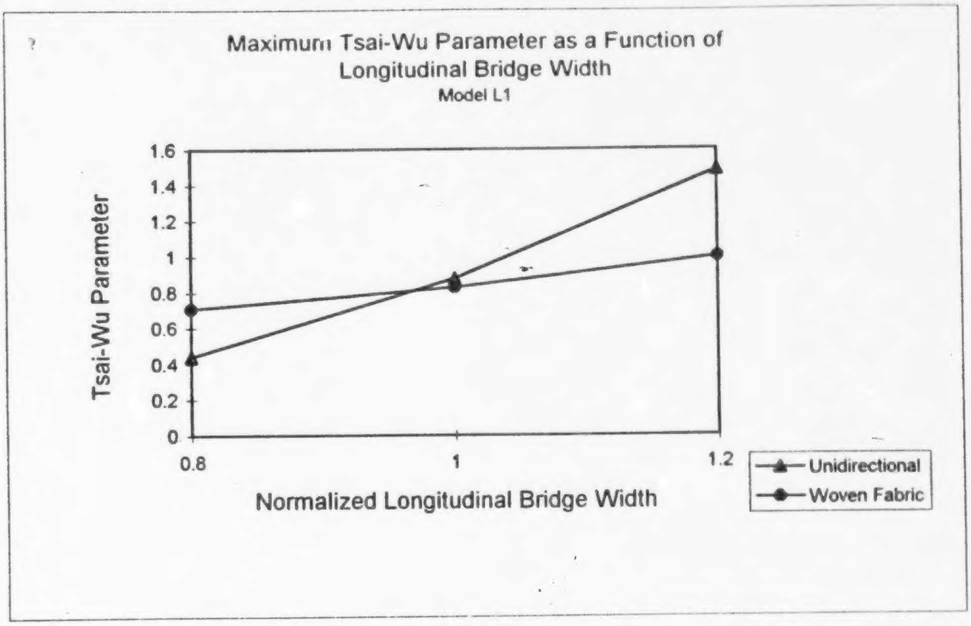

Figure 4 59 Maximum Tsai-Wu Parameter as a Function of Longitudinal Bridge Width, Model L1

CHAPTER 5

CONCLUSIONS AND RECOMMENDATIONS

5.1 Conclusions

The two critical layers of a multilayer composite pipe have been studied. Geometric configurations and composite forms have been analyzed using the finite element method and parametric analysis. A greater understanding has been developed of the stresses caused by internal pressure and secondary bending, and the effects of design variables on these stresses.

Layers 1 and 2 were subjected to secondary bending in the regions where elastomeric strips of other layers provided little radial support. This secondary loading induced normal and shear stresses in the composite materials for which unidirectional material is not ideally suited. Layers of woven fabric material provided transverse and shear strength in the locations where the unidirectional composite was particularly vulnerable, while the unidirectional core provided great longitudinal strength.

The following summarizes the significant results of the parametric study.

Typical Design

Layer 1 experienced high transverse and radial stresses and shear stress S_{TR}. Layer 2 experienced high radial stresses and shear stress S_{LR}. The Tsai-Wu parameter was highest in Layer 1. Thus Layer 1 is the critical layer.

Variation in Cross Bridge Width

Variations in cross bridge width had negligible effect on Layer 1, while in Layer 2, shear stress S_{LR} increased as the bridge width increased.

Variation in Cross Bridge Angle

Variations in cross bridge angle had negligible effect on Layer 1, while in Layer 2, all stresses decreased slightly as the angle approached 90°.

Variation in Percentage of Woven Fabric

In Layer 1, there was a decrease in stresses in the unidirectional material as the amount of woven fabric was increased. In Layer 2, there was a slight increase in stresses as the amount of woven fabric was increased.

Variation in Longitudinal Bridge Width

As the longitudinal bridge width increased, there was a significant increase in all stresses in Layer 1.

It was seen that the woven fabric was of greatest use in layer 1, where loading caused high transverse and shear S_{TR} stresses at the top and bottom of the strip. It was shown that the woven fabric was essential to layer 1 and that if all other factors are kept constant, a higher proportion of woven fabric may improve the performance of layer 1. However, this may not be practically possible as the introduction of woven fabric decreases the longitudinal modulus of the strip and greatly affects the performance of the pipe in terms of axial growth and rotation.

The benefits of layers of woven fabric were not as positive for layer 2 as for layer 1. There was less significant transverse loading and the woven fabric would seem to decrease the longitudinal strength of the composite. But given the not insignificant transverse loading in the bridge region, the presence of the woven fabric served to maintain long term strength of the composite. In this case, a reduction of the thickness of the woven fabric composite is a possible method of slightly increasing the strength of layer 2.

As has been known since the initial prototype testing and finite element analysis, the width of the outer hoop and layer 2 elastomers must be minimized. Layer 2 is not as sensitive to the width of the cross bridge as layer 1 is to the width of the longitudinal bridge, but both bridges must remain small. The angle at which the outer hoop crosses the inner hoop does not largely affect the stresses in layers 1 or 2. Generally, larger angles are better, but the difference is not significant.

5.2 Recommendations

There are other factors, not studied in this analysis, which may serve to minimize the effects of secondary bending. For example, the percentage α of composite material has not been studied in detail. A higher value would permit smaller bridge widths while maintaining composite strength. This would provide a greater pressure capacity of the pipe.

Reliability of the results of the finite element model would be greatly improved with a better knowledge of the material properties of the composite materials. A vigourous testing program to determine the material properties would allow a more accurate prediction of the point of failure of the pipe.

Visco-elastic behaviour of the composite materials should also be investigated. The long term life of the pipe is dependent on the ability of the materials to retain their strength over long periods of time. Any long term study will require knowledge of the visco-elastic nature of the out-of-plane composite material properties.

It was found in this study that changes in the cross bridge angle had little effect on the stresses in the composite. Knowing this, the finite element model could be further simplified by using a cross bridge angle of 90°. By taking advantage of the subsequent planes of symmetry which were not available at any other angle, this would lead to a reduction of the number of elements required. This may permit the generation of a simplified comprehensive model which could be used with smaller computing facilities.

REFERENCES

1. Bouey, S. and Freiheit, R.,*Pressure Testing Report*, Composite Technologies Inc., 1995 (Confidential)

2. D. Budney, *Personal Communication*, 1994

3. P. Craig and J. Summerscales, *Poisson's Ratios in Glass Fibre Reinforced Plastics*, Composite Structures, 1988, volume 9, pp 173-188.

4. R.M. Christensen, *Mechanics of Composite Materials*, John Wiley, New York, 1979.

5. E. Graff and G. Springer, *Design of Composite Straps*, Composite Structures, 1991, pp 187-211.

6. Z. Hashin, *Viscoelastic Fibre-Reinforced Materials*, AIAA Journal, 1966, volume 4, pp 1411.

7. Z. Hashin and B.W. Rosen, *The Elastic Moduli of Fibre-Reinforced Materials*, Journal of Applied Mechanics, 1964, volume 31, pp 223.

8. R. Hill, *Theory of Mechanical Properties of Fibre-Strengthened Materials: I. Elastic Behaviour*, Journal of Mechanical Physics and Solids, 1964, volume 12, pp 199.

9. T. Ishikawa and T Chou, *Elastic Behaviour of Woven Hybrid Composites*, Journal of Composite Materials, January 1982, volume 16, pp 2-19.

10. T.J. Lu, X. Ji and X.R. Gu, *The Effect of Resin Properties on the Strength of Filamentary Wound Structures*, Journal of Strain Analysis, 1989, volume 24 number 2, pp 107-113.

11. M. Nahas, *Survey of Failure and Post-Failure Theories of Laminated Fiber-Reinforced Composites*, Journal of Composites Technology and Research, 1996, volume 8, number 4, pp 138-153.

12. Y.S.N. Reddy and J.N. Reddy, *Linear and Non-linear Failure Analysis of Composite Laminates with Transverse Shear*, Composites Science and Technology, 1992, volume 44, pp 227-255.

13. D. She, *Flexible Composite Tubular Structures*, M.Sc. Thesis, University of Alberta, 1993.

14. G.D. Sims, A.F. Johnson and R.D. Hill, *Mechanical and Structural Properties of a GRP Pultruded Section*, Composite Structures, 1987, volume 8, pp 173-187.

15. J.J.Stoker, *Differential Geometry*, Wiley-Interscience, New York, 1969, pp 63.

16. Tsai, S.W., *A Survey of Macroscopic Failure Theories for Composite Materials*, Technical Report, AFWAL-TR 84-4025.

17. Tsai, S.W and Wu, E.M., *A General Theory of Strength for Anisotropic Materials*, Journal of Composite Materials, 1971, volume 5, pp 58-80.

APPENDIX 1

CYLINDRICAL APPROXIMATION

In order to simplify the helical geometry, the helical strips have been approximated by a cylinder with an equivalent radius r_s. The radius at a point is determined through differential geometry as follows (Stoker, 1969).

The curvature of a curve in space κ is defined as

$$\kappa = \frac{1}{r} = \frac{|X' \times X''|}{|X'|^3} \tag{A1.1}$$

where r_o is the pipe radius and **X** is the definition of a point on the curve. The definition of a helix in cartesian coordinates with wrap angle ϕ, angle of rotation Θ and with the axis of the cylinder in the z-direction, as in Figure 2.7, is

$$X = r_o\cos\theta\hat{i} + r_o\sin\theta\hat{j} + \theta r_o\cot\phi\hat{k} \tag{A1.2}$$

The first and second derivatives are

$$X' = -r_o\sin\theta\hat{i} + r_o\cos\theta\hat{j} + r_o\cot\phi\hat{k}$$

$$X'' = -r_o\cos\theta\hat{i} - r_o\sin\theta\hat{j}$$

The numerator of equation A1.1 is thus

$$\begin{aligned} X' \times X'' &= [(-r_o\cot\phi)(-r_o\sin\theta)]\hat{i} + [(r_o\cot\phi)(-r_o\cos\phi)]\hat{j} \\ &\quad +[(-r_o\sin\theta)(-r_o\sin\theta) - (r_o\cos\theta)(-r_o\cos\theta)]\hat{k} \\ &= r_o^2\sin\theta\cot\phi\hat{i} - r_o^2\cos\theta\cot\phi\hat{j} + r_o^2(\sin^2\theta + \cos^2\theta)\hat{k} \end{aligned}$$

or

$$X \times X'' = r_o{}^2\sin\theta\cot\phi\hat{i} - r_o{}^2\cos\theta\cot\phi\hat{j} + r_o{}^2\hat{k} \tag{A1.3}$$

with the magnitude being

$$
\begin{aligned}
|X' \times X''| &= [r_o^4\sin^2\theta\cot^2\phi + r_o^4\cos^2\theta\cot^2\phi + r_o^4]^{\frac{1}{2}} \\
&= [r_o^4\cot^2\phi(\sin^2\theta + \cos^2\theta) + r_o^4]^{\frac{1}{2}} \\
&= r_o^2(\cot^2\phi + 1)^{\frac{1}{2}}
\end{aligned}
$$

or

$$|X' \times X''| = r_o^2(\cot^2\phi + 1)^{\frac{1}{2}} \tag{A1.4}$$

The denominator of equation A1.1 is

$$
\begin{aligned}
|X'|^3 &= [(r_o^2\sin^2\theta + r_o^2\cos^2\theta + r_o^2\cot^2\phi)^{\frac{1}{2}}]^3 \\
&= r_o^3(\cot^2\phi + 1)^{\frac{3}{2}}
\end{aligned}
\tag{A1.5}
$$

thus the curvature at a point is

$$
\begin{aligned}
\kappa &= \frac{r_o^2(\cot^2\phi + 1)^{\frac{1}{2}}}{r_o^3(\cot^2\phi + 1)^{\frac{3}{2}}} \\
&= \frac{1}{r_o(\cot^2\phi + 1)}
\end{aligned}
$$

or

$$\kappa = \frac{\sin^2\phi}{r_o} = \frac{1}{r_s} \tag{A1.6}$$

and the effective strip radius is

$$r_s = \frac{r_o}{\sin^2\phi} \tag{A1.7}$$

This radius is used in the generation of the model to approximate the behaviour of the helix. It should be noted that the axis of the rectangular cross section of the strip corresponds with the axis of the radius of curvature of the strip. That is, bending about the minor axis of the strip causes a change in strip radius.

APPENDIX 2
MATERIAL PROPERTIES

A2.1 Introduction

Use of a finite element model requires a detailed characterization of the materials being used. The stress-strain relationship for the 3-dimensional case is

$$\begin{Bmatrix} \epsilon_{11} \\ \epsilon_{22} \\ \epsilon_{33} \\ \epsilon_{12} \\ \epsilon_{13} \\ \epsilon_{23} \end{Bmatrix} = \begin{bmatrix} \frac{1}{E_1} & -\frac{\nu_{12}}{E_1} & -\frac{\nu_{13}}{E_1} & 0 & 0 & 0 \\ -\frac{\nu_{21}}{E_2} & \frac{1}{E_2} & -\frac{\nu_{23}}{E_2} & 0 & 0 & 0 \\ -\frac{\nu_{31}}{E_3} & -\frac{\nu_{32}}{E_3} & \frac{1}{E_3} & 0 & 0 & 0 \\ 0 & 0 & 0 & \frac{1}{G_{12}} & 0 & 0 \\ 0 & 0 & 0 & 0 & \frac{1}{G_{13}} & 0 \\ 0 & 0 & 0 & 0 & 0 & \frac{1}{G_{23}} \end{bmatrix} \begin{Bmatrix} \sigma_{11} \\ \sigma_{22} \\ \sigma_{33} \\ \sigma_{12} \\ \sigma_{13} \\ \sigma_{23} \end{Bmatrix} \qquad \text{(A3.1)}$$

In the general orthotropic case this involves 12 elastic constants. There are six Poisson's ratios, 3 tensile moduli and 3 shear moduli. Determination of these properties for the materials in use involves a rigorous experimental or analytical process. As noted above, two fibre-resin systems were employed in the composite strips. Layers of glass fibre fabric reinforced vinyl ester surrounded an inner core of unidirectional glass fibre-reinforced vinyl ester. The elastic constants are determined for each as follows.

A2.2 Constituent Material Properties

The properties of the constituent materials, that is, the vinyl ester resin and the glass fibres, are shown in Table A2.1.

Table A2.1 Constituent Material Properties

Derekane Vinyl Ester Resin	
Modulus (ksi)	490
Strength (ksi)	11.5
ν	.35
G_m (ksi)	181
K_m (ksi)	544
E-Glass Fibres	
Modulus (ksi)	10,500
Strength (ksi)	550,000
ν	.2
G_f (ksi)	4,375
K_f (ksi)	5,833

The shear moduli and the bulk moduli of the above isotropic materials have been determined using the equations

$$G = \frac{E}{2(1+\nu)} \tag{A3.2}$$

$$K = \frac{E}{3(1-2\nu)} \tag{A3.3}$$

A2.3 Composite Material Properties

Because composite materials are generally used as thin laminates and less often as thick components, most of the material property data available is oriented towards characterization of laminates. This means that the out of plane properties, namely ν_{23} and G_{23} for the unidirectional material are not readily available. Thus for this analysis, these values have been estimated using the theoretical approximations as is explained below.

A2.3.1 Unidirectional Composite Material Properties

The unidirectional material is transversely isotropic about the 1-direction (the fibre direction), and the following relationships can be applied,

$$\begin{aligned} E_2 &= E_3 \\ \nu_{12} &= \nu_{13} \\ G_{12} &= G_{13} \end{aligned} \qquad \text{(A3.4)}$$

With the elastic relationships

$$\begin{aligned} \nu_{21} &= \frac{E_1}{E_2}\nu_{12} \\ \nu_{32} &= \frac{E_2}{E_3}\nu_{23} \end{aligned} \qquad \text{(A3.5)}$$

only E_1, E_2, ν_{12}, ν_{23}, G_{12} and G_{23} need be determined in order to completely characterize the unidirectional material. Most of these properties are supplied by DOW, the manufacturer of the vinyl ester resin. However as noted above, the out of plane properties ν_{23} and G_{23} are not supplied. To determine these we employ the composite cylinders model (Hashin and Rosin, 1964) as well as additional approximations by Hill (1964) and Hashin (1966). This analysis uses constituent properties to determine the composite elastic properties. It is based on a model of a fibre encased by a cylinder of resin, assuming the ratio a/b to be constant for all fibres in the composite, a and b being the fibre and resin radii respectively.

The Poisson's ratio ν_{23} is estimated as:

$$\nu_{23} = \frac{K_{23} - G_{23} - 4\nu^2_{12}G_{23}K_{23}/E_{11}}{K_{23} + G_{23} + 4\nu^2_{12}G_{23}K_{23}/E_{11}} \tag{A3.6}$$

where K_{23} is the plane strain bulk modulus and is calculated as:

$$K_{23} = k_m + \frac{G_m}{3} + \frac{c}{[k_f - k_m + \frac{1}{3}(G_f - G_m)]^{-1} + \frac{(1-c)}{(k_m + \frac{4}{3}G_m)}} \tag{A3.7}$$

where $c = (a/b)^2$ is the fibre volume fraction.

The transverse shear modulus can be approximated by

$$G_{23} = G_m\left[1 + \frac{c}{\frac{G_m}{G_f - G_m} + (K_m + \frac{7}{3}G_m)(2K_m + \frac{8}{3}G_m)^{-1}}\right] \tag{A3.8}$$

Given the above approximations, the material properties of the unidirectional material are summarized in Table A2.2. The strengths are also added, having been obtained by the manufacturer.

Table A2.2 Unidirectionally Reinforced Material Properties

Property	Value
E_1	5,500,000 psi
$E_2 = E_3$	1,490,000 psi
$\nu_{12} = \nu_{13}$	.3
ν_{23}	.56
$G_{12} = G_{13}$	590,000 psi
G_{23}	320,000 psi
σ_{1t} / σ_{1c}	125,000 / 87,700 psi
$\sigma_{2t} = \sigma_{3t}$ / $\sigma_{2c} = \sigma_{3c}$	4,870 / 18,700 psi
$\sigma_{12} = \sigma_{13}$	20,100 psi
σ_{23}	9,700 psi

A2.3.2 Woven Fabric Material Properties

The woven fabric must also be characterized. Given the infinite range of fibre forms that are available with different yarn sizes, types of weave, number of yarns in each direction, and tightness of the weave, it is much more difficult to characterize woven fabric composites than unidirectional composites. Because of this, some typical values have been assumed, and some approximations have been made in order to characterize the material (Sims, 1987; Lu, 1989; Craig, 1988; Whitcomb, 1991).

The woven fabric is assumed transversely isotropic about the 2-axis. The woven fabric material properties have been summarized in Table A2.3.

Table A2.3 Woven Fabric Reinforced Material Properties

Property	Value
$E_1 = E_2$	2,320,000 psi
E_3	1,490,000 psi
$\nu_{13} = \nu_{23}$	.3
ν_{12}	.15
$G_{13} = G_{23}$	590,000 psi
G_{12}	590,000 psi
$\sigma_{1t} = \sigma_{2t}$ / $\sigma_{1c} = \sigma_{2c}$	36,000 / 36,000 psi
σ_{3t} / σ_{3c}	4,870 / 18,700 psi
$\sigma_{13} = \sigma_{23}$	20,100
σ_{12}	20,000

APPENDIX 3

CONTACT SURFACE PRESSURE GRADIENTS

A comprehensive finite element model was used to determine the characteristics of the contact pressures acting between layers 1 and 2. This model was not used extensively for the entire study because of limited access to the necessary computing facilities. However, the contact pressure patterns found between the layers in this model were used to replace the presence of the additional composite strips in the simplified model.

The comprehensive model was generated as shown in Figure A3.1 in which the contact surfaces are clearly identifiable. Considering only the portion of the surface of the layer 2 strip which contacts the layer 1 strip, Figure A3.2 shows the radial stress in this area. The effect of the cross bridge is easily visible, as are the regions where outer hoop composite strips restrain radial expansion.

Figures A3.3 and A3.4 are graphs of the radial stress on this surface at two cross sections: in the centre of the cross bridge region at A-A and in one of the restrained regions at B-B as is shown in Figures A3.1 and A3.2. It is clear that the surface pressures underneath the cross bridge at A-A are noticeably less than those found elsewhere. These two pressure gradients were approximated, as shown by the linear representation in Figures A3.2 and A3.3, and were applied directly to the contact surfaces of Model L2. The sudden increase in contact pressure at the edge of the strip was not modelled in Model L2. The high levels of radial stress were inconsistent with visual observation which did not indicate any type of compressive failure at the strip edges.

Figure A3.5 shows the radial displacement of the contact surface of the layer 1 strip of the comprehensive model. This displacement field was then emulated in Model L1 by application of a pressure field. Figure A3.6 shows the displacements of the contact surface of Model L1, having had a pressure gradient applied to it. It can be seen that these displacement fields closely match those of Figure A3.5. The pressure field which was applied to Model L1 was modified for each parametric variation, in order to give the identical displacements for the contact surface. It was assumed that the displacements of this surface would remain constant regardless of parametric variations in layer 1. This is not strictly true, as modifications to any one layer will affect the deformations of all layers; however, for the parametric analysis of this study, this factor was kept constant in order to evaluate the effects of other variations on each layer individually.

The above procedure was applied to Models L1 and L2 for all parametric variations in longitudinal bridge width, cross bridge angle and percentage of woven fabric. However, the effect of variations in cross bridge width on the contact pressures were studied further as is explained below.

To determine how the contact pressures under the cross bridge were affected by the cross bridge width, another two-layer finite element model was generated, experiencing cross bridge constraints as in Model L2, as is shown in Figure A3.7. Using this model, the cross bridge width was varied and the subsequent change in contact pressures between layers 1 and 2 was determined. Figure A3.8 shows a graph of the contact pressure along the centre of the strip. The edge and centre of the cross bridge are indicated. It can be seen that the contact pressures generally increased slightly as the width increased. However, this was not constant along the entire length of the strip. Given this non-constant relationship and the fact that the changes in contact pressure were less than 4%, the contact pressures were not altered for the study of cross bridge width.

However, the radial expansion in the region of the cross bridge was altered as the cross bridge width increased. In order to determine the magnitude of this affect, Model L2 was run with variations in cross bridge width. The displacement field of the Model L2 contact surface was determined for each case and the changes were noted. These changes were then applied to the contact surface of Model L1. This allowed indirect determination of the effects of variations in cross bridge width on the layer 1 stresses.

In summary, as the cross bridge width increased, the changes in contact pressure between layers 1 and 2 were negligible but the changes in radial displacement of layer 1 were not and were applied to Model L1 for this study.

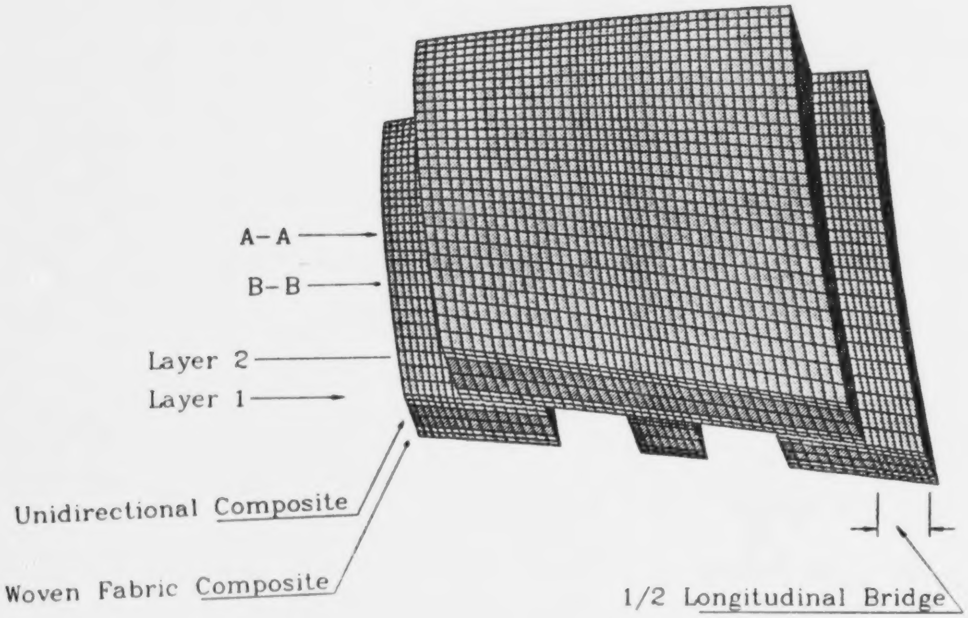

Figure A3.1 Comprehensive Model

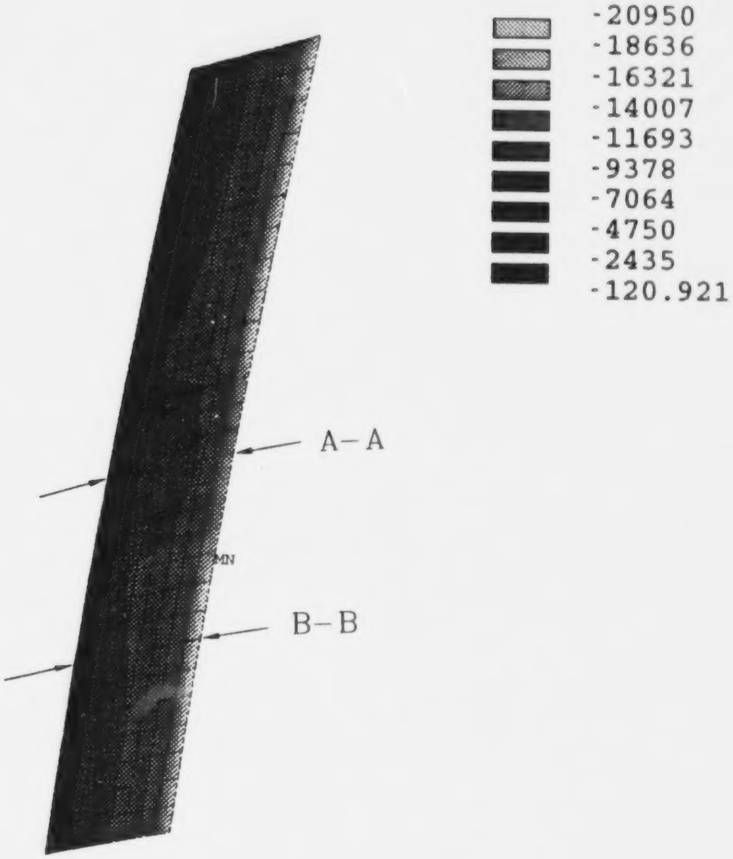

Figure A3.2 Contact Pressure at Contact Surface of Layer 2 of Comprehensive Model

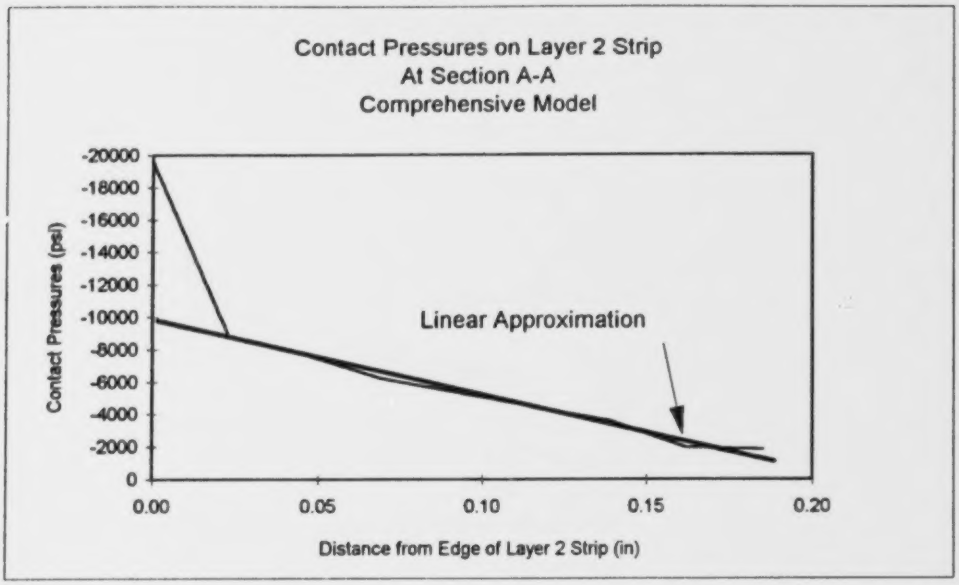

Figure A3.3 Graph of Contact Pressure at A-A of Contact Surface of Layer 2 of Comprehensive Model

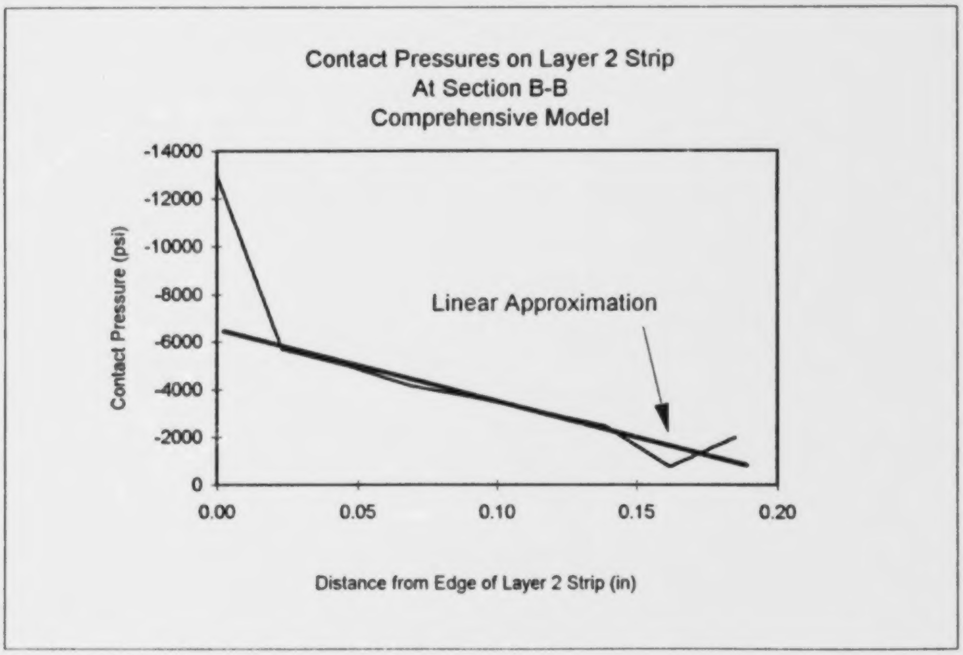

Figure A3.4 Graph of Contact Pressure at B-B of Contact Surface of Layer 2 of Comprehensive Model

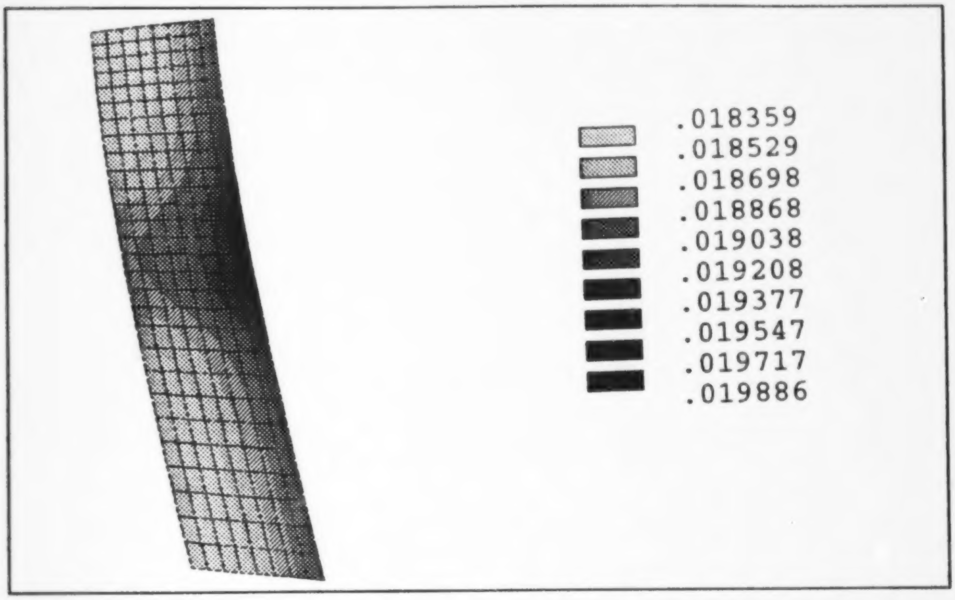

Figure A3.5 Radial Displacement of Contact Surface Layer 1 of Comprehensive Model

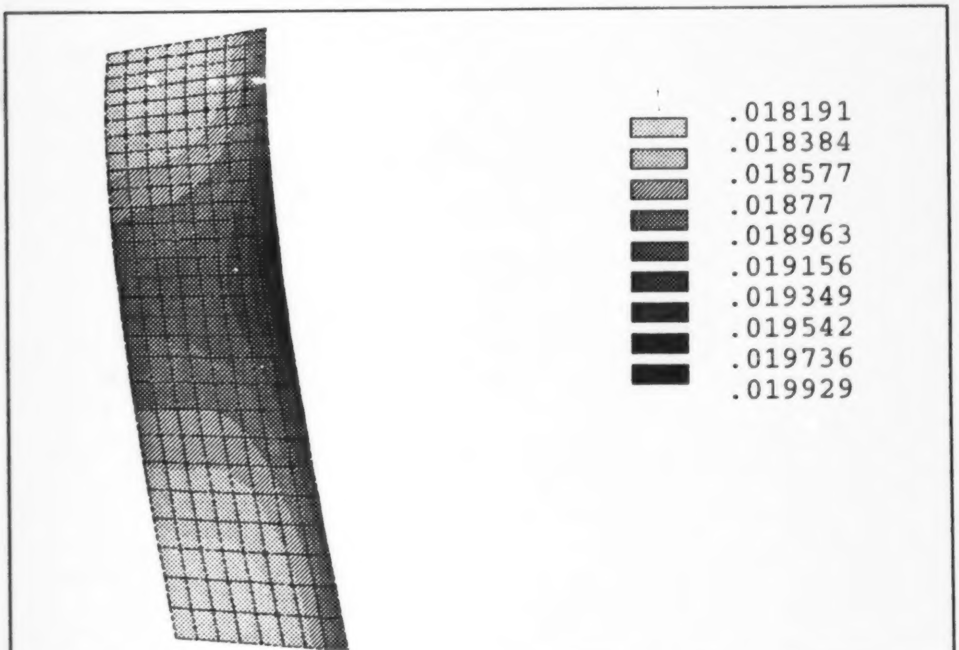

Figure A3.6 Radial Displacement of Contact Surface of Layer 1, Model L1

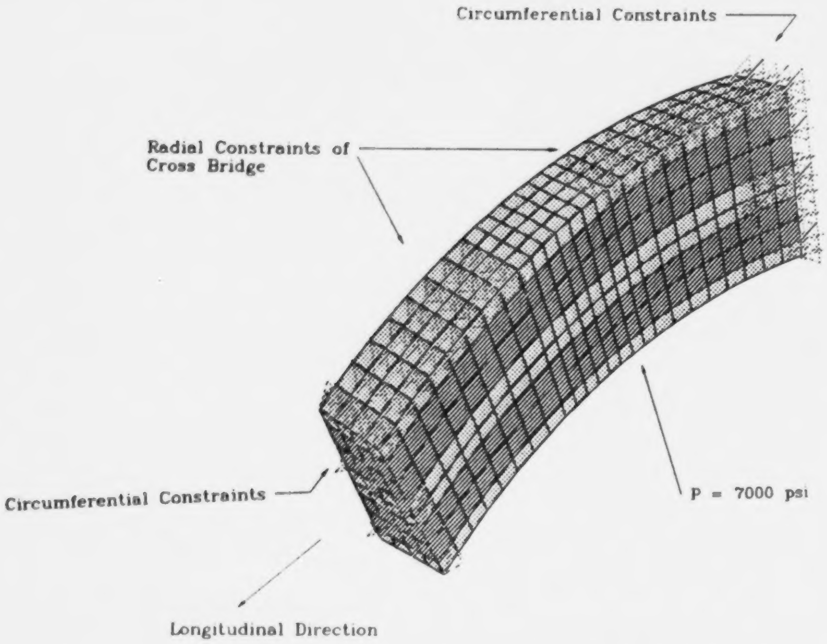
Circumferential Constraints
Radial Constraints of Cross Bridge
Circumferential Constraints
P = 7000 psi
Longitudinal Direction

Figure A3.7 Two Layer Cross Bridge Finite Element Model

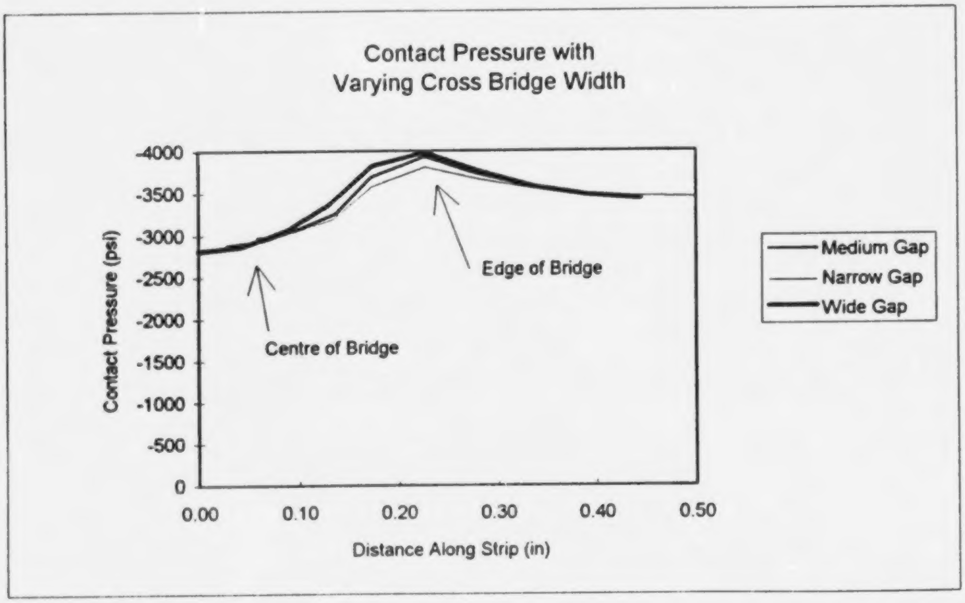

Figure A3.8 Graph of Contact Pressure of Two Layer Cross Bridge Finite Element Model

APPENDIX 4
FAILURE CRITERIA

A4.1 Introduction

In order to compare the effects of material and geometric variations to be applied to the model, a number of possible failure criteria are available. In this study, two such criteria are used. The Maximum Stress Criterion indicates the dominant mode of failure through identification of significant component stresses, while the Tsai-Wu criterion employs interaction factors to predict an ultimate failure point.

In both failure criteria, the material strengths are related to the principal directions of the composite. For the unidirectional and woven fabric composites in use, these directions correspond to the orthotropic material properties of each.

A4.2 Maximum Stress Failure Criterion

The basic Maximum Stress Criterion (Reddy and Reddy, 1991) is often used for isotropic materials and in situations where loading is generally unidirectional. It is easy to use and simply requires that each component stress is less than the strength in that direction.

$$\begin{aligned} \sigma_1 &= X_T \;\; or \;\; X_C \\ \sigma_2 &= Y_T \;\; or \;\; Y_C \\ \sigma_3 &= Z_T \;\; or \;\; Z_C \\ \sigma_{12} &= R \\ \sigma_{13} &= S \\ \sigma_{23} &= T \end{aligned}$$

where X,Y,...T are the strengths corresponding to the stresses σ_{ii} and the subscripts $_T$ and $_C$ designate tensile or compressive values.

This criterion can also be written in polynomial form:

$$(\sigma_1 - X_T)(\sigma_1 + X_C)(\sigma_2 - Y_T)(\sigma_2 + Y_C)(\sigma_3 - Z_T)(\sigma_3 + Z_C)$$
$$x(\sigma_4 - R)(\sigma_4 + R)(\sigma_5 - S)(\sigma_5 + S)(\sigma_6 - T)(\sigma_6 + T) = 0$$

The limitation of this criterion is that it does not allow for interaction between the stresses. That is, failure is not indicated until at least one of the stresses exceeds the strength in that direction; the presence of additional stresses does not affect this result. notwithstanding this limitation, one benefit of this criterion is that it indicates the dominant mode of failure. This is directly applicable to experimental observations of composite materials when it is often clear that the specimen failed in tension as opposed to shear or vice-versa.

A4.3 Tsai-Wu Failure Criterion

An alternate theory for the failure of anisotropic materials has been proposed by Tsai and Wu (Tsai and Wu, 1971). Though several have been proposed (Nahas, 1986), that proposed by Tsai and Wu is the most general and has been found to correspond well with experimental data (Graff, 1991). While not indicating the mode of failure, this criterion allows for interaction between the stresses and by doing this, is a much more realistic analytical tool. Like many advanced failure theories it starts with the general assumption that there exists a failure surface in stress-space in the form:

$$f(\sigma_k) = F_i\sigma_i + F_{ij}\sigma_i\sigma_j = 1$$

where $f(\sigma_k)$ is designated the Tsai-Wu parameter, i,j,k = 1,2...6 and F_i and F_{ij} are second and fourth rank tensors respectively. F_i has been written in abbreviated form with F_i (i = 1,2,...6) representing the 6 component strengths of the symmetric second order strength tensor. Similarly, F_{ij}, with 36 components, represents the fourth order tensor having 81 components.

The resultant matrices are related to engineering constants and strengths in the following manner:

$$F_i = \begin{bmatrix} \dfrac{1}{X_T} - \dfrac{1}{X_C} \\ \dfrac{1}{Y_T} - \dfrac{1}{Y_C} \\ \dfrac{1}{Z_T} - \dfrac{1}{Z_C} \\ 0 \\ 0 \\ 0 \end{bmatrix}$$

$$F_{ij} = \begin{bmatrix} \dfrac{1}{X_T X_C} & \dfrac{C_{XY}}{\sqrt{X_T X_C Y_T Y_C}} & \dfrac{C_{XZ}}{\sqrt{X_T X_C Z_T Z_C}} & 0 & 0 & 0 \\ & \dfrac{1}{Y_T Y_C} & \dfrac{C_{YZ}}{\sqrt{Y_T Y_C Z_T Z_C}} & 0 & 0 & 0 \\ & & \dfrac{1}{Z_T Z_C} & 0 & 0 & 0 \\ & & & \dfrac{1}{R^2} & 0 & 0 \\ & & & & \dfrac{1}{S^2} & 0 \\ & & & & & \dfrac{1}{T^2} \end{bmatrix}$$

where C_{XY}, C_{XZ}, and C_{YZ} are constants. The interaction terms F_{12}, F_{13}, F_{23} relating the normal stresses have been proposed by Tsai (Tsai, 1978). Several tests, such as a biaxial planar tensile test, have been proposed in order to determine the parameters; however, such testing is significantly more complex than current prototype testing. Tsai found that by setting $C_{XY} = C_{XZ} = C_{YZ} = -1/2$, a good match with experimental data was found. This estimate was used for this study.

APPENDIX 5
MESH REFINEMENT

A5.1 Introduction

The two models generated, L1 and L2, were optimized with regards to mesh refinement. The optimal mesh was determined by performing an analysis using three different meshes for each model.

A5.2 Model L1

The woven fabric layers were modelled with two elements through the thickness while the unidirectional was modelled with three elements through the thickness. The additional element for the unidirectional was added because this layer experienced a high level of transverse bending about the axis of the strip. This bending introduced high stresses at the outside edges of the unidirectional layer and stresses close to zero at the centre. When the centroidal stresses were calculated for the Tsai Wu failure criteria, an artificially low Tsai-Wu failure criteria resulted that did not reflect the high stresses at the surface. By increasing the number of elements through the thickness, this factor was minimized. The number of elements through the thickness was limited to three because of computational limitations.

As noted above, given the limited number of elements permitted through the thickness of the layer, three meshes were generated for this model, and the stresses from each were compared. Figures A5.1 to A5.5 show the variation of stress with mesh refinement, for the woven fabric and unidirectional layers. It can be seen that in each case, there is little variation from the second model to the third. Thus, for Model L1, the moderate mesh was adopted for further study. Figure A5.6 shows Model L1 with the final mesh.

A5.3 Model L2

Both the woven fabric and the unidirectional material of this layer were modelled with two elements through the thickness. A third element was deemed unnecessary for the unidirectional layer of this model as the stresses due to transverse bending were minimal. The 'T' section received additional elements through the thickness because of a stress concentration at the junction with the main part of the strip.

Once again, three meshes were generated. Figures A5.7 to A5.2 show the variation in stresses due to mesh refinement. There is a larger difference between meshes 2 and three in this case, notably regarding the shear stresses. However, as the stresses are converging, and because the stresses are relatively low compared to the strengths in this direction, the moderate mesh was adopted once again. Figure A5.13 shows Model L2 with the final mesh.

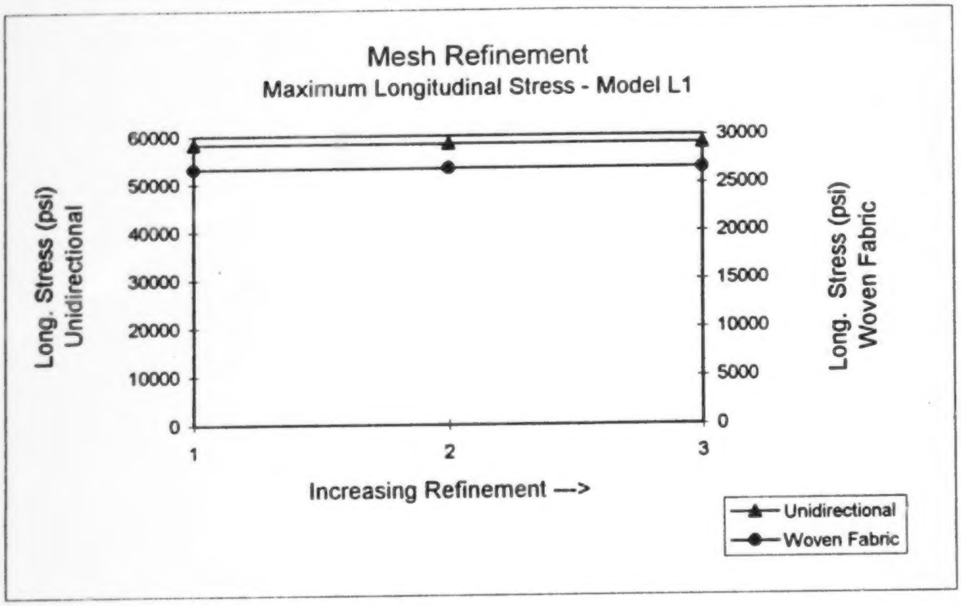

Figure A5.1 Variation of Maximum Longitudinal Stress with Mesh Refinement, Model L1

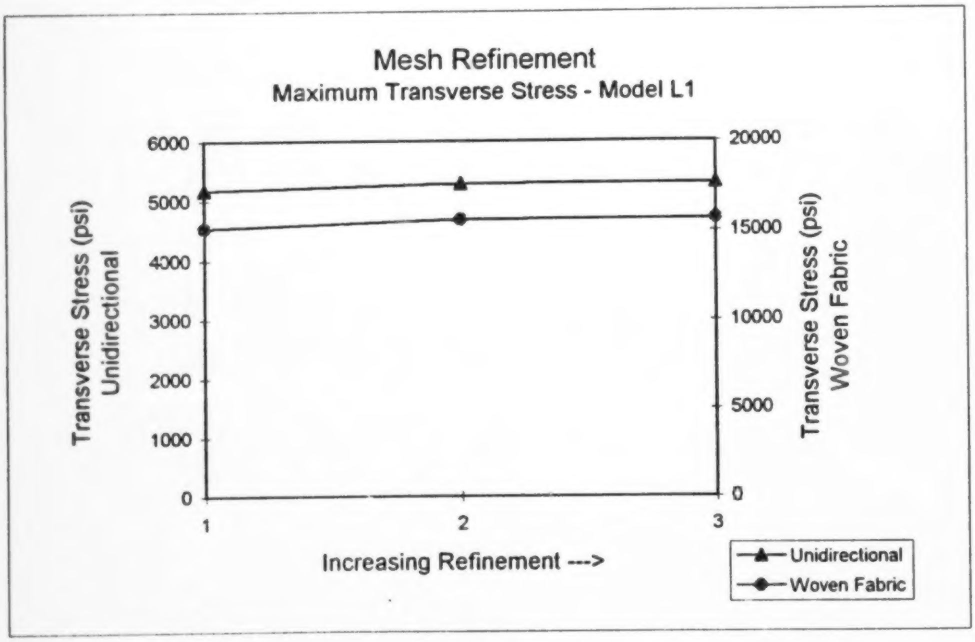

Figure A5.2 Variation of Maximum Transverse Stress with Mesh Refinement, Model L1

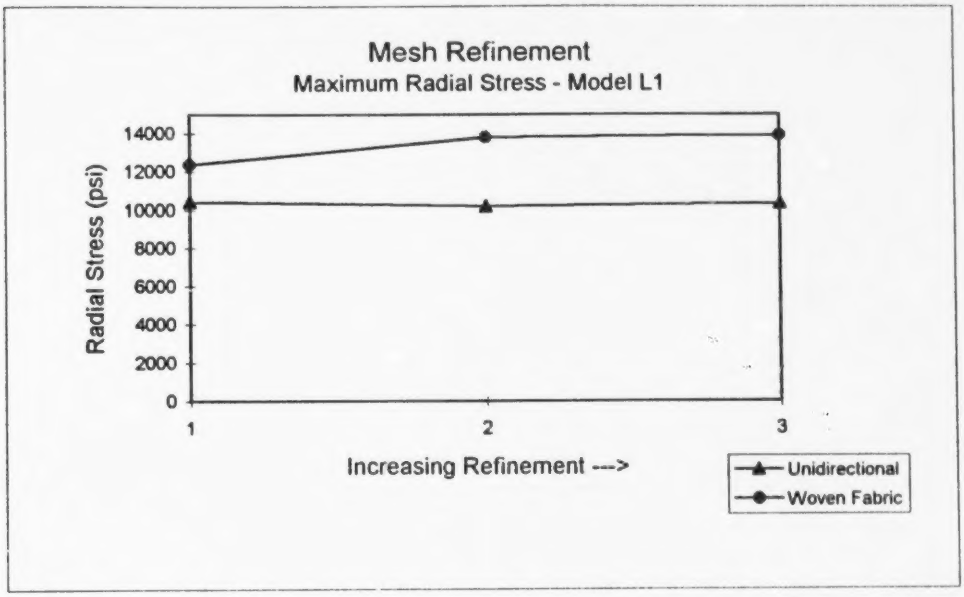

Figure A5.3 Variation of Maximum Radial Stress with Mesh Refinement, Model L1

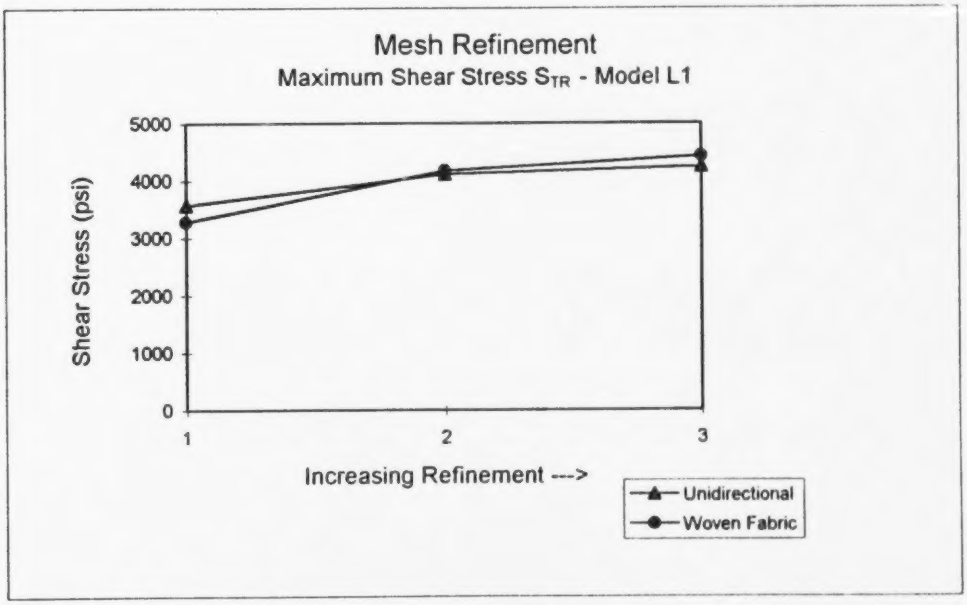

Figure A5.4 Variation of Maximum Shear Stress S_{TR} with Mesh Refinement, Model L1

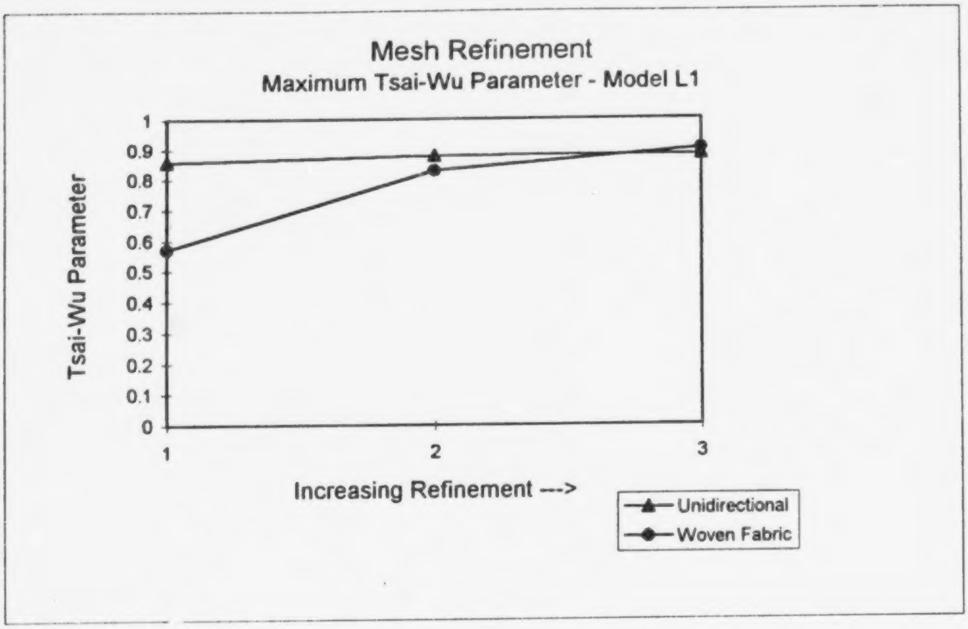

Figure A5.5 Variation of Maximum Tsai-Wu Parameter Mesh Refinement, Model L1

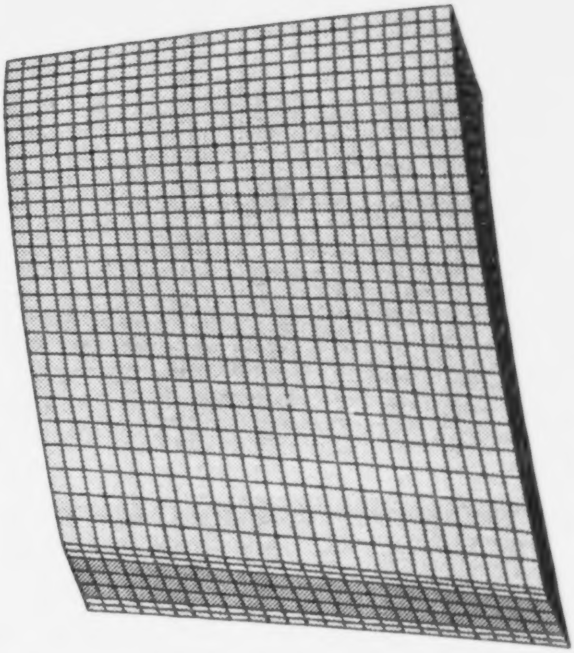

Figure A5.6 Final Mesh Density of Model L1

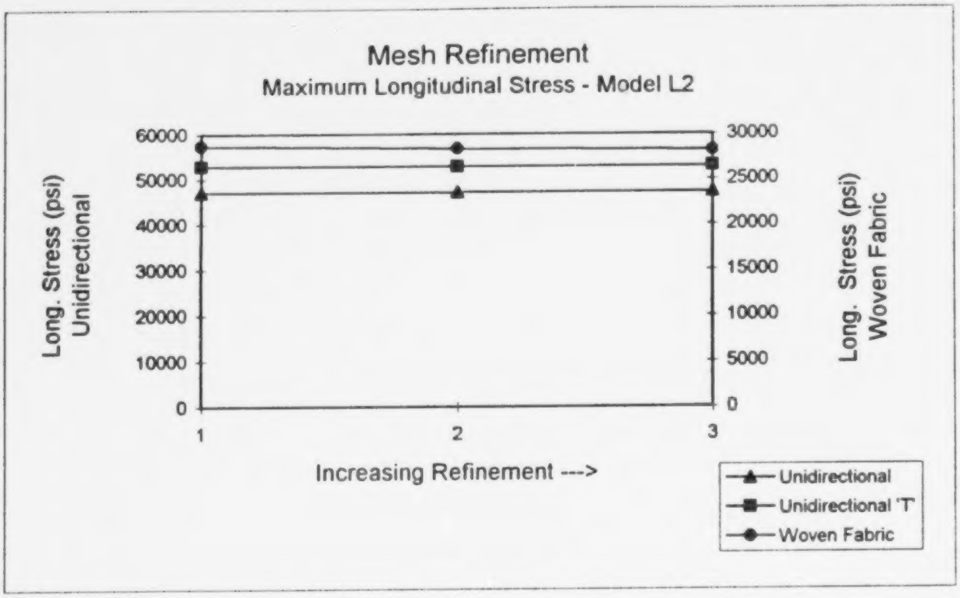

Figure A5.7 Variation of Maximum Longitudinal Stress with Mesh Refinement, Model L2

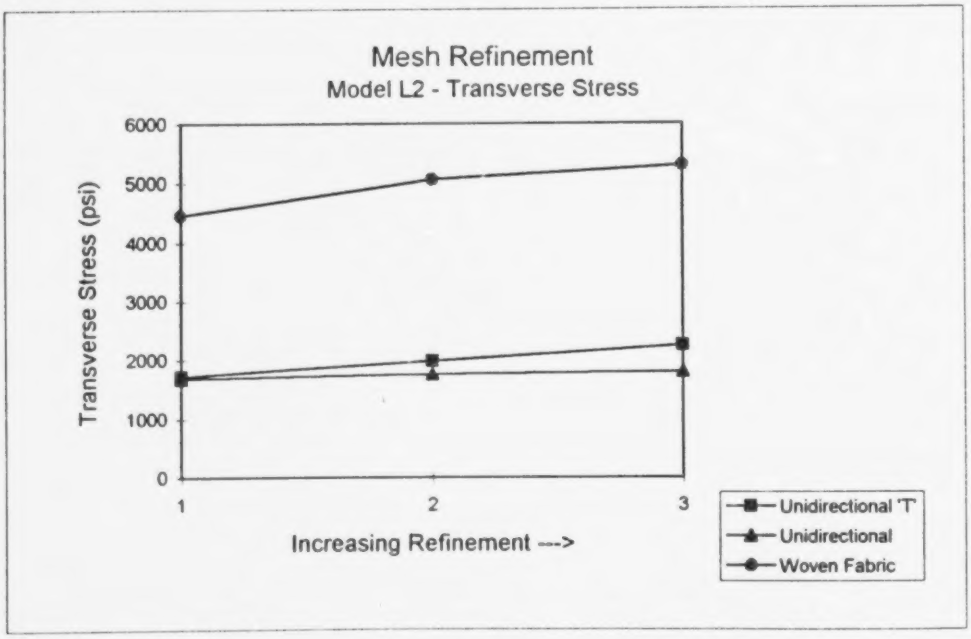

Figure A5.8 Variation of Maximum Transverse Stress with Mesh Refinement, Model L2

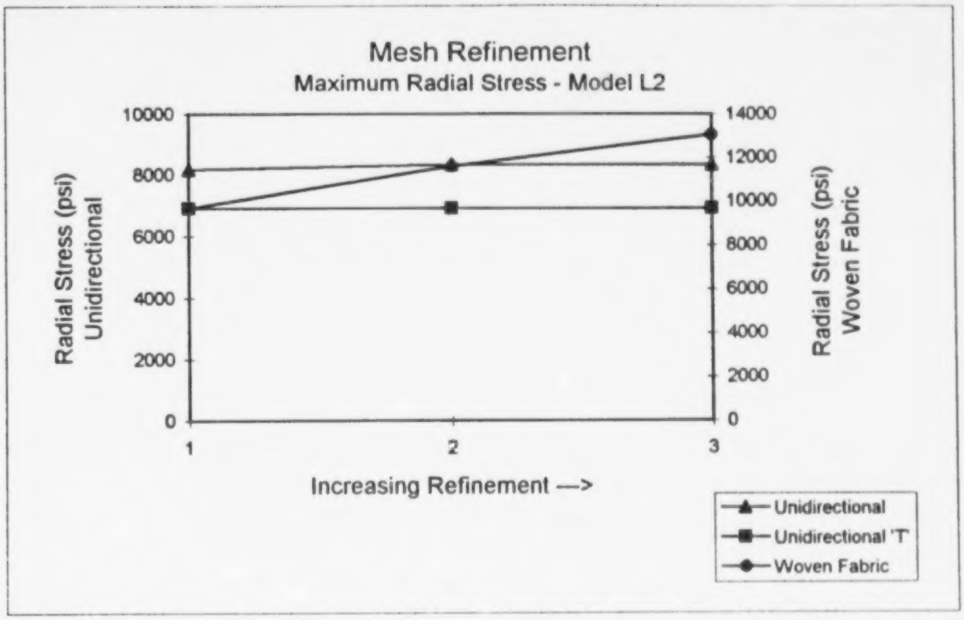

Figure A5.9 Variation of Maximum Radial Stress with Mesh Refinement, Model L2

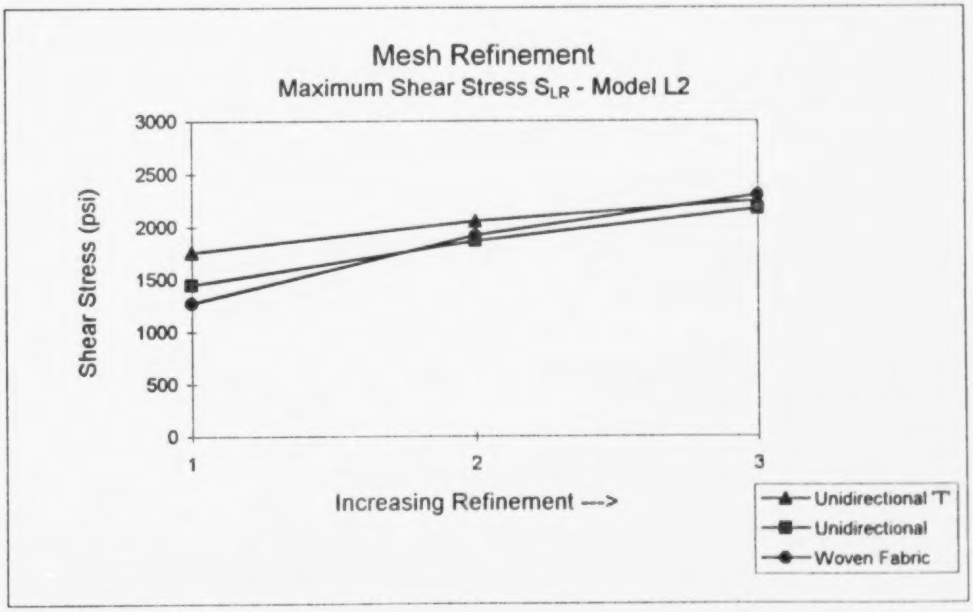

Figure A5.10 Variation of Maximum Shear Stress S_{LR} Mesh Refinement, Model L2

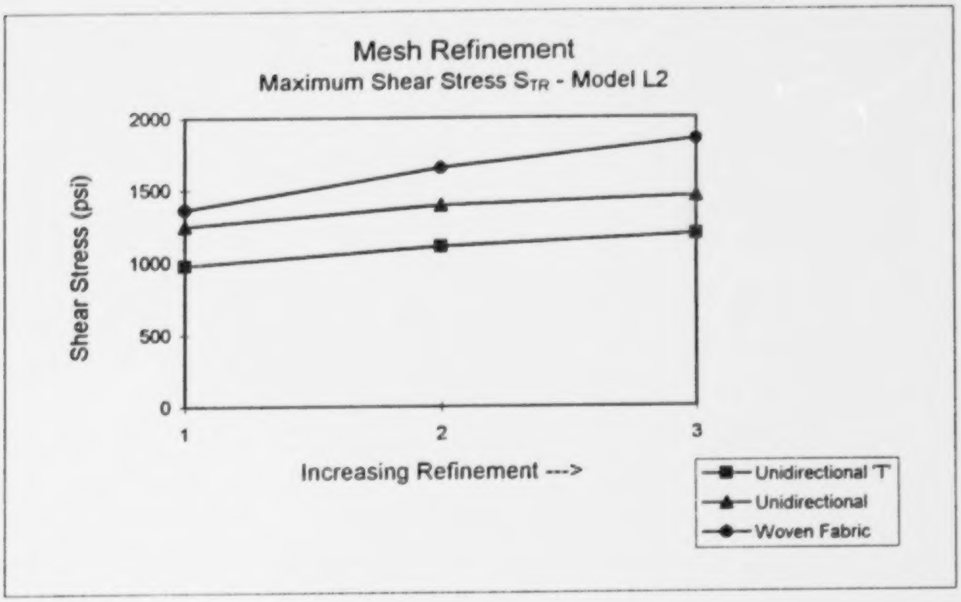

Figure A5.11 Variation of Maximum Shear Stress S_{TR} with Mesh Refinement, Model L2

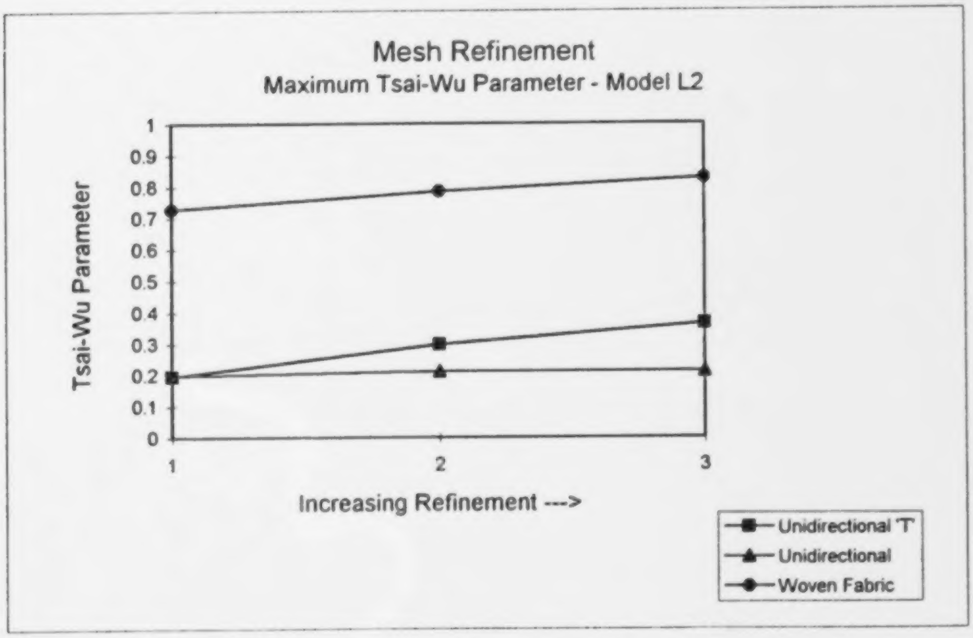

Figure A.5.12 Variation of Maximum Tsai-Wu Parameter with Mesh Refinement, Model L2

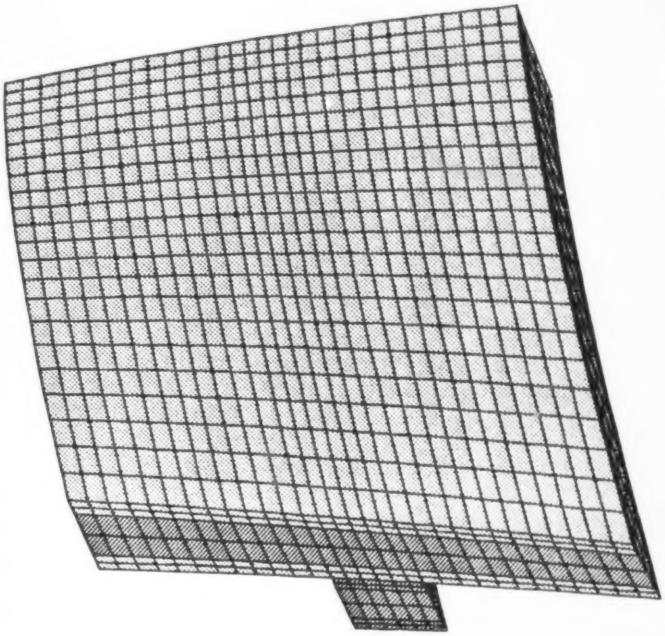

Figure A5.13 Final Mesh Density of Model L2